NUREG-0956

SAND84-0410
Vol. 3

Uncertainty in Radionuclide Release Under Specific LWR Accident Conditions

Volume III
S_2D Analyses

Prepared by
R. J. Lipinski, D. R. Bradley, J. E. Brockmann, J. M. Griesmeyer,
C. D. Leigh, K. K. Murata, D. A. Powers, J. B. Rivard,
A. R. Taig, J. Tills, and D. C. Williams

Sandia National Laboratories
Albuquerque, NM 87185

April 1985

SAND84-0410
Vol. 3
R5

Uncertainty in Radionuclide Release Under Specific LWR Accident Conditions

Volume III
S_2D Analyses

Prepared by
R. J. Lipinski, D. R. Bradley, J. E. Brockmann, J. M. Griesmeyer,
C. D. Leigh, K. K. Murata, D. A. Powers, J. B. Rivard,
A. R. Taig*, J. Tills**, and D. C. Williams

Sandia National Laboratories
Albuquerque, NM 87185

April 1985

Prepared for
Office of Nuclear Regulatory Research
U.S. Nuclear Regulatory Commission
Washington, D.C. 20555

*On attachment from Safety and Reliability Directorate, United Kingdom Atomic Energy Authority

**J. Tills and Associates, Inc.

ABSTRACT

An estimation of the uncertainty in the calculated radiological source term for an assumed S_2D accident in the Surry plant has been made. The major conclusions of the study are:

- The method of calculating a specific source term for a particular LWR accident, as demonstrated in the BMI-2104 reports, allows the determination of the effect on the source term of various phenomena uncertainties.

- For the S_2D accident a very important uncertainty is whether or not the core materials in the reactor cavity are coolable by the continuous flow of water from the sprays. This uncertainty leads to a late-time source term uncertainty that ranges from about a megacurie of suspended radioactivity, down to many orders of magnitude lower. The uncertainty in debris coolability also induces a larger uncertainty in the early source term than was found in the TMLB' analyses (reported in Volume II). The uncertainty in debris coolability is primarily due to uncertainty in debris configuration after contacting water in the reactor cavity.

- At late times another important uncertainty is the effectiveness of the containment sprays. This single uncertainty leads to a factor of ten uncertainty in late-time source term, all of it upward with respect to the BMI-2104 evaluation.

- In all cases considered, the total suspended aerosol radioactivity declined by a factor of one hundred in one hundred minutes or less. This is due to the cleansing action of the sprays.

CONTENTS

CONTENTS (Continued)

LIST OF FIGURES

FIGURES (Continued)

FIGURES (Continued)

LIST OF TABLES

ACKNOWLEDGEMENTS

The authors wish to thank B. Lucero of Tech. Reps., Inc. for her invaluable aid in typing and preparation of this document and M. Watkins of Tech. Reps., Inc. for her aid in getting figures made.

1. INTRODUCTION

The radiological consequences of a reactor accident are determined, in large part, by the magnitude and characteristics of the radioactivity release, or radiological "source term," from the plant. Important characteristics of the source term, other than magnitude of release of the many radionuclides involved, include physical and chemical nature of the released species, release timing and duration, and thermal-hydraulic features of the accompanying gas discharge (sensible heat, velocity and direction of ejection, etc.). One aim of studies of severe-accident phenomena is to provide an improved understanding of accident progression and hence, ultimately of this radiological source term.

In 1975, the Reactor Safety Study (RSS) published by the U.S. Nuclear Regulatory Commission (NRC) provided estimates of the radioactive source terms that might result from a severe core-damage accident in a nuclear power plant.[1] In those areas where detailed knowledge of the phenomena that might take place in the accident was not available, the estimates given in the RSS were intended to be conservative (i.e., the intent was to bound the radiological source term resulting from the hypothetical accident).

Since publication of the RSS, there have been substantial advances in the state of knowledge concerning the nature of severe accidents in nuclear power plants and of the fission-product release that might be associated with such accidents. These developments have indicated that the source-term estimates in the RSS might be overly conservative. In response to this concern, the NRC in 1980 requested a reevaluation of the assumptions and methods used to derive the radiological source-term estimates of the RSS. This reexamination resulted in the publication in 1981 of a report, "Technical Bases for Estimating Fission Product Behavior During LWR Accidents (NUREG-0772)."[2]

The computational tools (mathematical models coded into computer language) for performing the massive, complex calculations needed to model the phenomena of a severe accident in a nuclear power plant have likewise undergone improvements since the publication of the RSS, and particularly since the events at TMI-2. As part of the continuing source-term reassessment, the NRC is sponsoring a demonstration (headed by Battelle's Columbus Laboratories [BCL]) of a calculational procedure for the mechanistic determination of source terms. The approach adopted in the BCL determination of source terms represents a departure from that used in the RSS. It is recognized in the new effort that the release of fission products from the reactor fuel, and the subsequent behavior of the fission products, depend continuously on the nature and the timing of accident phenomena as well as on the details of nuclear plant construction. Models for the estimation of fission-product release and behavior are embedded in accident-analysis codes that incorporate the effects of the various phenomena characteristic of specific sequences of events within the plant. In this sense, the estimation of the radioactive source terms is being placed on a technical, mechanistic foundation similar to those long used in severe-accident analyses to calculate source terms for hydrogen and steam. Preliminary results of the BCL study are available in draft form; final results will be published in the volumes of a report series designated BMI-2104.[3]

Extensive peer review of interim results from the reevaluation has suggested that considerable uncertainty still exists in the estimation of severe-reactor-accident source terms. To appreciate more fully the quality of the current state of the art in estimating severe-accident source terms, an estimate of the uncertainty in model predictions is essential. Comparison of the reassessed source-term estimates with the estimates from the RSS, and application of the new radioactive-release estimates, would be more meaningful if there were information available concerning the magnitude of the uncertainty associated with the estimates and

whether that uncertainty was preferentially up or down with respect to the base case.

Sandia National Laboratories, Albuquerque (SNLA), has been estimating the uncertainty in the results of Battelle's recalculations. The SNLA effort is referred to here as the Quantitative Uncertainty Estimation for the Source Term (QUEST). The results of the QUEST study are described in general terms in Volume I of this report; detailed descriptions, supporting data, and analyses are contained in Volumes II, III, and IV.

References

1. U.S. Nuclear Regulatory Commission, "Reactor Safety Study - An Assessment of Accident Risks in U.S. Commercial Nuclear Power Plants", WASH-1400 (NUREG-75/014) (Washington, DC: U.S. Nuclear Regulatory Commission, 1975).

2. U.S. Nuclear Regulatory Commission, "Technical Bases for Estimating Fission Product Behavior During LWR Accidents," NUREG-0772 (Washington, DC: U.S. Nuclear Regulatory Commission, 1981).

3. J. A. Gieseke, P. Cybulskis, R. S. Denning, M. R. Kuhlman, and K. W. Lee, Radionuclide Release under Specific LWR - Accident Conditions -- Volumes I - VII (Drafts), BMI-2104 (Columbus, OH: Battelle's Columbus Laboratories, 1983).

2. OBJECTIVES

2.1 Objectives

The objective of the QUEST study is to estimate the uncertainty in selected specific radiological source terms as calculated in the BCL study. These determinations are meant to be examples of uncertainty in specific source terms, just as the BMI-2104 results are examples of source terms for specific LWR accident conditions.

The scope of the study was limited. Only three combinations of plant and accident sequences are considered:

- the TMLB' and S_2D accident sequences in the Surry plant (a large, dry, pressurized-water reactor [PWR])

- the TC accident sequence in the Grand Gulf plant (a boiling-water reactor [BWR] with a Mark III containment)

Operator intervention is not considered in these accidents. This volume deals only with the second of these three plant-sequence combinations, the Surry plant with the S_2D accident sequence. Volume II deals with the TMLB' analysis and QUEST methodology in detail. Descriptions of the above plants and sequences may be found in BMI-2104; paraphrases of these descriptions are provided in Appendix A of this volume for convenience.

2.2 Source-Term Characterization

The radiological source term in this study is divided into the following species groups: Cesium iodice (CsI), cesium hydroxide (CsOH), tellurium (Te), refractory fission products (RFP), and inert aerosols. Refractory fission products include barium (Ba), lanthanum (La), cerium (Ce), strontium (Sr), neodymium (Nd), praseodymium (Pr), and samarium (Sm), as well as the actinides

neptunium (Np) and plutonium (Pu). Inert aerosols include structural materials, control-rod materials, and concrete components.

The source term will be characterized for each of the aerosol groups described as the suspended mass and total aerosol radioactivity within containment as a function of time, assuming no containment failure. This characterization allows separation of the question of containment failure likelihood or mode from the question of potential source-term magnitude.

3. METHODS

3.1 Overview of Accident Source-Term Determination

A severe nuclear-reactor accident progresses through many phases, all of which contribute to the nature of the radiological source term. As the water in the reactor vessel is removed, the core heats up due to the decay heat of fission products and oxidation of the clad on the fuel. The heatup causes the vaporization of fission products and structural materials, which may condense and form aerosols.

The vapors and aerosols produced in-vessel may plate out or settle out on surfaces within the reactor coolant system (e.g., in the upper plenum, piping, or steam generator). Later heating of these surfaces may cause revaporization of the deposited materials. As the accident progresses, hot materials drop to the bottom of the reactor vessel and eventually melt a hole in the bottom. Core materials are released from the vessel, and the associated steam and gas flow may resuspend some of the aerosols deposited inside the vessel. The combination of all the above processes is a net retention of vapors and aerosols within the reactor coolant system.

If the molten core materials are ejected from the reactor vessel at high pressure (as they may be in the S_2D sequence), aerosols may be formed during the ejection process. In the cavity, if the core materials are not permanently cooled by water, the molten debris will attack the concrete. The resulting melt-concrete interactions provide an additional major source of aerosols.

The aerosols released from the reactor vessel and the aerosols produced ex-vessel mix in the containment atmosphere, agglomerate, and deposit onto containment surfaces. The containment and recirculation sprays, which are operating during an S_2D accident, help deplete aerosols and fission-product gases from the containment

atmosphere. The amount suspended at the time of containment failure is a measure of the potential amount that could be released from the containment building if containment fails. Additional important factors are the amounts after containment failure that settle, that are generated from melt-concrete interactions, and that are resuspended by gas flow or by water entrainment from flashing pools of water. The result of the above processes is a net retention of aerosols in the containment building. That which is not retained constitutes the radiological source term.

The suite of codes used in BMI-2104 models many of the features of the accident progression described above. Figure 3-1 displays

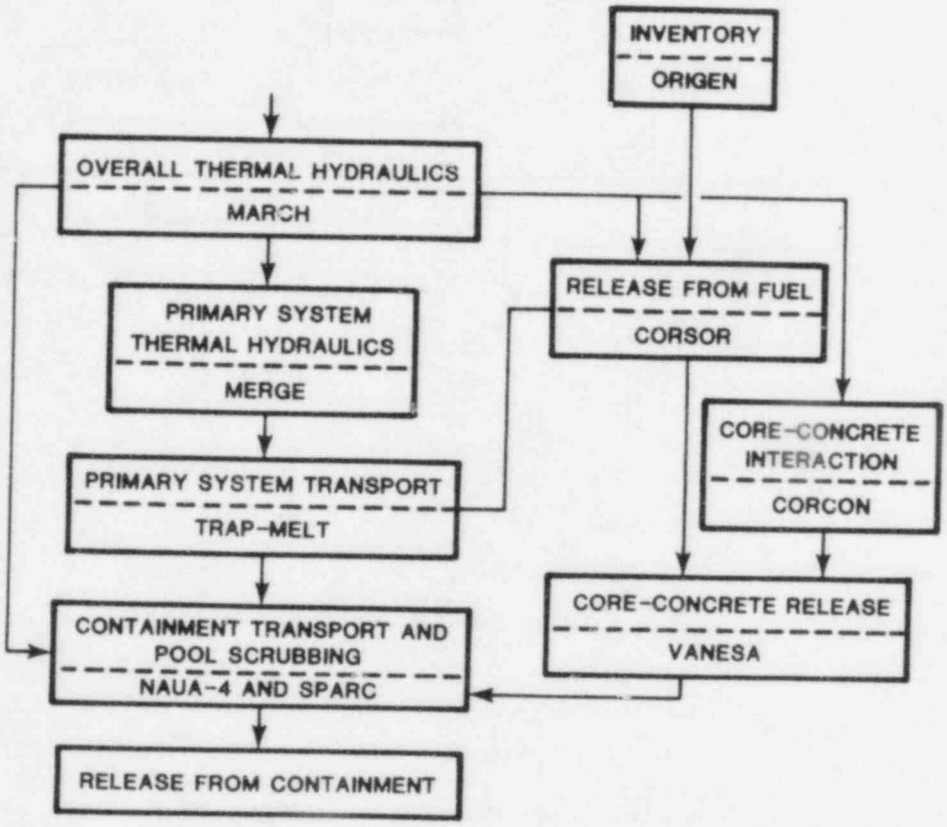

Figure 3-1 Relationships among codes used in determination of source-term code-input uncertainty.

the relationships among the various codes used in determining the radiological source term. A description and assessment of each of these codes may be found in Reference 1.

The ORIGEN code determines the fission-product inventory in the core. (The uncertainty in ORIGEN is negligible and so is not addressed in this study.) The MARCH 2.0 code calculates the overall accident thermal hydraulics, including the rate of water removal from the reactor coolant system (RCS), core temperature and clad-oxidation rates during the meltdown process, the time of vessel breach, and the temperatures of the molten materials released from the vessel. The fuel temperatures calculated by MARCH are given to the CORSOR code, which calculates fission-product release rates from fuel within the RCS. The gas-flow rates and temperatures calculated by MARCH are given to the MERGE code, which calculates gas and surface temperatures along the flow path out of the RCS. The temperatures calculated by MERGE are used by the TRAP-MELT code, along with the fission product release rates obtained from CORSOR, to determine the amount of fission-product retention in the RCS.

The CORCON code calculates temperature and gas-flow rates through the melt during core-concrete interactions, using initial melt mass, composition, and temperatures determined by MARCH. The VANESA code calculates the aerosol-release rate during core-concrete interactions using time-dependent melt temperatures and gas-flow rates from CORCON. NAUA-4 calculates the agglomeration and settling of aerosols within the containment building and removal of aerosols by containment spray. NAUA uses aerosol sources from CORSOR (after attenuation by TRAP-MELT) and VANESA, and steam-condensation rates from MARCH. SPARC calculates the retention of fission products in the suppression pool in a BWR.

As the modeling of a severe accident progresses, uncertainty develops in two ways. First, uncertainty can be introduced at a particular stage of the calculation because the knowledge or models of that particular stage of the accident are not accurate. For

example, the release-rate coefficients for CORSOR are uncertain. Sometimes certain phenomena are omitted from the models for simplicity. For example, NAUA does not treat turbulent agglomeration of aerosols. These are all sources of uncertainty. The second way uncertainty develops is by propagation. Uncertainty introduced into the analysis in a previous stage will be propagated through the present stage and amplified or attenuated by the physical processes considered. For example, uncertainties in fuel-temperature history produced by MARCH can yield very large uncertainties in fission-product release in CORSOR.

3.2 Components of the Source-Term Uncertainty

In the TMLB' analysis (reported in Volume II) the uncertainty in the source term was divided into two components:

- Code-input uncertainty (δ_c), which is the variation in the calculated source term due to justifiable variations in the input to the computer codes used in BMI-2104 (MARCH 2.0, MERGE, CORSOR, TRAP-MELT, CORCON, VANESA, NAUA, and SPARC)

- Phenomena uncertainty (δ_p), which is the uncertainty in the calculated source term due to uncertainties in known phenomena that are important to the source term.

The code-input uncertainty indicates the range in source terms that might be calculated by different users of the code suite used in BMI-2104. The phenomena uncertainty includes not only some uncertainties that are addressed in δ_c but also some that are not addressed in δ_c either because the models of the uncertain phenomena are not affected by changes in code-input parameters, or because the phenomena are not included in the codes. The δ_c analyses are obtained using the previously described BMI-2104 code suite. The δ_p analyses use the BMI-2104 code suite as well as additional codes (such as the CONTAIN code for containment phenomena) and seperate scoping calculations.

δ_p is a more complete estimate of the present state of uncertainty than is δ_c and encompasses δ_c. It was found in the TMLB' analysis that δ_p was greater than δ_c, although it was not too much greater, and that δ_c did not offer any significant insights not found in δ_p. Thus for the present S_2D analysis, only δ_p will be considered.

The determination of δ_p involves a two-stage process. First, the important sources of uncertainty are identified, and the range over which each might vary is determined. Second, the sources of uncertainty are combined and propagated to determine their effects on the amount of suspended or released radionuclides.

3.3 Determination of Sources of Uncertainty and their Ranges

The uncertainty in suspended radionuclides comes from many sources. Every stage of the severe-accident sequence can contribute to the final uncertainty. Only those sources that strongly influence the magnitude and nature of suspended radionuclide release from containment are considered for this study.

Compiling a list of potential sources of phenomena uncertainty involves reviewing literature on accident progression, investigating experimental results for unexpected effects, and considering alternate models for accident behavior. Fortunately, a research program at Sandia National Laboratories has recently completed a review of phenomena uncertainties in severe accidents.[2] Although the uncertainties listed in that study are not quantified, the extensive list provides a basis for consideration in this study.

The first step in identifying which phenomena uncertainties are important to the source term is to determine how those uncertainties can be handled quantitatively. For those instances where the phenomena can be addressed directly through code-input parameters in the BMI-2104 codes, simply varying those code-input parameters will solve the problem. For those cases where the phenomena exist in the

codes but are not addressable by code-input parameters, simple code modifications can be made to add new input parameters. In the event the phenomenon is missing, the choice is threefold: The phenomena can be added to the code, a more advanced code that already includes the phenomenon can be used, or extensive scoping calculations can be done.

Once the methods for handling the phenomena uncertainties are developed, identification of the important ones can be made by a backward progression. That is, the phenomena and parameters that strongly affect the suspended aerosol concentration in the containment building are determined first. These are input parameters to and models in the CONTAIN code, which is used in place of NAUA for the containment phenomena modeling. Next, the phenomena and parameters that strongly affect the input parameters to CONTAIN are identified. These are input parameters to and models in the VANESA code. This backward progression is continued until a chain of parameters and models that strongly affect the suspended aerosol concentrations in containment is identified.

In addition to identifying the individual sources of uncertainty, it is necessary to estimate over what ranges they might vary. Only after such an estimation is made can the sources be combined and propagated to yield the net uncertainty in the radiological source term. The ranges for the sources of uncertainty are determined in two ways: First, when data are available for a parameter, the uncertainty range is determined from the scatter in the data. Second, when data are not available, the uncertainty range is determined from predictions of alternate models. The ranges are described in Section 5.

3.4 Combining and Propagating Uncertainties

Three methods of combining and propagating code and phenomena uncertainties are considered. First, it is possible to vary a single input parameter about a given base case (specifically, a

BMI-2104 case) and examine the effect of such variation on the estimated radiological source term. This approach yields a measure of the relative size and importance of each parameter. At the end of this process, however, it is difficult to combine the individual parameter uncertainties into an overall uncertainty estimate. The QUEST study makes limited use of this approach.

Second, it is feasible to perform sensitivity studies on the component codes of the suite under consideration. This approach gives an indication as to which parameters are important to a given code. In addition, the relative influence of these parameters on the source term can be estimated by linking the sensitivity studies of the various codes. Again, the resultant uncertainties are not readily combined into an overall uncertainty statement. This approach is used for the purpose of obtaining background data for application to the major methodology adopted for combining and propagating individual uncertainties, described below.

In the third approach, a specific value is chosen for each input parameter or uncertain phenomenon from within the uncertainty range for that parameter of phenomenon. This set of input values is then used in calculating a specific radiological source term. This process is repeated until the range in possible radiological source terms becomes apparent. This approach allows the combination of uncertain parameters in a manner that avoids inconsistencies (such as assuming 100% oxidation of zirconium metal both in-vessel and ex-vessel in order to maximize both in-vessel and ex-vessel aerosol generation).

In order to minimize the number of full source-term calculations that need to be performed, the input parameters may be consciously chosen with regard for those that would lead to high or low calculated source terms. Sensitivity studies on component codes, and scoping calculations, can aid the selection process. The source terms produced by the first few calculations cannot be

guaranteed to span the full space that is possible, but they should give a quick estimate of the full span.

The tools used for the spanning calculations are the suite of codes used in BMI-2104. They are modified for the δ_p calculations to determine the effect of uncertain phenomena. In addition, some individual codes are replaced with other codes or with extensive scoping calculations that have a greater flexibility to span the ranges of phenomena uncertainties of interest.

3.5 References

1. T. S. Kress, Review of the Status of Validation of the Computer Codes Used in the NRC Accident Source Term Reassessment - Study (BMI-2104), Draft, ORNL/TM-8842 (Oak Ridge, TN: Oak Ridge National Laboratories, 1984).

2. J. B. Rivard, V. L. Behr, R. G. Easterling, J. M. Griesmeyer, F. E. Haskin, S. W. Hatch, A. M. Kolaczkowski, R. J. Lipinski, M. P. Sherman, A. R. Taig, and A. J. Wickett, Identification of Severe Accident Uncertainties, SAND83-1689, NUREG/CR-3440 (Albuquerque, NM: Sandia National Laboratories, forthcoming).

4. SENSITIVITY STUDY RESULTS

Limited sensitivity studies were performed for MARCH, CORSOR, CORCON, VANESA, NAUA, and CONTAIN for the TMLB' accident in Surry. The results are presented in Volume II of the QUEST reports. Because an S_2D accident is similar to a TMLB' accident (except for the presence of sprays), full sensitivity studies for all these codes were not repeated for the S_2D accident. However, because of the importance of the sprays in removing aerosols from the containment atmosphere, a sensitivity study in spray droplet size was performed with the CONTAIN code.

The sensitivity study was performed relative to a base case which is similar to the S_2D case reported in the Volume V draft of BMI-2104. The amounts of CsI, Te, and aerosols radioactivity suspended in containment as a function of time are shown in Figures 4-1, 4-2, and 4-3, respectively, for assumed average spray drop sizes of 300, 400, and 2000 μm. (The basis for these drop sizes is discussed in Section 5.4.) A case with no sprays present is also shown. There is no discernable difference between 300 and 400 μm drop sizes, but 2000 μm yields substantially less depletion of aerosols, and lack of sprays shows even less depletion.

The behavior of CsI is different than that of Te or the inert aerosols. The CsI is all released in a short period of time prior to, and during vessel failure. It then depletes from the containment atmosphere in an exponential decay with a rather short time constant. The aerosols are produced continuously in the melt-concrete interactions. The combined process of depletion and replenishment yields a steady value for the amount of Te suspended in the containment atmosphere. The aerosol radioactivity behavior is a combination of the CsI and Te behavior since radioactive aerosols are produced both before and after vessel failure.

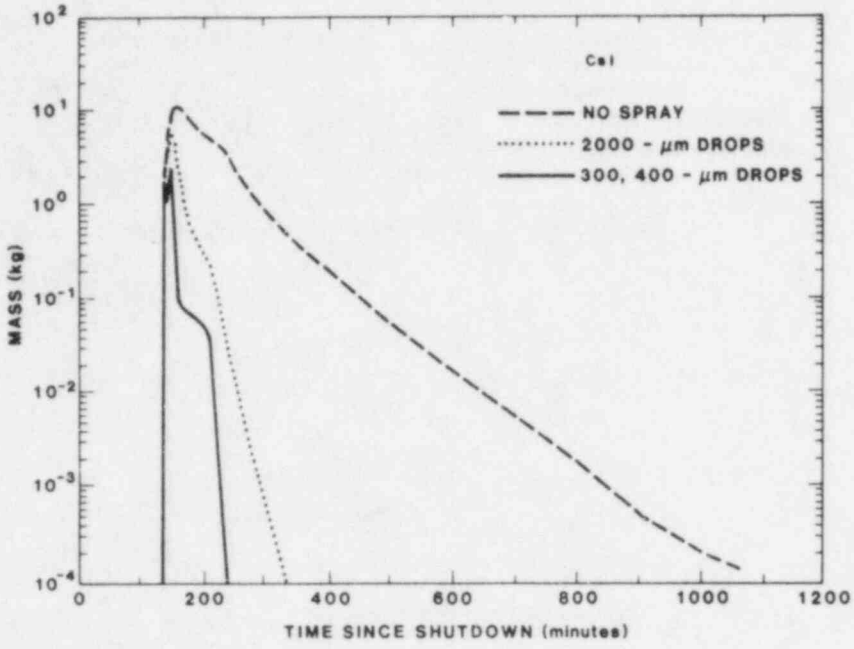

Figure 4-1 Suspended CsI mass vs. time for various spray conditions

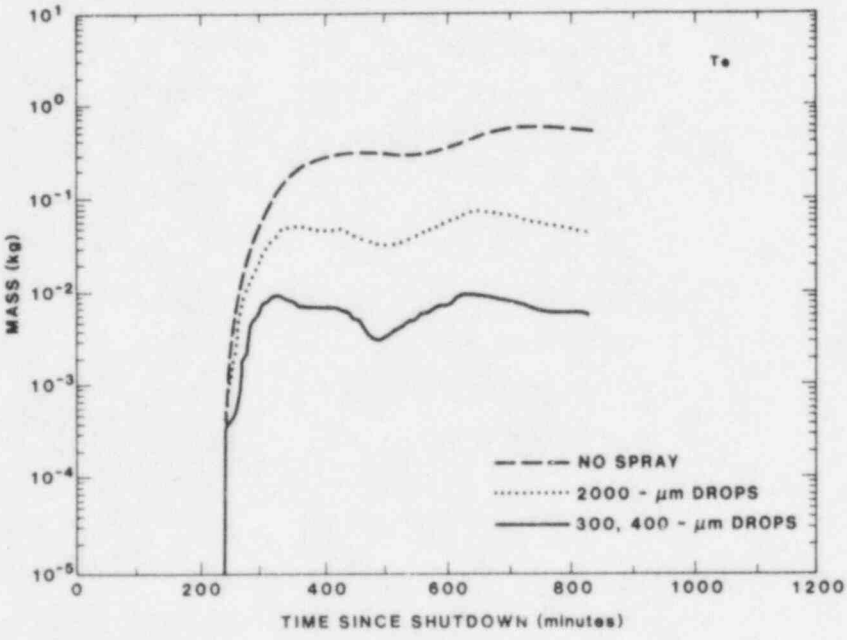

Figure 4-2 Suspended Te vs. time for various spray conditions

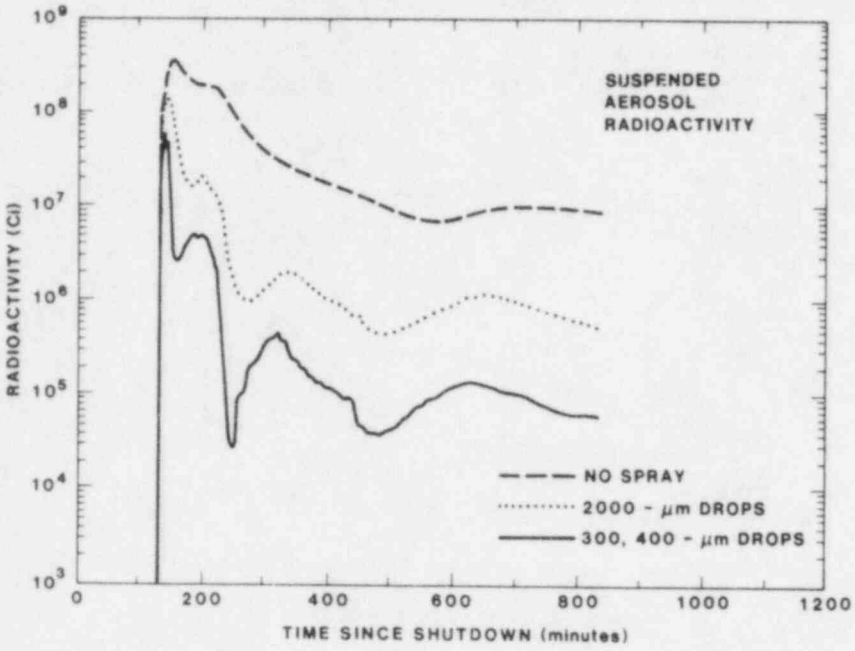

Figure 4-3 Suspended aerosol radioactivity vs. time for various spray conditions

The amount of suspended aerosol radioactivity with a drop size of 2000 μm is about ten times greater than for the BMI-2104 base case value of 400 μm. This indicates that the source term uncertainty will be at least a factor of 10 upwards with respect to the BMI-2104 base case for the S_2D accident sequence. The suspended aerosol radioactivity at late times without sprays is about ten times greater than with sprays with 2000 μm diameter drops and about a hundred times greater than with sprays with 400 μm diameter drops. This demonstrates the importance of sprays in the source term calculations.

5. SOURCES OF UNCERTAINTY AND THEIR RANGES

The uncertainty in the potential radionuclide release during an LWR accident comes from many sources. Every stage of the severe-accident sequence can contribute to the final uncertainty. However, only those sources of uncertainty that strongly influence the magnitude and nature of the potential radionuclide release are considered in this study.

The identification of the influential sources of uncertainty is based on sensitivity studies (primarily those performed for the TMLB' analysis reported in Volume II, plus that described in Section 4), on the experiences of persons familiar with the codes, and on reviews of severe-accident phenomena. Some important phenomena uncertainties were identified in the TMLB' analysis. Additional phenomena uncertainties will be discussed in this section.

In addition to identifying the individual sources of uncertainty, it is necessary to determine over what range they might vary. Only after such a determination is made can the sources be combined and propagated to yield the net uncertainty in the radiological source term. The ranges for the sources of uncertainty will be determined from scatter in available data and from alternate models describing the phenomena of interest. That is, every range must be technically justified. These ranges and their justifications are presented in this section.

5.1 Phenomena Uncertainties and Their Ranges

The suite of codes used in the Battelle study contains various phenomenological uncertainties.[1,2] These uncertainties arise from modeling that does not accurately describe the processes under consideration, either because of approximations used or because the processes themselves are not currently well understood. In

addition, some uncertainties arise because some processes are not included in the codes, sometimes because the processes have only recently been discovered or recognized as important. An extensive list of phenomena uncertainties in LWR severe accidents has been developed recently at Sandia National Laboratories.[3] The uncertain phenomena that are considered to be important to the radiological source term will be described in this subsection. In addition to identifying the sources of phenomena uncertainty and their ranges, the means by which the effect of these uncertainties on the source term is quantified will also be discussed.

The accident sequences are divided into four sequential regimes within which the uncertain phenomena will be discussed. The four regimes are:

1. In-vessel production of fission-product, control-rod, and structural vapors and aerosols

2. Net retention within the reactor coolant systems (RCS) (including the opposing influences of retention and resuspension or revaporization)

3. Ex-vessel production of radiological and inert aerosols

4. Net retention within the reactor containment building (RCB).

The in-vessel production regime is addressed by the MARCH and CORSOR codes. The net in-vessel retention regime is addressed by the MERGE and TRAP-MELT codes. The ex-vessel production regime is addressed by the CORCON and VANESA codes. The net ex-vessel regime is addressed by the NAUA code.

5.2 Phenomena Uncertainties Found in the TMLB' Analysis

Most of the uncertain phenomena identified in Volume II as important in the TMLB' sequence are also important in the S_2D accident. These include uncertainties in fuel temperature, fuel configuration, fission-product release rate coefficients, retention in the reactor coolant system (RCS), aerosol production during high-pressure melt ejection, and molten pool behavior. Two additional phenomena whose uncertainties are important for the analysis of the S_2D sequence are the effectiveness of the ex-vessel sprays and ex-vessel debris coolability. A summary of the important uncertain phenomena and uncertainty ranges identified as being important for the S_2D analysis is given in Table 5-1. A summary of additional phenomena not explicitly included in the TMLB' analysis is given in Table 5-2. More detailed explanation of the tables may be found in Volume II.

Some additional discussion is warranted concerning the uncertainty in retention of fission products in the RCS. In the TMLB' analysis, it was found that natural circulation in the reactor vessel and RCS could lead to large velocities (up to ~ 1 m/s). Current codes only consider net velocities produced by boiloff of the vessel water. Since net boiloff velocities in the TMLB' accident are typically 0.001 to 0.01 m/s, natural circulation could easily dominate the thermal-hydraulics and introduce large uncertainty into the fission-product retention calculations.

In an S_2D accident, the time from the start of core melt to core collapse is half of the time in the TMLB' accident (15 minutes vs. 30 minutes), so the net steam velocities are not that much different. Thus although fission products are released continually from the RCS (through the break) in the S_2D accident (unlike the puff release at vessel failure in TMLB'), the uncertainty in retention of fission-products in the RCS is comparable for an S_2D accident as it is for a TMLB' accident.

Table 5-1 Sources and ranges of phenomena uncertainty considered in δ_p calculations

Regime	Source	Range
In-vessel production of vapors and aerosol	Meltdown progression and clad oxidation	Modeled by MARCH
	Release rates of volatile fission products, control-rod materials, and structural materials	0.1x to 10x nominal
	System boundary conditions	
In-vessel net retention of vapors and aerosols	Natural circulation between core, plenum and other volumes	
	Revaporization from heating of surfaces	10% to 99% net retention
	Aerosol depletion factors	
	Aerosol resuspension from gas flow during breach	
Ex-vessel production of aerosols	Aerosol generation during high-pressure melt ejection	8 to 800 kg
	Debris coolability	0 to 100%
	Interlayer molten pool heat transfer	1x to 20x nominal
	Surroundings heatup	ES = 0.001 - 1.0
Ex-vessel net retention of aerosols	Multicompartmentalization	1,5
	Number of aerosol components	7
	Turbulent-energy-dissipation rate	10^{-5}-0.02 m^2/s^3
	Coupling between aerosol behavior and containment-atmosphere thermodynamics	included
	Spray droplet size	300-2000 μm
	Aerosol resuspension from gas flow at containment failure	0 to 25%
	Water reentrainment from flashing after containment failure	

Table 5-2 Phenomena not explicitly considered in δ_p calculations

Phenomenon	Reason for Neglect
Boron chemistry	Difficult to quantify effect; partially included in the 10% to 90% RCS retention range.
Steam explosions	Effect on source term similar to that of high-pressure melt ejection. (Effect on containment not within scope of this study.)
Vessel depressurization before failure	Modeled by means of small melt-ejection aerosol source
Delayed melting of outer rows of fuel elements and delay in fission-product release	Effect of quantities involved is included in net RCS retention range, but effect of delay is not. Some question on how material escapes vessel.
Revaporization of deposited fission products in RCS	Effect of quantities involved is included in net RCS retention range, but effect of delay is not. Some question of how material escapes vessel.
Hydrogen burns	Model development needed; could alter aerosol form
Diffusiophoresis	Included in CONTAIN calculations; effect of uncertainty in diffusiophoresis is small
Reevolution of iodine gas from evaporating pools	Effect partly engulfed by effects of resuspension at containment failure
Radioactive decay chains	$^{132}Te \rightarrow {}^{132}I$ is included in calculations and seems to be chain with strongest effect on late suspended radioactivity

5.3 The Effect of Water in the Reactor Cavity

An important difference between an S_2D accident and a TMLB' accident is the availability of recirculating water in the containment sprays. This spray water can find its way into the reactor cavity. Water in the reactor cavity during an S_2D accident in the Surry plant has the potential to strongly affect the source term by allowing the possibility of (1) debris coolability which would eliminate melt-concrete aerosol generation, (2) scrubbing of melt-concrete aerosols if the water lies above a molten pool, and (3) ex-vessel steam explosions. About half of the spray water falling into the refueling cavity will drain into the reactor cavity and half will drain into the refueling canal. After the canal is filled with water, all the water falling into the refueling cavity will drain into the reactor cavity.

The area of the refueling cavity is about 110 m^2, and the cross-sectional area of the containment building is about 1100 m^2, so about 10% of the spray water falls into the refueling cavity. (See Figure 5-1 from the Surry FSAR.[4]) The volume of the refueling canal is about 28 m^3. The containment sprays activate at 20 minutes after the start of the accident and deliver 0.404 m^3/s of water, with 0.040 m^3/s falling into the refueling cavity. The sprays draw from the refueling water storage tank (RWST), which has an inventory of 1320 m^3 of water available for the sprays. Thus, they can continue spraying for 54.5 minutes.

The recirculation sprays activate at 25 minutes into the accident and feed off the reactor coolant system (RCS) water that enters the containment building during the RCS blowdown, plus the containment spray water that is coming from the RWST. The recirculation sprays deliver 0.884 m^3/s, with 0.088 m^3/s falling into the refueling cavity. During the five minutes that the containment sprays are operating alone, the refueling canal receives 12 m^3 of water. After that, the combined flow into the refueling cavity is 0.128 m^3/s, half of which goes into the refueling canal.

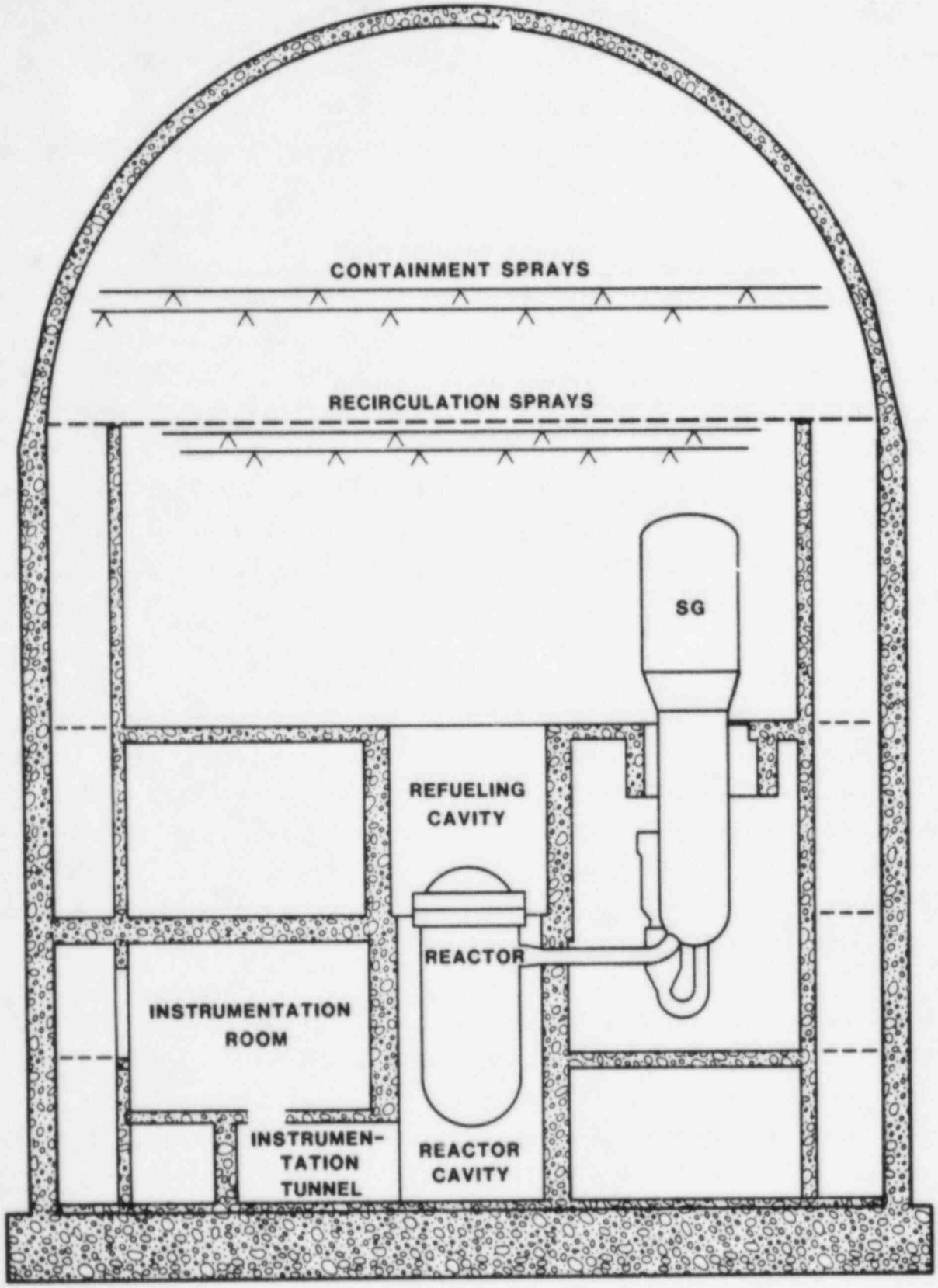

Figure 5-1. Surry Plant (from reference 1)

The canal then fills up in another 2.1 minutes, which corresponds to 27.1 minutes into the accident. By this time, the reactor cavity has received 28.3 m^3 of water, and then begins to receive water at the combined rate of 0.128 m^3/s.

The cross-sectional area of the reactor cavity and instrumentation tunnel is 57 m^2. The floor to the instrumentation room is about 5 m above the cavity floor. So the volume of water that will "fill" the reactor cavity is 285 m^3. This takes a total of (285 - 28.3)/0.128 = 2005 s = 33.4 minutes after the refueling canal has ben filled. So the reactor cavity (with the instrumentation tunnel) is filled with 6 m of water at about 60 minutes after the accident has begun. This is well before the predicted time of vessel failure at 148 minutes. (The BMI-2104 S_2D calculations have 118 m^3 of water in the reactor cavity at this time).

It is difficult to tell with conviction (using FSAR diagrams) just at what level the reactor cavity will begin to spill into other areas. The entrance into the instrumentation room is through a vertical box that may be able to contain water until the level is another meter or so above the floor level. (See Figure 5-1.) On the other hand, there is an air duct at a slightly lower level that may be able to pass water, but it is not clear whether there is a lower level for it to spill into.

The importance of the various possible levels for water spilling is that for some of the higher levels, the water is touching the bottom of the reactor vessel well before fuel debris enters the lower plenum. Depending on how well this water pervades the vessel insulation, the cooling effect of the water (boiling heat transfer) could alter the mode of vessel failure, possibly driving the location up to above the water level. On the other hand, if local failure takes place at the instrumentation tubes in spite of the water, the melt would be ejected under high pressure directly into the water. The effect of this on possible steam explosions,

aerosol generation, or direct heating of the atmosphere by hot fragments is not well known.

The presence of water in the reactor cavity with continuous refilling via the recirculation sprays raises the possibility of permanent debris coolability if the melt fragments and quenches during the ejection process and forms a bed of particulate debris. The 0.040 m^3/s flow rate into the cavity from the recirculation sprays alone is enough to remove about 85 MW of power by boiling (neglecting any subcooling in the water). So there is an adequate heat sink for the debris. However, getting the decay heat out of the debris and to the water heat sink requires liquid water to penetrate fragmented and solid debris against a counter-flow of vapor generated by water boiling within the debris bed.

The criterion for debris coolability by coolant boiling has been studied extensively both analytically and experimentally. Models exist[5] that agree fairly well with most of the available data[6]. For uniformly mixed debris in the reactor cavity, assuming 100% of the core is involved, the debris will be coolable (and will not remelt) if the average particle diameter is larger than about 1 mm. If the average particle diameter of the entire bed, or of just the top 5 or 10 cm, is less than 1 mm, then the debris will dry out and remelt. Since the particle diameter and bed configuration following a melt ejection into water involving tens of thousands of kilograms of melt is not at all well known, the present state of uncertainty in debris coolability in the reactor cavity ranges from coolable to remelt.

In summary, the action of the containment sprays and recirculation sprays in the S_2D accident in Surry is sufficient to fill the reactor cavity and instrumentation tunnel with about 5 meters of water within 60 minutes after the start of the accident. Above about 5 meters the water would be expected to spill into adjacent areas. The water level may be high enough to submerge the bottom part of the vessel prior to the dropping of core debris into

the lower plenum of the vessel. This may affect the vessel failure mode and location, the amount of high-pressure melt ejection aerosol formation and containment atmosphere heating, and the possibility and consequences of an ex-vessel steam explosion. The presence of water in the cavity along with continuous feeding from the sprays allows the possibility of melt fragmentation, quenching, and permanent coolability. Although the present state of modeling for debris coolability is reasonably good, the uncertainty in debris particle size and bed configuration is so large that both coolable debris and non-coolable debris are reasonable possibilities.

5.4 Uncertainty Range for Surry Spray Drop Size

An additional important uncertain phenomenon is the effect of sprays on the suspended aerosols in containment. One important contributor to this uncertainty is dominated by the uncertainty in the appropriate droplet size to use in the CONTAIN code. The Surry FSAR[4] describes the sprays as follows: "In all spray headers, two nozzle sizes are used. The first, producing an average particle size of approximately 1000 microns average, covers a vertical cone measuring about 15 ft horizontally on either side of the spray headers. The second nozzle size produces particles of about 1500 microns average, and covers the remaining containment volume outside this cone." The uncertainty in the average drop size at Surry comes from two sources. First, there is uncertainty in the appropriate average to use in the aerosol codes. Possible appropriate averages are number median, linear median, surface median, and mass median. Arguments given in Appendix C suggest that reasonable values could range from about the linear median to the surface median. The existence of two different size spray nozzles widens the range that would come from a single-sized nozzle. Also, there is a scatter in performance from nozzle to nozzle which yields an additional uncertainty in average drop diameter.

The average drop diameter for various kinds of averages and different nozzle types are shown in Table 5-3 (from reference 2). The span in the average drop size over different definitions is about a factor of 1.6 for the three nozzles shown. The uncertainty span in the appropriate average is even larger than this since there is no experimental basis for aerosol collection by sprays on which to make a judgment on what average, if any, is appropriate for use in a particular aerosol code.

It is not specified in the FSAR what type nozzles are used in the Surry containment, nor what type average is meant in their description of drop size, but the averages referred to are likely mass medians, and the nozzles are probably similar to the 1713 and A80.

In tests conducted by Babcock and Wilcox with 22 Sprayco 1713A nozzles, the drop mass median diameters spanned a range from 680 to 1200 microns (95% prediction interval)[7]. Thus one might expect the number median diameters to range from about 425 to 750 microns. Similarly, one might expect the A80 sizes to range from about 1200 to 2000 microns for mass median, and from 700 to 1300 microns for number median.

Table 5-3. Various average drop sizes (microns) for various spray nozzles (Sprayco 1713, Spraying Systems 1 C6.3 and A80)[7]

Average	1713	1 C6.3	A80
Number median	660	870	980
Linear median	780	1020	1150
Surface median	915	1205	1360
Mass median	1080	1420	1600

Considering the above arguments, it is suggested that an appropriate uncertainty range for the effective spray drop diameter in the Surry plant is 300 to 2000 microns. The data in Table 1 could be interpreted as justifying the specification of a narrower range. However, there are other uncertainties in the aerosol collection efficiency of a falling drop in addition to the uncertainty in drop size. To some extent, the drop size is being used here as a surrogate for these other uncertainties, and it is judged that the range used here, 300-2000 microns, gives a reasonable representation of the overall source term uncertainty due to uncertainty in spray effectiveness. The reader is referred to Appendix C for a more detailed discussion of these issues.

5.5 References

1. J. A. Gieseke, "Summary of Source Term Analyses for Five LWR Plants," Trans Eleventh Water Reactor Safety Research Info Mtg, Gaithersburg, MD, October 24-28, 1983.

2. J. A. Gieseke, P. Cybulskis, R. S. Denning, M. R. Kuhlman, and K. W. Lee, Radionuclide Release under Specific LWR - Accident Conditions -- Volumes I-VII (Drafts), BMI-2104 (Columbus, OH: Batelle's Columbus Laboratories, 1983).

3. J. B. Rivard, V. L. Behr, R. G. Easterling, J. M. Griesmeyer, F. E. Haskin, S. W. Hatch, A. M. Kolaczkowski, R. J. Lipinski, M. P. Sherman, A. R. Taig, and A. J. Wickett, Identification of Severe Accident Uncertainties, SAND83-1689, NUREG/CR-3440 (Albuquerque, NM: Sandia National Laboratories, forthcoming).

4. Surry Power Station Units 1 and 2, Final Safety Analysis Report, Virginia Electric and Power Company, Richmond, Va. (1970).

5. R. J. Lipinski, A Coolability Model for Postaccident Nuclear - Reactor Debris, Nucl. Tech., 65, p. 53 (1984).

6. R. J. Lipinski, A Review of Debris Coolability Models, Proc. of Int. Mtg. on LWR Severe Accident Evaluation, Cambridge, Mass., Aug. 28 - Sept. 1, 1983, pg. 18.2-1.

7. N. A. Nitti, Babcock and Wilcox, letter to D. A. Powers, Sandia National Laboratories, February 14, 1983.

6. SOURCE-TERM UNCERTAINTY FROM UNCERTAIN PHENOMENA (δ_p)

The suite of codes used in the Battelle study contains various phenomenological uncertainties. These uncertainties arise from modeling that does not accurately describe the processes under consideration, either because of approximations used or because the processes themselves were not understood when the codes where written. In addition, some uncertainties arise because some processes are not included in the codes, sometimes because the processes have only recently been discovered or recognized as important. The phenomena uncertainties that are considered to be important to the radiological source term are discussed in Section 5, along with the range of uncertainty associated with them. In this section, these phenomena uncertainties will be combined and propagated to determine their effect on the radiological source term.

To determine δ_p, self-consistent sets of values for uncertain phenomena were chosen for full calculations, with each set yielding a specific radiological source term. The phenomena values were chosen from within uncertainty ranges based on technical assessments and described in Section 5. Values were chosen that might result in high source terms or low source terms. The resulting high and low calculated source terms then became an estimate of the current range of source-term uncertainty.

The method of calculation was to use the codes from the BMI-2104 study, where possible, and simulate the ranges in phenomena uncertainty by code modifications. Specifically, the MARCH code was used to span uncertainties in core-meltdown thermal hydraulics. The variation provided by the input parameters was judged to be adequate without modifying the code. The CORSOR code was modified by altering the release-rate coefficents. The MERGE and TRAP-MELT codes were not used because the range in uncertainty caused by

various phenomena not treated in the codes would have required code revisions beyond the time limitation set for this study. Rather, a single parameter for net in-vessel retention was used to span the range of phenomena possibilities. These possibilities include strong natural circulation, revaporization from structural heatup by decay heating or natural circulation from the core, and dry aerosol resuspension at vessel failure. The span used was based on extensive scoping calculations, including in-vessel application of the MAEROS aerosol code performed during the TMLB' analysis (see Appendix B of Volume II).

The CORCON code was modified to use a more realistic viscosity in the heat-transfer-coefficient determination for all cases (including the base case). The heat-transfer coefficient between melt layers was varied, and the emissivity for surroundings was also varied in order to simulate the possible presence of a cloud of hot aerosols above the molten pool.

Finally, the CONTAIN code was used in place of the NAUA code because, in addition to all the features found in NAUA, CONTAIN has coupled thermal hydraulics and aerosol behavior, multicomponent aerosol capability, turbulent agglomeration, and containment multicell capability. All of these additional features were used in the four cases, except the multicell capability. Because of time limitations, this capability was considered only in the sensitivity study reported in Volume II.

Three self-consistent source terms were calculated so as to consider the possibility of a high term at early time (just after vessel failure), the possibility of a high source term at late time (nominally 15 hours into the accident), and the possibility of a low source term (which turned out to be low for both early and late times). The three δ_p cases are called early-high, late-high, and low respectively.

Table 6-1 gives the general conditions for the various stages of an accident that would be expected to result in high or low source terms at early or late time.

For the early-high case, core temperatures and release rate coefficients at the high end of the uncertainty range are assumed. In addition, retention in the RCS is assumed to be at the low end of the uncertainty range. These conditions result in a high release of radionuclides at the time of vessel failure. The time of vessel failure is also a time when the containment experiences a pressure spike which can threaten containment integrity. This pressure spike comes from the quenching of hot ejected molten materials in either water or the containment atmosphere, hydrogen burns ignited by the hot melt, and release of high-pressure steam from the vessel. Thus the early-high case is of particular interest.

The ex-vessel aerosol production and retention are not as important to the early-high case as the in-vessel activities. However, they affect how much material is available to escape a failed containment. So as a secondary enhancement of the early-high source term, the ex-vessel aerosol production is assumed to be large

Table 6-1 Conditions expected to result in high or low source terms at early or late time

	Early-High	Late-High	Low
In-vessel production	Large	Small	Small
Net retention in RCS	Small	Small	Large
Melt-concrete areosol production	Large	Large	None
Retention in containment	Small	Small	Large

and retention in the containment small. The first involves melt temperatures at the high end of the uncertainty range in the CORCON calculation. In addition it is assumed that there is no water pool above the molten pool (the melt ejection process and small steam explosions are assumed to blow out the water). Low ex-vessel retention occurs by assuming the sprays fail when containment fails from overpressure. Because spray failure is linked to containment failure, the early-high case is not extended to late times as was done in the TMLB' analyses. As mentioned, these ex-vessel conditions are of secondary importance to the early-high case.

A high source term at late time will occur if fission products are not released from the fuel until the melt-concrete interaction. So for the late-high case the core temperatures and release rate coefficient at the low end of their ranges are assumed, and low in-vessel retention is also assumed. The ex-vessel melt-concrete aerosol generation is at the high end of its range. This includes assuming no water pool above the molten pool because of occasional small steam explosions blowing out the water. Finally, low aerosol depletion is achieved by assuming a spray drop size at the high end of the uncertainty range. Spray failure would yield even less depletion, but no reasonable means of failing the sprays (without also failing the containment building) could be identified.

For the low case, core temperatures and release rate coefficients at the low end of the uncertainty band are assumed and RCS retention at the high end of the uncertainty range is assumed. Since the in-vessel production of aerosols is fairly low in this case, and aerosol agglomeration depends strongly on concentration, in-vessel retention will be limited to only 90% (rather than 99%). Ex-vessel aerosol production is assumed to be low and ex-vessel retention large. Indeed, there is no melt-concrete aerosol production at all because the ejected melt is assumed to form mixed debris with fragment sizes larger than several millimeters. This results in the debris being coolable.

The approach used in the TMLB' analyses for a case that is low at late times was to have a large release of fission products in-vessel with strong in-vessel retention. This minimizes the late-time release of aerosols in melt-concrete interactions. However, in an S_2D accident, ex-vessel debris coolability is a very reasonable possibility, and it yields essentially no ex-vessel aerosol source. Therefore, a better low source term at late times involves a low release from fuel and is identical to the early-low case. This case has the added advantage of reducing the concern of late-time revaporization of volatile fission products deposited within the RCS.

The ranges of the various uncertain phenomena are discussed in Section 5. Whether the high or low ends of each range yields a high or low effect at each stage of the accident sequence may be determined from the sensitivity studies described in Volume II and in Section 4. This information leads to specific parameter values used for the four δ_p cases. These parameter values and the base-case values are listed in Table 6-2. The results from combining and propagating the sources of phenomenological uncertainty will now be presented. The intermediate results from each stage of the accident are discussed first, followed by the final results.

6.1 In-Vessel Production of Vapors and Aerosols

The range of in-vessel production of vapors and aerosols was determined by core thermal hydraulics and release phenomena. The uncertainty in core thermal hydraulics was assumed to be adequately covered by varying the input parameters to the MARCH code, which then involves broadly different meltdown scenarios. The uncertainty in the core-temperature history, as determined by MARCH, is then propagated through the CORSOR code with the addition of uncertainties in the release-rate coefficients.

Table 6-2 Specific parameter values used for δ_p calculations

Parameter	Base-Case	Early-High	Late-High	Low
In-Vessel Production:				
MARCH 2.0:				
TMELT (°C)	2277	2482	1927	1927
TFUS (°C)	2938	3052	2217	2217
NDZDRP (out of 24)	1	1	6	6
FDROP	0.02	0.75	0.02	0.02
DPART (mm)	12.7	3	1.5	1.5
FZMCR	1	0	1	1
WGRIDX (kg)	28 888	28 888	8 666	28 888
DP (mm)	12.7	0.25	12.7	12.7
Resulting:				
Clad oxidation (%)	60	92	38	38
Vessel failure time (minutes)	241	173	148	148
CORSOR:				
Release Coefficients	nominal	10 x base*	0.1 x base	0.1 x base
Net Retention in RCS:	55%	10%	10%	90%
Ex-Vessel Production:				
CORCON:				
Layer-layer h*	Low	Low	Low	N.A.**
Surroundings emissivity	1.0	0.001	0.001	
Net Retention in RCB:				
CONTAIN:				
SPDIAM (μm)	400	None***	2000	300

*Total aerosol release limited to 5000kg
**Coolable debris assumed
***Vessel failure pressure spike assumed to fail containment/sprays

The results of the MARCH runs for the base case and the three δ_p cases are shown in Figures 6-1 through 6-10. At this early stage in the calculations, some of the cases overlap almost exactly. Figures 6-1 and 6-2 show the peak and average core temperatures. These variations are the strongest contributers to the code-input source-term uncertainty during early times. They also influence the ex-vessel source-term generation by altering the inventory in the ex-vessel molten debris. Figures 6-3 and 6-4 show the fraction of core melted and the fraction of clad oxidized. In the low case, a rapid melting of the entire core results if the effective melt temperature for the core (TMELT) is low and if only a small fraction of core in the molten state is needed for slump. This minimizes the time at high temperatures for the fuel before vessel failure. The total fraction of clad oxidized varies from 38% to 92% by the time of vessel failure. This is due to a combination of variables in MARCH. At the start of melt-concrete interactions, the range is 38% to 100% because of additional oxidation during ex-vessel debris quenching and reheating.

The containment absolute pressures and temperatures are shown in Figures 6-5 and 6-6, respectively. The results shown are MARCH results using the INTER core-concrete interaction model. Since this study is interested in the suspended mass independent of containment failure and since INTER calculates much higher concrete-penetration rates than CORCON, the three δ_p cases do not allow concrete penetration (and thus containment depressurization). Relatively high containment pressures at the time of vessel failure (given in Table 6-2) are not predicted unless there is a simultaneous hydrogen burn. Such a burn may occur systematically if the molten materials serve as an ignition source. The possibility of early containment failure affects the perceived importance of the early-high and low cases but not the size of the in-containment source term itself. The high potential pressures also make a large-hole containment failure at early time more plausible than the base case would indicate. A large hole in containment would yield a larger release

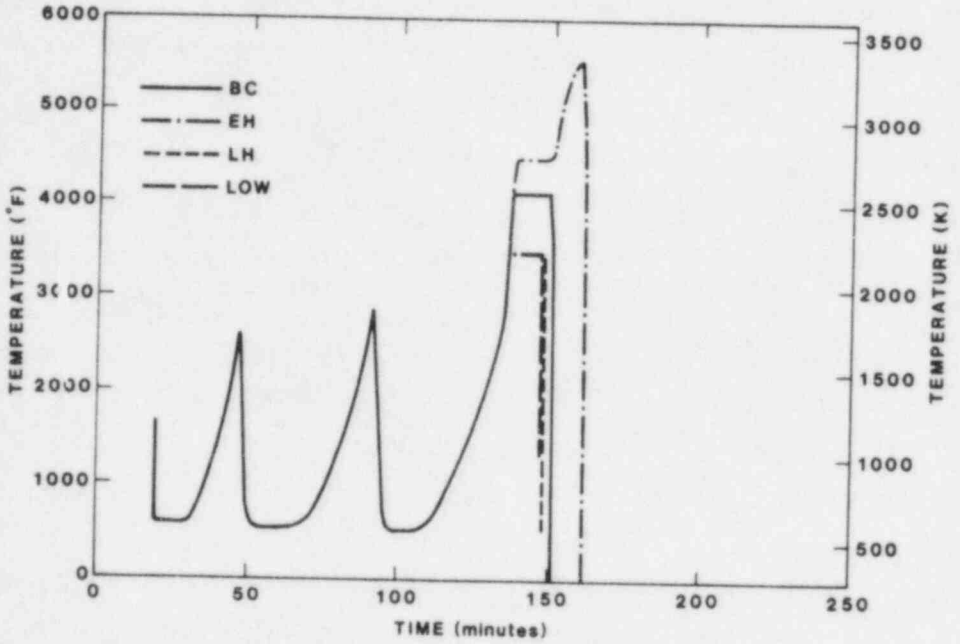

Figure 6-1 Maximum core temperature.

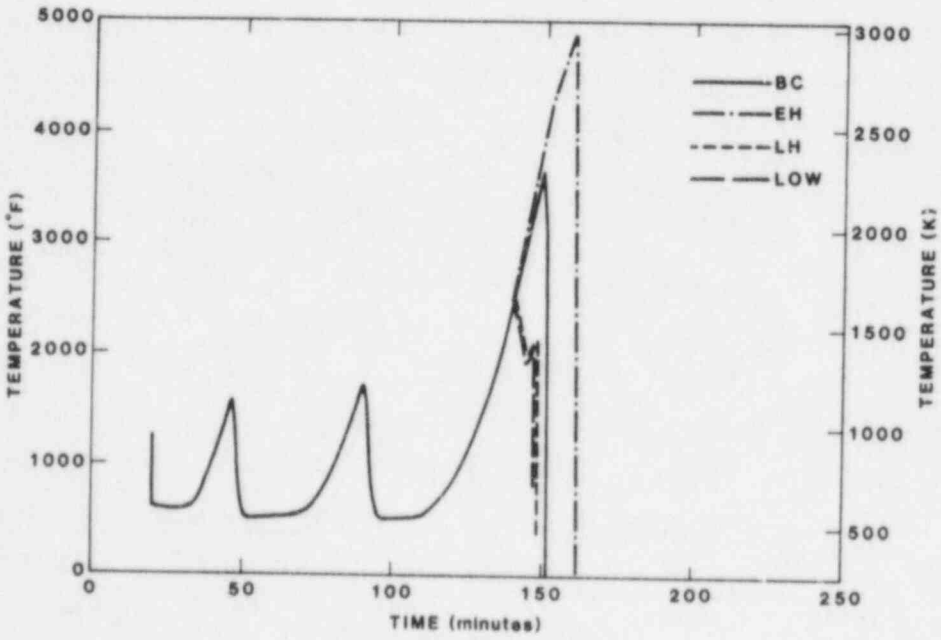

Figure 6-2 Average core temperature.

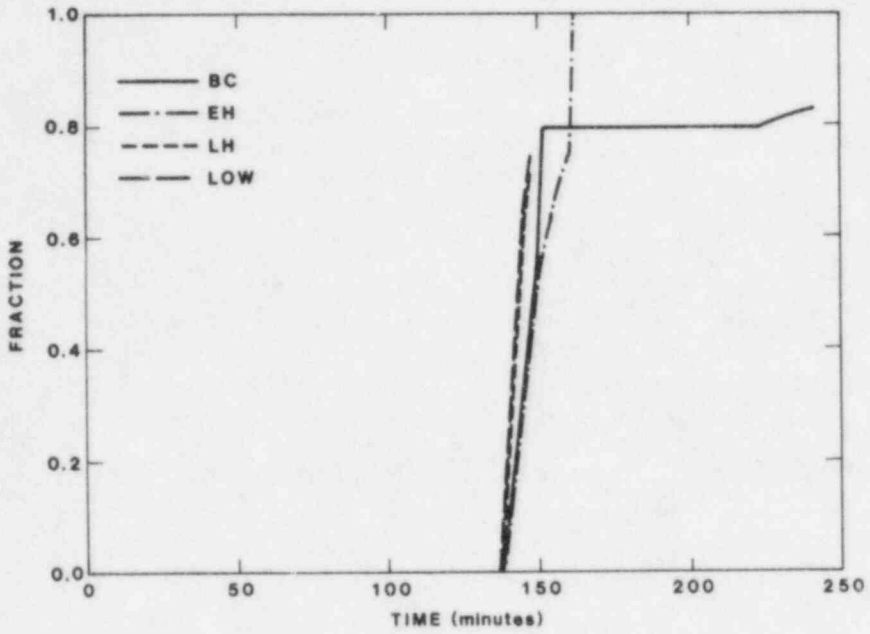

Figure 6-3 Fraction of core melted.

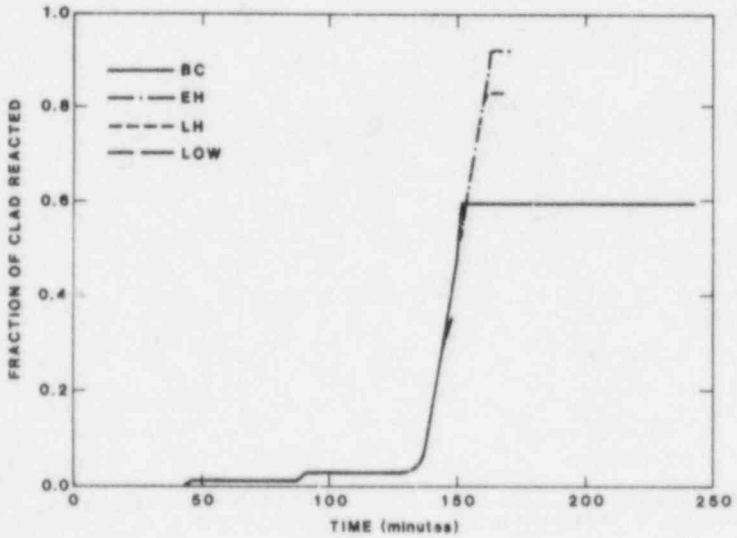

Figure 6-4 Fraction of clad reacted.

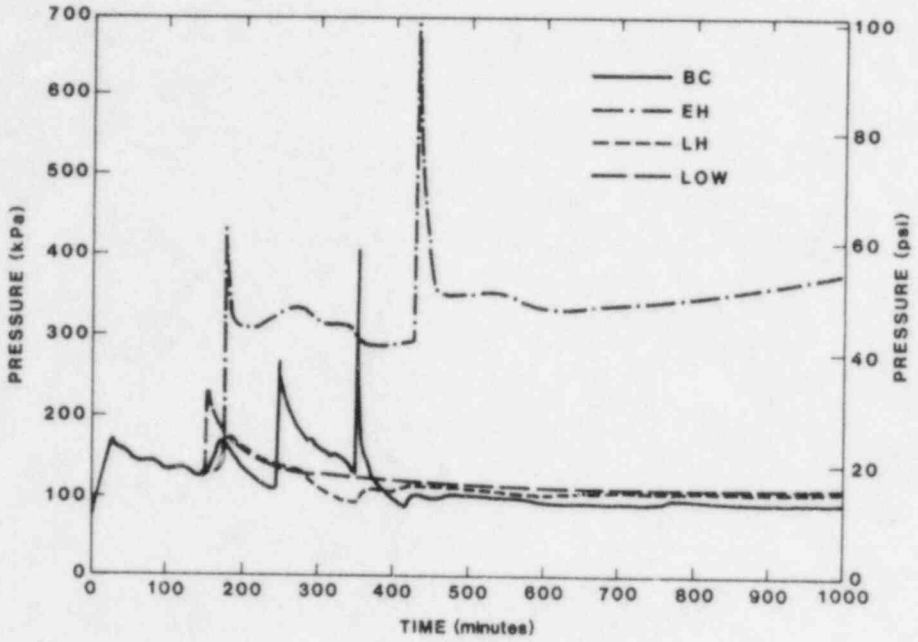

Figure 6-5 Total containment pressure (absolute).

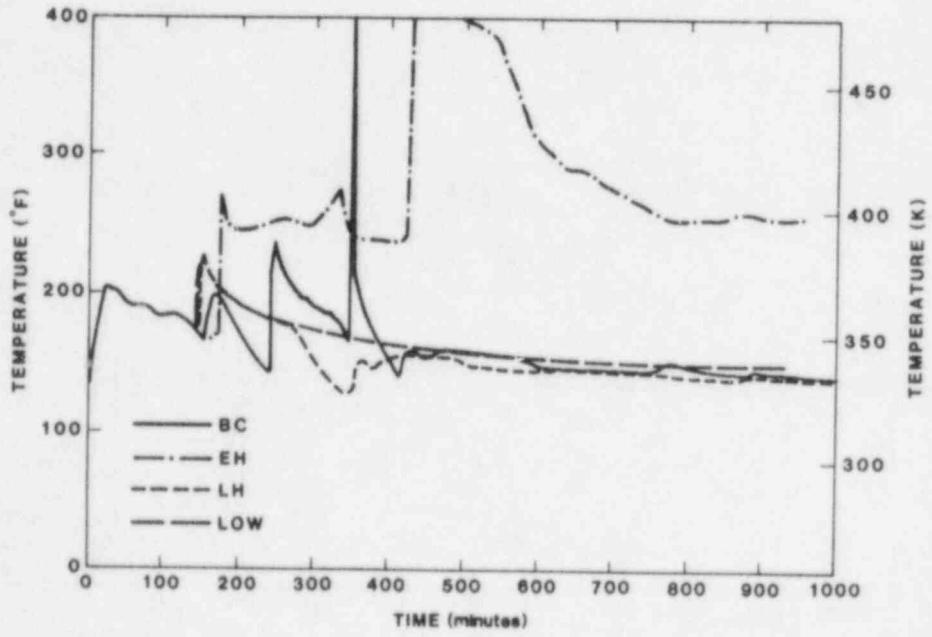

Figure 6-6 Compartment temperature.

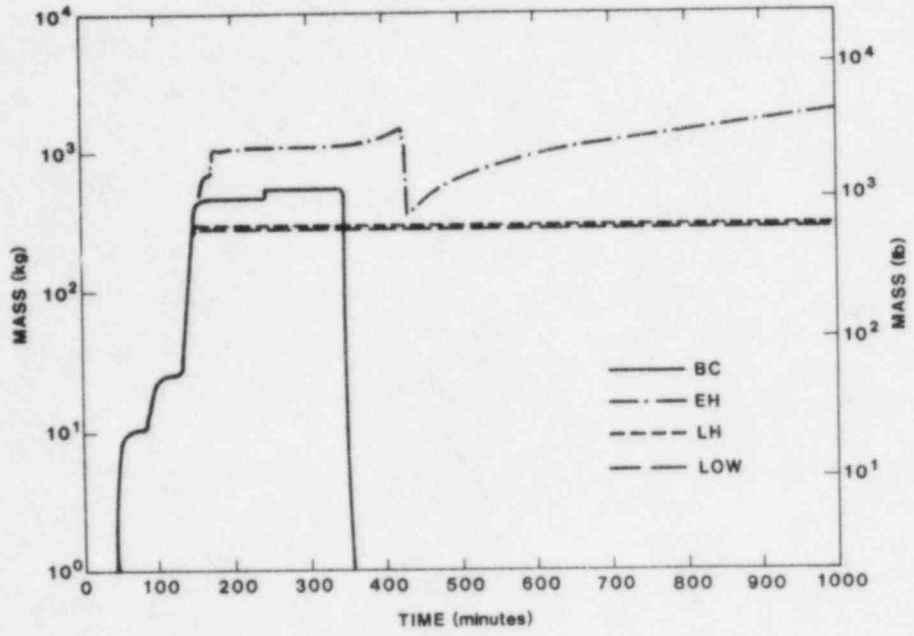

Figure 6-7 Containment hydrogen.

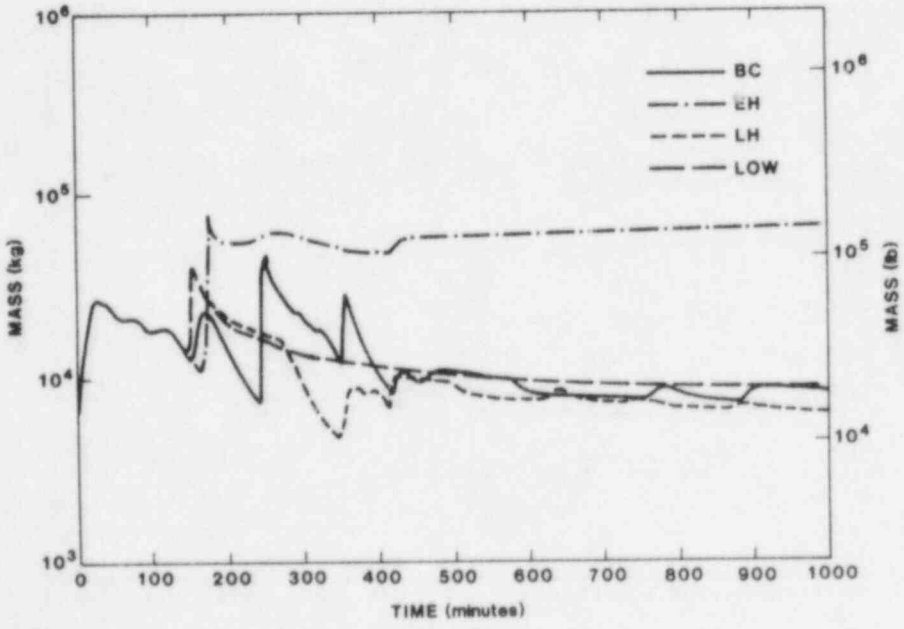

Figure 6-8 Containment steam and suspended liquid.

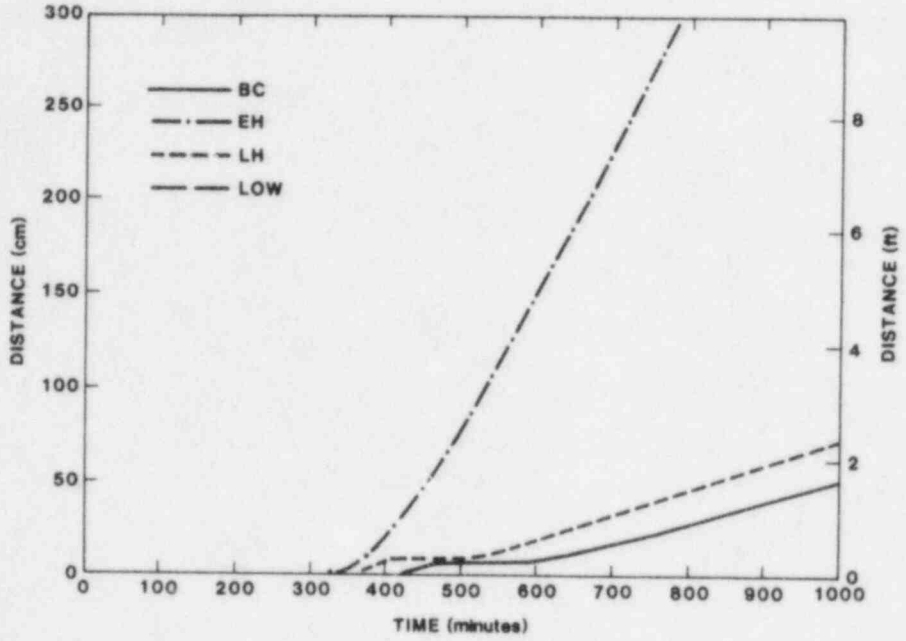

Figure 6-9 Vertical concrete penetration.

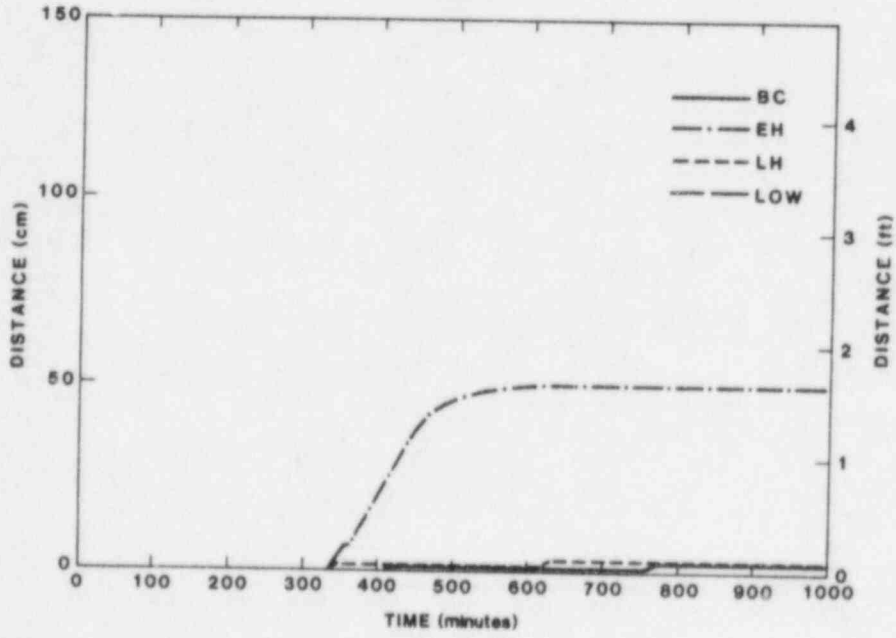

Figure 6-10 Radial concrete penetration.

from containment because there would be less time for postfailure settling.

Figures 6-7 and 6-8 show the containment hydrogen and suspended water. A span of a factor of ~30 exists in the hydrogen mass at early time, but there is not much variation in the final maximum values. Burns are predicted.

Figures 6-9 and 6-10 show the vertical and radial concrete penetration. The vertical penetration is sensitive to the initial mass of steel in the melt. A steel mass only slightly less than that used in the base case will result in a much-reduced penetration rate at late time.

6.2 In-Vessel Aerosol Production

The core temperatures determined by MARCH are used as input to the CORSOR code and combined with variations in release rate coefficients to determine how much of the fission product inventory might be released from the fuel. The core inventories of materials available for release are given in Table 6-3. Figures 6-11 through 6-14 display the fractional release versus time of cesium, iodine, and tellurium for a "base case" and upper- and lower-bound calculations. The upper-bound calculation corresponds to early-high. The lower bound corresponds to both late-high and low. Figure 6-4 displays a similar plot for the sum of all remaining fission products. Table 6-4 contains corresponding information on the final release fractions from the core materials of all the species treated by CORSOR (and by analogy, those species not treated in CORSOR).

The upper-bound results for volatiles (Figures 6-11 through 6-14) are unsurprising: Cesium, iodine, and tellurium are released in their entirety from the core at times somewhat earlier than those encountered in the base-case run. Releases of lower volatility materials (Figure 6-4) show a greater difference from the base case.

Table 6-3 Inventories of radionuclides and structural materials for Surry

Fission Products		Actinides/Structural	
Element	Mass (kg)	Element	Mass (kg)
Kr	13.4	U	70,210
Rb	14.7	Pu	469
Sr	47.6	Np	24.6
Y	22.9	Cr	8,130
Zr	179	Mn	159
Mo	155	Fe	51,880
Tc	37.1	Ni	4,517
Ru	104	Zr	16,460
Rh	104	Sn	262
Pd	52.5	Ag	2,750
Ag	2.4	In	505
Sb	0.8	Cd	173
Te	25.4		
I	12.4		
Xe	260		
Cs	131		
Ba	61.2		
La	62.3		
Ce	131		
Pr	50.7		
Nd	171		
Sm	34.0		

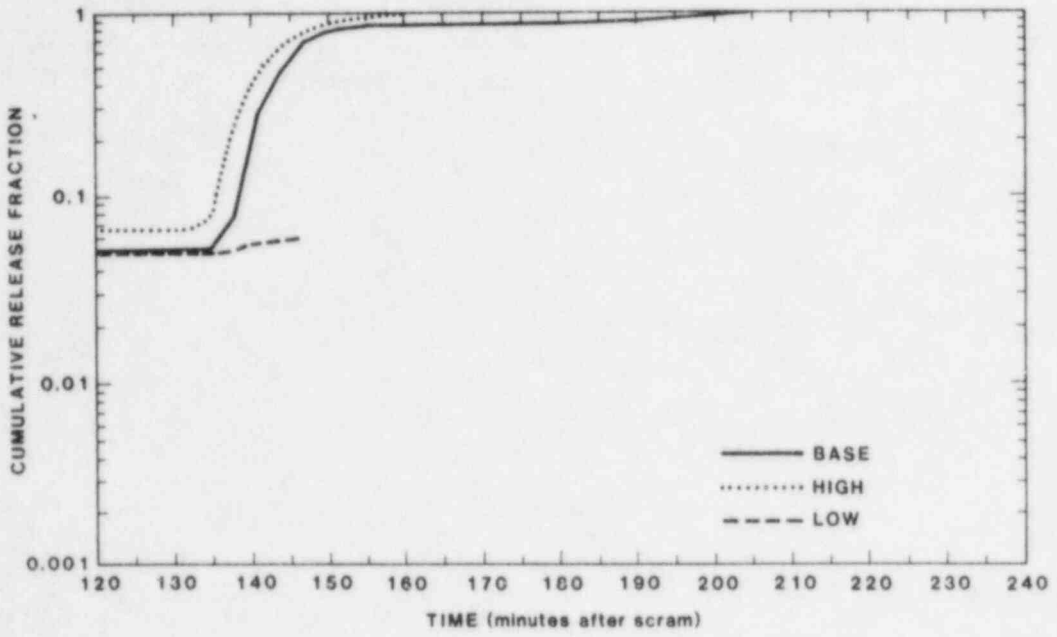

Figure 6-11 Cesium release as a function of time.

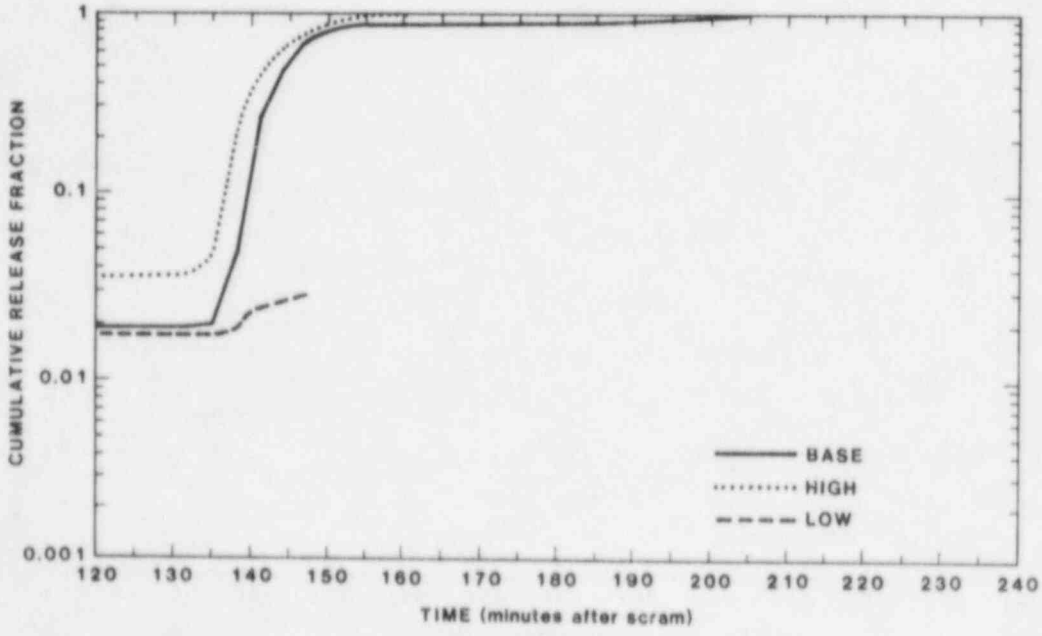

Figure 6-12 Iodine release as a function of time.

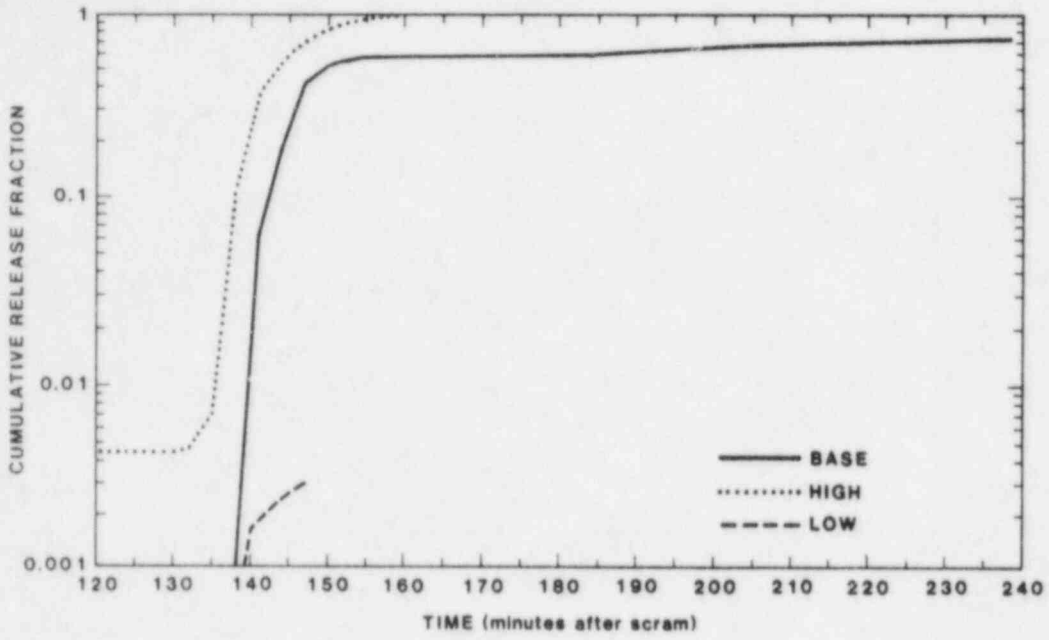

Figure 6-13 Tellurium release as a function of time.

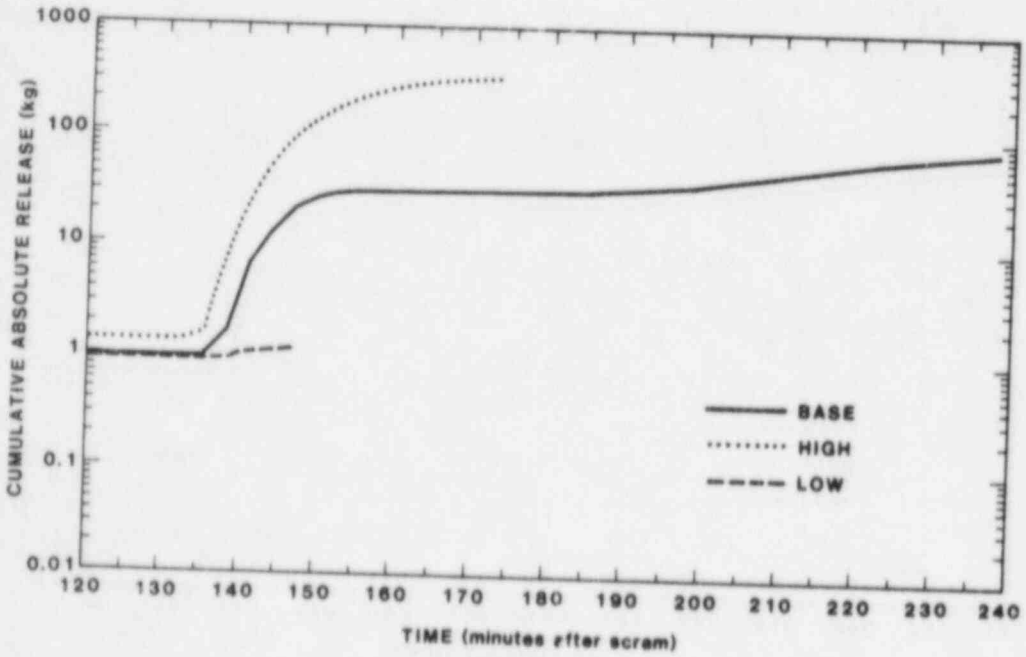

Figure 6-14 Remaining fission-product aerosol release as a function of time.

Table 6-4 Release fraction from core materials

Species Name	Base-Case Release Fract.	High Release (EH)	Low Release (LH and Low)
Fission products:			
SE	0.73958	1.00000	0.00305
BR	1.00000	1.00000	0.02887
KR	1.00000	1.00000	0.04172
RB	1.00000	1.00000	0.06149
SR	0.15240	0.94650	0.00005
Y	0.00068	0.04877	0.00000
ZR	0.00035	0.00373	0.00000
MO	0.18401	0.82743	0.00029
TC	0.01543	0.19392	0.00001
RU	0.01542	0.19392	0.00001
RH	0.01543	0.19391	0.00000
PD	0.01542	0.19392	0.00001
AG	0.99854	1.00000	0.00295
SB	0.82799	1.00000	0.00082
TE	0.73958	1.00000	0.00305
I	1.00000	1.00000	0.02887
XE	1.00000	1.00000	0.04172
CS	1.00000	1.00000	0.06150
BA	0.35328	0.99412	0.00026
LA	0.00068	0.04877	0.00000
CE	0.00068	0.04876	0.00000
PR	0.00068	0.04877	0.00000
ND	0.00068	0.04877	0.00000
SM	0.00068	0.04877	0.00000
Actinides:			
UO2	0.00068	0.04877	0.00000
PU	0.00068	0.04877	0.00000
Structures:			
CR	0.03378	0.28404	0.00002
MN	0.03378	0.28404	0.00002
FE	0.03378	0.28404	0.00002
NI	0.03378	0.28404	0.00002
ZR	0.00035	0.00334	0.00000
Control rods:			
SN	0.81806	0.92284	0.00622
AG	0.48841	0.85629	0.16560
IN	0.14743	0.75569	0.06607
CD	0.79228	0.94252	0.46168

*EH, LH, and Low refer to early-high, late-high, and low cases, respectively.

Lower-bound results indicate the potential for very small releases of all species. Of particular interest is a release of only 3% of iodine and 6% of cesium by the time of vessel failure. If the core debris forms from fracturing of non-molten fuel and if the debris is coolable ex-vessel, the early-low source term could have very little Cs and I in it.

6.3 Net Retention in the RCS

The net retention values for the high and low cases, as given in Table 6-2, were used in conjunction with the masses released from core materials to obtain the net release of aerosols from the RCS at the time of vessel breach. These net release values are summarized in Table 6-5. For the base case, the net release was distributed over time prior to vessel failure as indicated in the time-dependent retention tables given in an early draft of BMI-2104. For the other cases, the net release was emitted as a single puff at vessel failure.

6.4 Ex-Vessel Aerosol Production

The major ex-vessel aerosol source comes from melt-concrete interactions. The melt-concrete source term is driven primarily by the oxide-phase temperature and the gas-generation rate. The oxide- and metal-phase temperatures, H_2O and CO_2 releases, and axial and radial penetration for the base case plus the upper- and lower-bound cases are shown in Figures 6-15 through 6-20. The base case is similar to that used in the BMI-2104 calculations and includes the problem in CORCON with viscosity at the melt-concrete interface (see Volume II). A modified version of CORCON with an attempt at correcting this problem was used in the three δ_p cases. The net effect is cooler debris at late time with more gas flow and more concrete penetration. The axial penetration is still less than that predicted by INTER (see Figure 6-9), but the radial penetration is comparable to INTER predictions.

Table 6-5 Net release of aerosols from RCS at time of vessel breach (fraction of initial core inventory)

Species Name	Base Case	Early High	Late High	Low
Fission Products:				
SE	0.40677	0.90000	0.00274	0.0003
BR	0.55000	0.90000	0.02598	0.0029
KR	0.55000	0.90000	0.03755	0.0042
RB	0.55000	0.90000	0.05534	0.0061
SR	0.08382	0.85185	0.00004	0.0000
Y	0.00037	0.04389	0.00000	0.0000
ZR	0.00019	0.00336	0.00000	0.0000
MO	0.10121	0.74469	0.00026	0.0000
TC	0.00849	0.17453	0.00001	0.0000
RU	0.00848	0.17453	0.00001	0.0000
RH	0.00849	0.17452	0.00000	0.0000
PD	0.00848	0.17453	0.00001	0.0000
AG	0.54920	0.90000	0.00265	0.0003
SB	0.45539	0.90000	0.00074	0.0001
TE	0.40677	0.90000	0.00274	0.0003
I	0.55000	0.90000	0.02598	0.0029
XE	0.55000	0.90000	0.03755	0.0042
CS	0.55000	0.90000	0.05535	0.0062
BA	0.19430	0.89471	0.00023	0.0000
LA	0.00037	0.04389	0.00000	0.0000
CE	0.00037	0.04388	0.00000	0.0000
PR	0.00037	0.04389	0.00000	0.0000
ND	0.00037	0.04389	0.00000	0.0000
SM	0.00037	0.04389	0.00000	0.0000
Actinides:				
UO2	0.00037	0.04389	0.00000	0.0000
PU	0.00037	0.04389	0.00000	0.0000
Structures:				
CR	0.01858	0.25564	0.00002	0.0000
MN	0.01858	0.25564	0.00002	0.0000
FE	0.01858	0.25564	0.00002	0.0000
NI	0.01858	0.25564	0.00002	0.0000
ZR	0.00019	0.00301	0.00000	0.0000
Control rods:				
SN	0.44993			
AG	0.26863			
IN	0.08109			
CD	0.43575			

Figures 6-21 and 6-22 show the total and tellurium aerosol-emission rates, respectively. A comparison with Figures 6-15 through 6-20 shows that the aerosol-emission rate responds more strongly to oxide temperature than to gas-generation rate. The range in aerosol-emission is as much as a factor of 20. In general, the rate decreases by a factor of 10 over ten hours.

The peaks shown in Figures 6-21 and 6-22 in aerosol-emission rate for the base case and late-high case are due to a large zirconium-metal component in the initial melt composition. It is not known whether these peaks would be supported by experiments. The heat from oxidizing zirconium metal is only a small fraction of (a few percent) of the decay heat and should not, by itself, produce a temperature peak.

One important omitted phenomenon in ex-vessel aerosol generation is the effect of isotope decay chains, in particular, the production of iodine-132 from the decay of tellurium-132. Iodine-132 would be sparged from the melt quite readily and would add significantly to the radioactivity released from the melt. This phenomenon was not included in the δ_p calculation, but it is discussed in Volume II.

6.5 Net Retention in Containment: Source-Term Uncertainty from Uncertain Phenomena (δ_p)

For the purposes of this study, the uncertainty in the source term is expressed as the uncertainty in the mass of suspended radionuclides in containment. These suspended masses are calculated using the CONTAIN code.

Figures 6-23 through 6-27 display the suspended mass in containment versus time since reactor shutdown for CsI, CsOH, Te, RFP, and inert solids. Figure 6-28 displays the total suspended aerosol radioactivity. In all these figures, it is assumed that there is no containment failure. This leaves the time of failure as

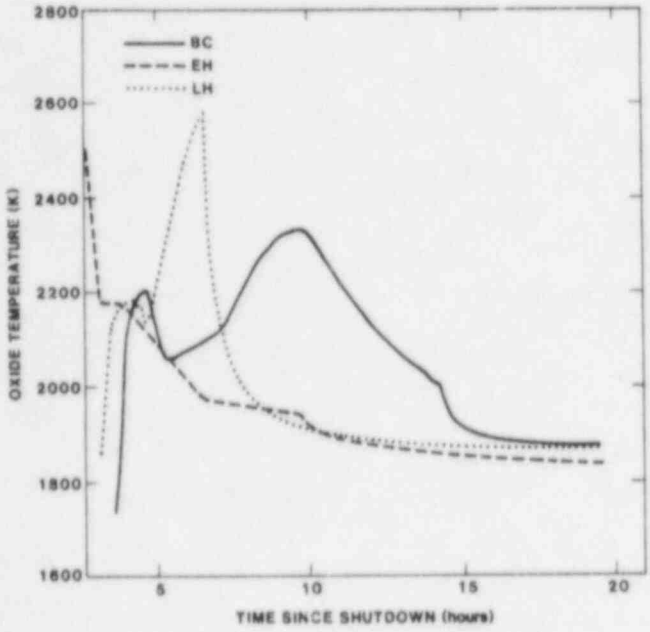

Figure 6-15 Oxide-phase temperatures.

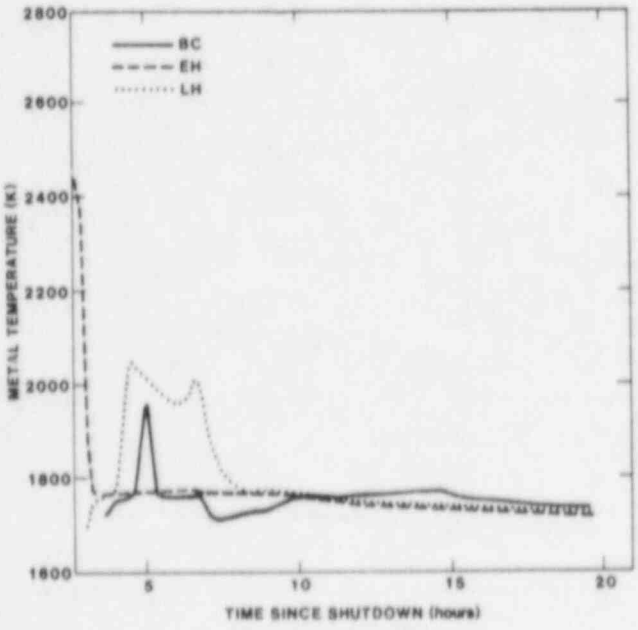

Figure 6-16 Metal-phase temperatures.

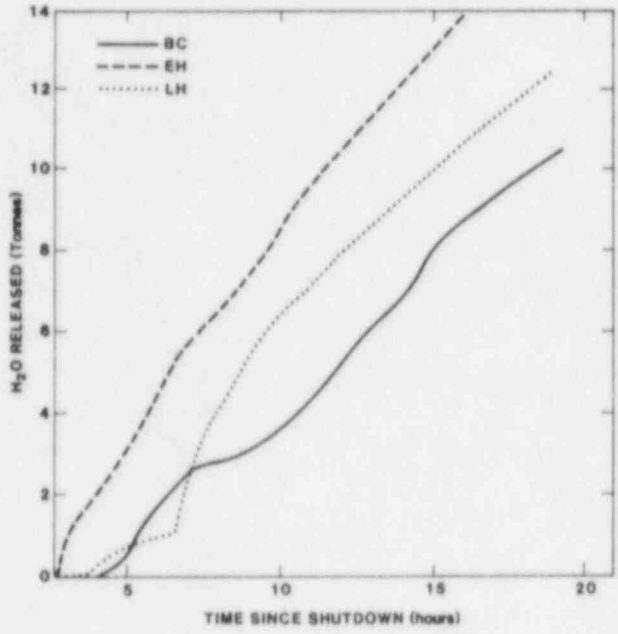

Figure 6-17 Water release.

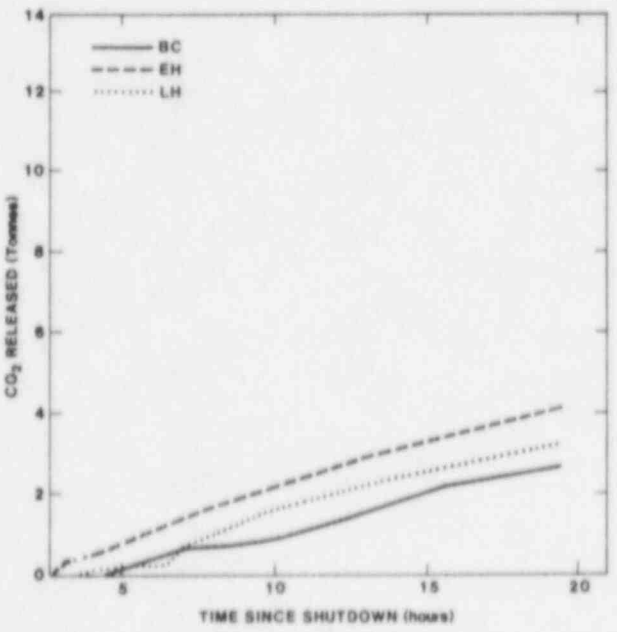

Figure 6-18 Carbon dioxide released.

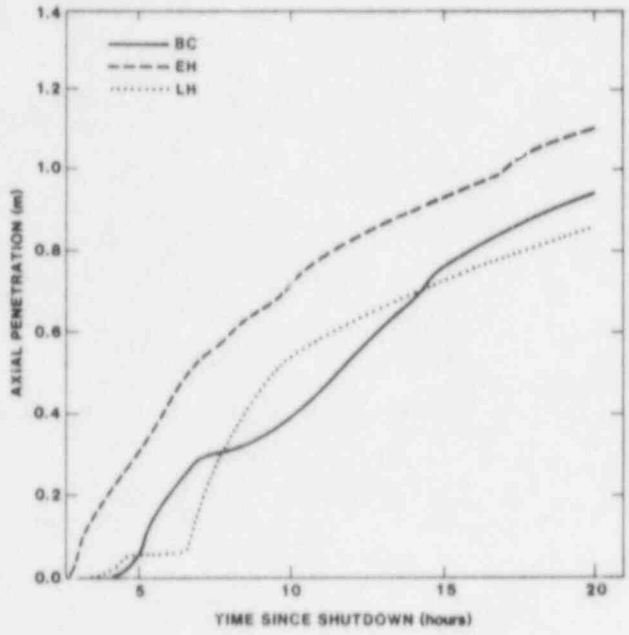

Figure 6-19 Axial penetration.

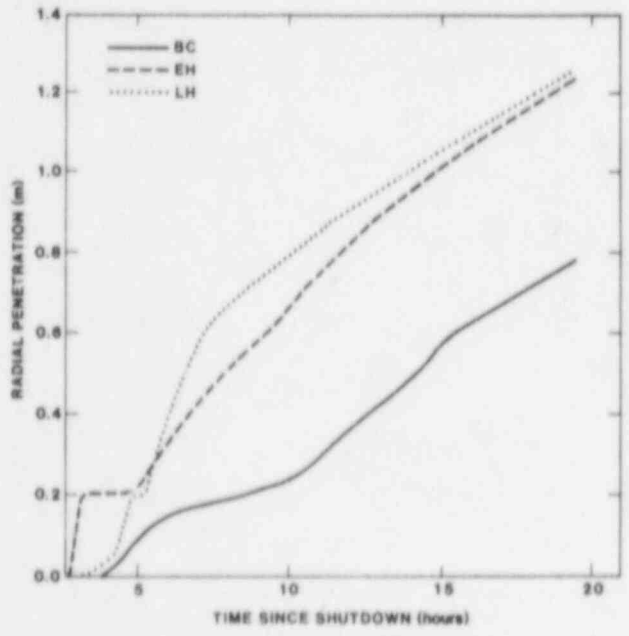

Figure 6-20 Radial penetration.

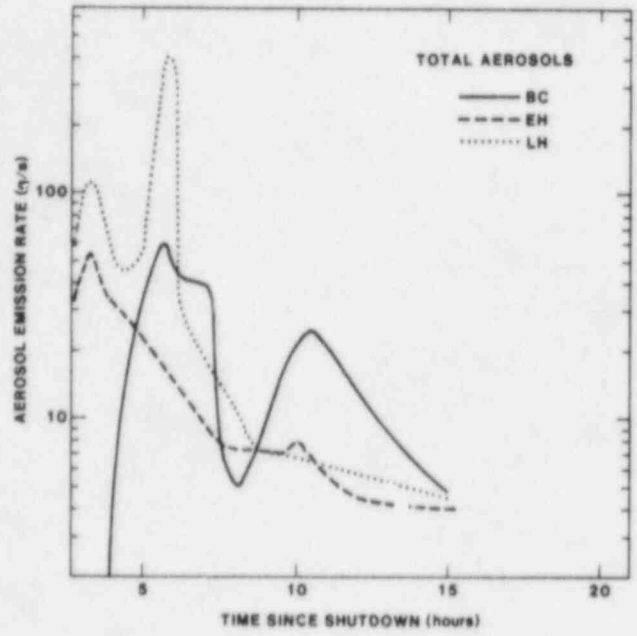

Figure 6-21 Total aerosol emission rates.

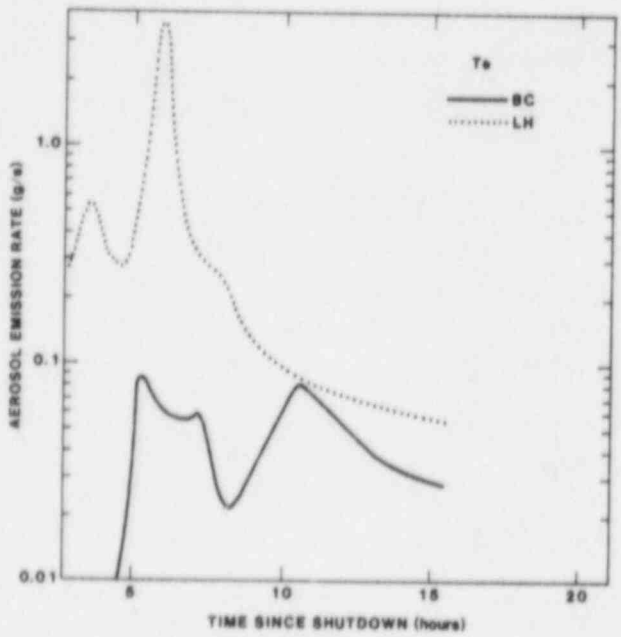

Figure 6-22 Te aerosol emission rates.

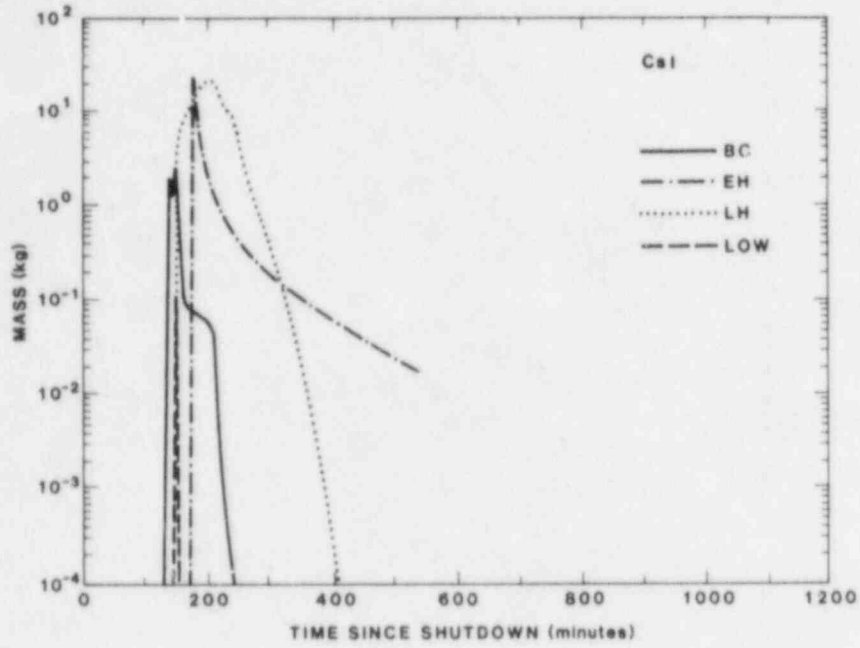

Figure 6-23 Suspended CsI mass versus time since shutdown.

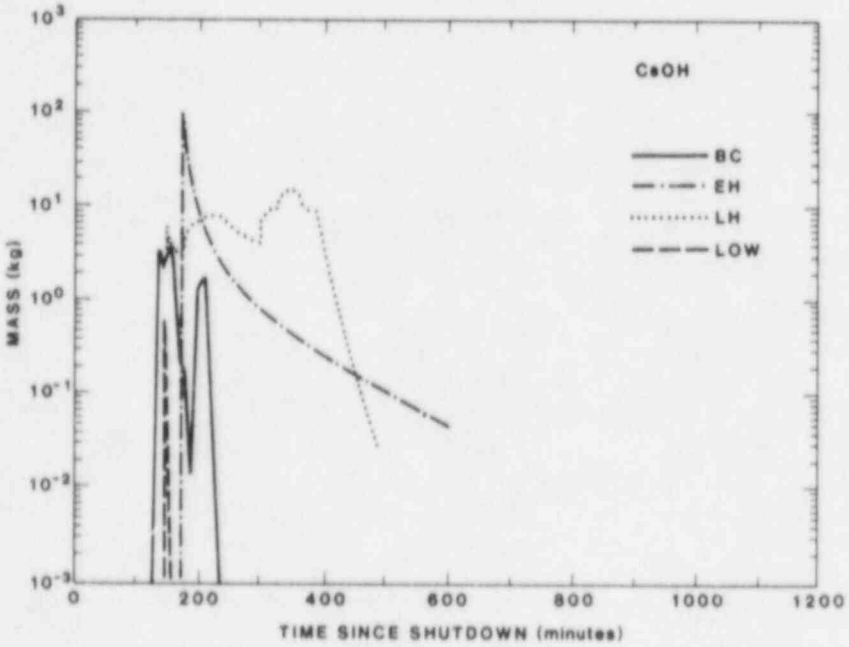

Figure 6-24 Suspended CsOH mass versus time since shutdown.

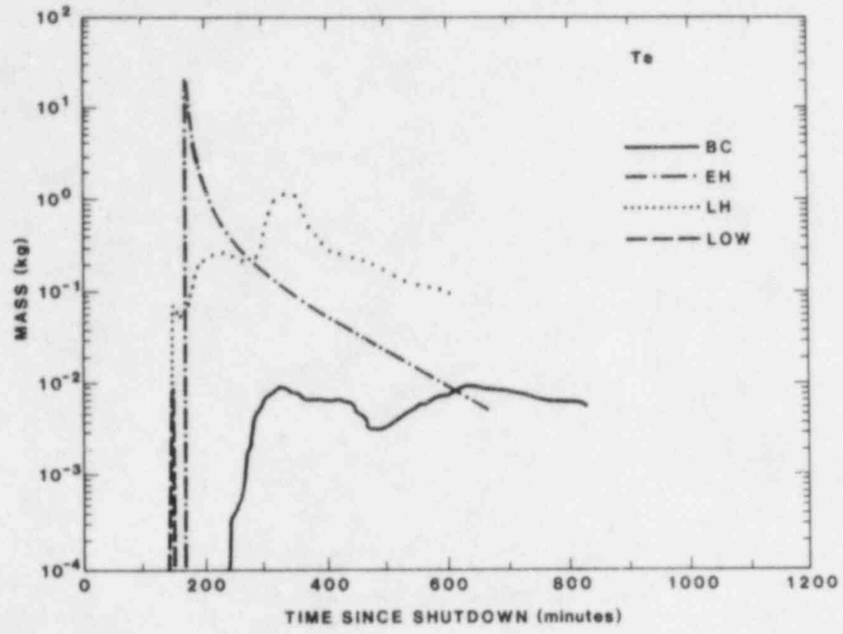

Figure 6-25 Suspended Te mass versus time since shutdown.

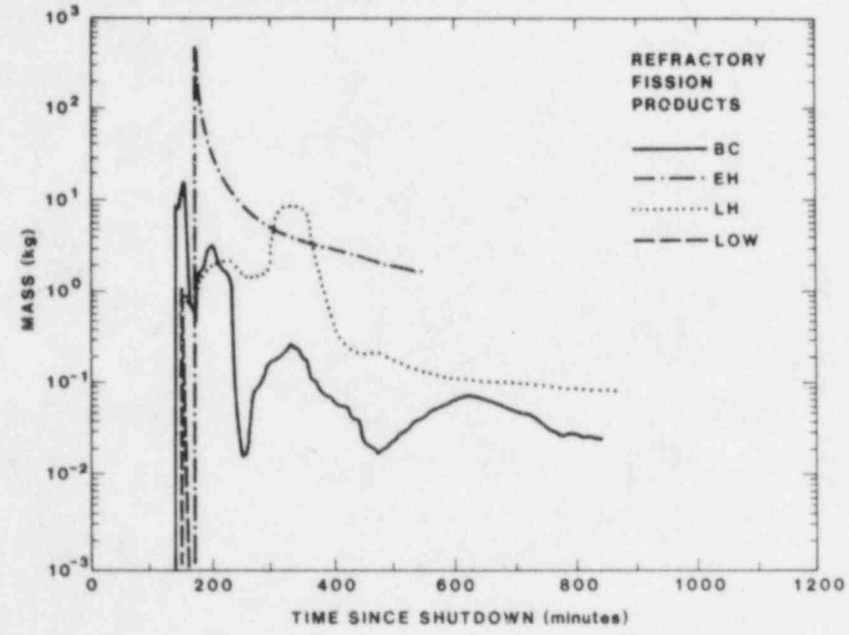

Figure 6-26 Suspended RFP mass versus time since shutdown.

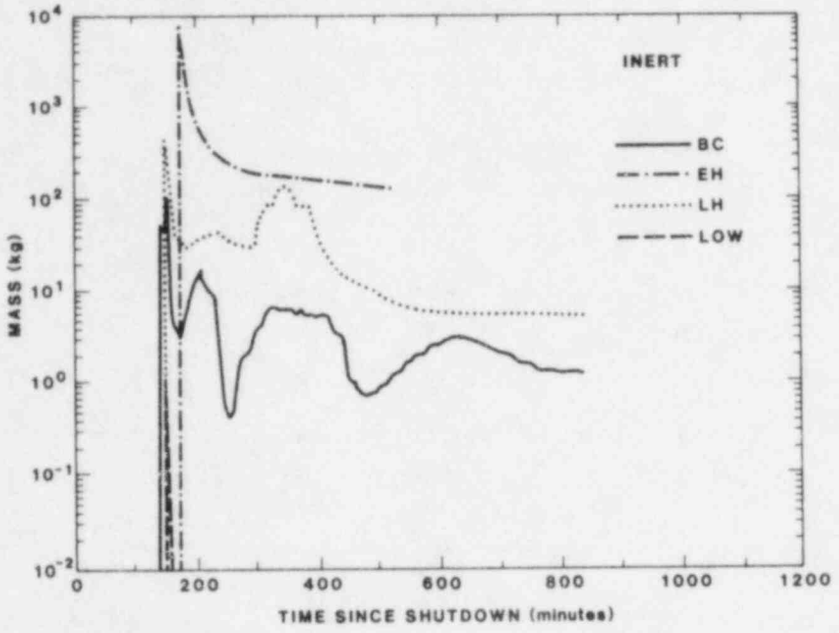

Figure 6-27 Suspended inert aerosol mass versus time since shutdown.

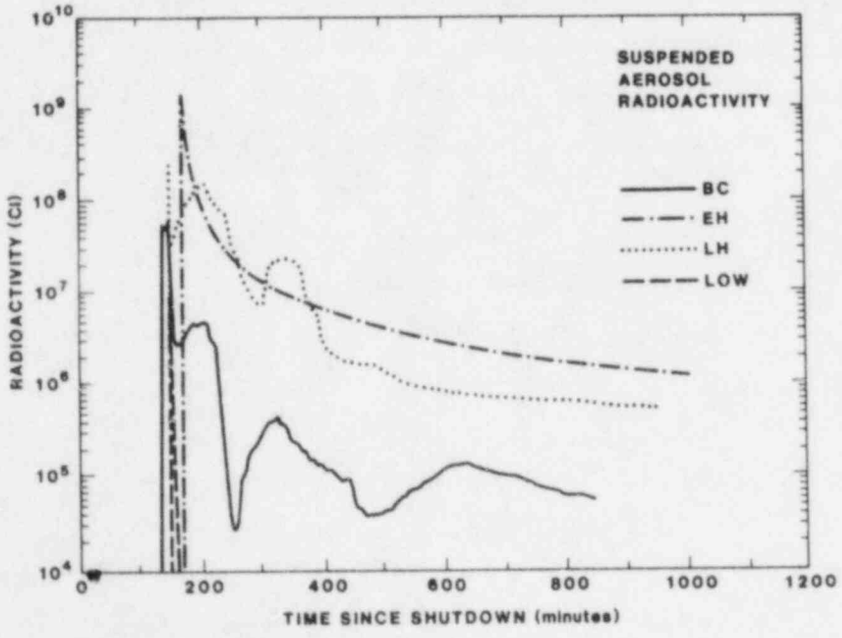

Figure 6-28 Total suspended aerosol radioactivity versus time since shutdown.

a free parameter. The early-high case is the only case in which spray failure is assumed. Since spray failure was judged to be plausible only due to a substantial containment failure, the early-high case was not carried out much beyond the time of vessel failure.

The CsI and CsOH aerosols are all released before and shortly after vessel failure in the cases considered. Thus their behavior in the containment building is like a puff release: the concentration declines very rapidly with time.

The uncertainty in suspended CsI and CsOH mass at the time of vessel failure (about 150 to 300 minutes) spans a factor of about 200 (ratio of high value to low value). This uncertainty is due partly to uncertainty in the amount of cesium and iodine released from fuel in-vessel and partly to the uncertainty in retention in the RCS. In the TMLB' analysis the uncertainty in in-vessel release of Cs and I was not as important because if all the Cs and I were not released in-vessel, they would be released rapidly ex-vessel in the melt-concrete interaction. Indeed this behavior is shown in the S_2D late-high case. However, in the low case, in which coolable ex-vessel debris is assumed (see Section 5.3), Cs and I are not released ex-vessel. Thus the uncertainty in in-vessel release is more important.

At late time (about 900 minutes) the amounts of suspended CsI and CsOH are very low and insignificant for the cases considered. However, two phenomena have the potential to change this general result. The first is revaporization of CsI and CsOH that has deposited on RCS surfaces and heated them with their decay heat. If this reheat and revaporization all occurs before vessel failure, then all the CsI and CsOH will be released as a puff at vessel failure and will settle out rapidly in containment. This is essentially the behavior shown for the early-high case. However, if the revaporization is much slower (e.g., because the elements are spread over a larger surface in the RCS), then a slow continuous

release could occur which would continuously replenish the CsI and CsOH settling in containment. A quasi-steady value of suspended mass would be reached. The value would depend on the rate at which CsI and COH were being revaporized, which could be determined only by a detailed structures heatup calculation. However, if the revaporization is spread over 10 to 20 hours, a steady value of about 0.5 kg of CsI would be expected. (This estimate is based on comparison with the tellurium plot, which will be discussed shortly.)

The second phenomenon that could lead to high suspended iodine values at late times is the decay of ^{132}Te into ^{132}I. If this decay takes place in a molten pool, the ^{132}I will be rapidly released. The total suspended mass of ^{132}I would be very small (less than 1 gram), but the radioactivity would be comparable to that from all other late-time sources. This phenomenon is discussed more completely in the TMLB' report (Volume II).

The suspended Te and refractory fission products (RFP) masses are shown in Figures 6-25 and 6-26. At the time of vessel failure the uncertainty ranges from essentially total Te release from the vessel down to a value 3000 times lower. The high end corresponds to nearly 100% release of Te from fuel and then resuspension of aerosols deposited within the RCS. The resuspension occurs during the very vigorous blowdown at the time of vessel failure. The early-time uncertainty for both the Te and the RFP is due to uncertainty in the in-vessel release from the fuel and the net retention in the RCS.

The amount of suspended Te and RFP at late times is small because of the presence of sprays, but not totally negligible in all cases. The late-high case is about a factor of ten higher than the base case primarily because of an assumed average spray drop size of 2000 μm (instead of 400 μm, as used in the BMI-2104 calculations). With coolable ex-vessel debris (the low case) no Te or RFP are generated to replace settling aerosols. Thus the late-time Te and

RFP source term in that case is many orders of magnitude lower than the late-high or base case and is totally negligible.

In the late-high case, about 10 kg of Te is released from the ex-vessel molten pool over 10 hours. Thus the suspended mass of Te at that time (about 0.2 kg) gives an indication of how much CsI would be suspended if its 25 kg mass revaporized from the RCS over about 10 hours. The inert aerosols show a behavior similar to that of the refractory fission products.

Since CsI and CsOH dominate the source term at early time and Te and RFP dominate at late times, it would be convenient to have a single combined measure of the source term. One such measure is the total radioactivity on suspended aerosols and is shown in Figure 6-28.

The uncertainty at vessel failure ranges from about 1 GCi down to a factor of 1000 lower. The high case is composed about equally of volatile and refractory fission products. The low case is dominated by CsI. At late times, the high case is about 1 MCi and is a factor of ten higher than the base case value reported in BMI-2104. The low case is many orders of magnitude lower than the base case; this is due to the ex-vessel debris being coolable and eliminating the source of aerosols from the melt-concrete interaction.

An exception to the rule that coolable debris implies negligible late-time source terms occurs if there is significant revaporization of CsI and CsOH from RCS surfaces. If this revaporization occurs over about 10 hours, a quasi-steady level of about 5 MCi suspended in containment would result. This value is higher than the late-high case shown in Figure 6-28.

6.6 Cumulative Release from Containment

The above discussions considered only the suspended masses in containment, assuming no failure. If containment fails at a particular time, the amount that escapes depends on the fraction of steam and air that escapes during depressurization, the amount of aerosol settling that occurs during depressurization, the amount driven out by melt-concrete gas generation after depressurization, and aerosol resuspension. The uncertainty in containment hole size was found to be quite large, so the hole sizes that were assumed correspond primarily to a parametric variation. The effect of hole size on release of suspended aerosols from containment has been addressed in the TMLB' analysis and will not be repeated here. It was found that with overpressure failure, large holes are possible that can release essentially all suspended aerosols at the time of failure. Conversely, small holes are also possible that release only a percent or so of suspended aerosols.

6.7 Summary

The suspended mass of various radionuclides that might result during an S_2D accident is not accurately known because of uncertainties in the phenomena that produce suspended radionuclides in containment. The range of uncertainty in suspended aerosol radioactivity at the time of vessel failure is a factor of about 1000. The uncertainty at late times is many orders of magnitude, but the source term at that time is over 100 times smaller than at early times. Cesium iodine dominates the suspended radionuclides immediately following vessel failure. Tellurium and refractory fission products dominate at late time. Hence a considerable number of fission products must be considered when the source term is assessed.

The source-term uncertainty near the time of vessel failure is dominated by in-vessel processes. Particularly important uncertainties are

- Core-temperature histories

- Release rates from fuel for given temperature and gas-flow conditions

- Natural circulation paths within the RCS

- Net retention of fission products within the RCS (including effects of revaporization and resuspension

The source-term uncertainty at late time (about 15 hours into the accident) is dominated by ex-vessel processes. Particularly important uncertainties are

- Whether or not the ex-vessel debris is coolable

- Effective spray droplet diameter

7. SUMMARY AND CONCLUSIONS

An estimation of the uncertainty in the calculated radiological source term for an assumed S_2D accident in the Surry plant has been made. The major conclusions of the study are:

- The method of calculating a specific source term for a particular LWR accident, as demonstrated in the BMI-2104 reports, allows the determination of the effect on the source term of various phenomena uncertainties

- For the S_2D accident a very important uncertainty is whether or not the core materials in the reactor cavity are coolable by the continuous flow of water from the sprays. This uncertainty leads to a late-time source term uncertainty that ranges from about a megaCurie of suspended radioactivity, down to many orders of magnitude lower. The uncertainty in debris coolability also induces a larger uncertainty in the early source term than was found in the TMLB' analyses (reported in Volume II). The uncertainty in debris coolability is primarily due to uncertainty in debris configuration after contacting water in the reactor cavity.

- At late times another important uncertainty is the effectiveness of the containment sprays. This single uncertainty leads to a factor of ten uncertainty in late-time source term, all of it upward with respect to the BMI-2104 evaluation.

- In all cases considered, the total suspended aerosol radioactivity declined by a factor of one hundred in one

hundred minutes or less. This is due to the cleansing action of the sprays.

It should be noted that these conclusions are the result of a scoping look at the uncertainties for a particular plant and accident. More refinement on the uncertainty bands could be achieved with additional effort. Scoping estimates for other plants and sequences will have to be made before it can be determined how generally applicable these conclusions are.

APPENDIX A

The Surry Plant and the S_2D Sequence

QUEST considers three combinations of plant and accident sequence:

- The Surry plant (a large, dry pressurized-water reactor [PWR]) with the TMLB' and S_2D accident sequences (believed to dominate risk in this plant)

- the Grand Gulf plant (a boiling-water reactor [BWR] with a Mark III containment) with the TC accident sequence (believed to be risk-dominant for this plant).

NOTE: Volume III of this report deals only with the second of these three plant-sequence combinations, i.e., the Surry plant with the S_2D accident sequence. The other plant-sequence combinations are dealt with in other volumes of this report.

The Surry unit is a pressurized-water reactor, embodying a pressure vessel 157 inches (4 m) in diameter with 157 fuel assemblies, designed by Westinghouse. Detailed plant data are provided in Table A-1. The reactor is designed to operate at a nominal power of 2441 MW (thermal) and a reactor-coolant-system absolute pressure of 15.5 MPa (2250 psi). The containment is a steel-lined, reinforced concrete structure with a free volume of 1.8 x 10^6 ft^3 (51 x $10^3 m^3$); it is operated subatmospherically with initial absolute pressure and temperature of 10 psi (69 kPa) and 100°F (38°C), respectively. Figure A-1 illustrates the layout of the containment.

Table A-1 Surry plant data [adapted from BMI-2104, Vol V]

Nominal power	2 441 MW (thermal)	(8 329 × 10^6 Btu/hour)
Internal energy of water	246.9 × 10^6 Btu	(2.605 × 10^{11} J)
Sensible heat in the core	16.35 × 10^6 Btu	(1.725 × 10^{10} J)
Total water in the system	423 200 lb	(192 000 kg)
Aug. temperature (Excl. pres.)	572°F	(300°C)
Pressure (gage)	2 280 psi	(15.7 MPa)
Reactor coolant system volume	8 387 ft^3	(237.5 m^3)
Pressurizer volume, total	1 336 ft^3	(37.8 m^3)
water	816 ft^3	(23.1 m^3)
steam	520 ft^3	(14.7 m^3)
Three accumulators, total volume	4 350 ft^3	(123.2 m^3)
water volume	2 775 ft^3	(78.58 m^3)
pressure (gage)	665 psi	(4.59 MPa)
temperature	120°F	(49°C)
Containment recirculation spray 2 systems, flow each	3 500 gpm	(0.22 m^3/s)
Containment free volume	1.8 × 10^6 ft^3	(5.1 × 10^4 m^3)
Initial temperature	100°F	(38°C)
Initial pressure (absolute)	10 psi	(69 kPa)
Dewpoint	80°F	(27°C)
Primary system hot metal	1 686 285 lb	(764 886 kg)
Temperature	572°F	(300°C)

Containment Heat Sinks

	Thickness	Area
Walls inside containment	1.0 ft (0.30 m)	3 320 ft^2 (308 m^2)
Walls inside containment	2.0 ft (0.61 m)	27 600 ft^2 (2 560 m^2)
Walls inside containment	3.0 ft (0.91 m)	19 400 ft^2 (1 800 m^2)
Walls inside containment	4.0 ft (1.2 m)	5 000 ft^2 (465 m^2)
Walls inside containment	6.5 ft (2 m)	2 100 ft^2 (195 m^2)
Containment wall	4.5 ft (1.4 m)	46 747 ft^2 (4 340 m^2)
Dome	2.5 ft (0.76 m)	25 000 ft^2 (2 320 m^2)
Floor above foundation mat	2.0 ft (0.61 m)	11 250 ft^2 (1 050 m^2)
Foundation mat	10.0 ft (3 m)	11 250 ft^2 (1 050 m^2)
Containment liner		
Walls	0.38 in. (9.7 mm)	46 747 ft^2 (4 343 m^2)
Dome	0.50 in. (13 mm)	25 000 ft^2 (2 323 m^2)
Floor	0.25 in. (6.4 mm)	11 250 ft^2 (1 045 m^2)
Miscellaneous metal - 1 200 000 lb (540 000 kg)		

Core	
Equivalent diameter	119.7 in. (3.04 m)
Active height	144.0 in. (3.66 m)
L/D	1.202
Total cross sectional area	78.3 ft^2 (7.27 m^2)
No. of fuel assemblies	157
Rods per assembly	204
Pitch	0.563 in. (14.3 mm)
Assembly dimensions	8.426 in. square (214 mm square)

Table A-1 Surry plant data [adapted from BMI-2104, Vol V] (Continued)

Core (Continued)			
Fuel rod diameter			0.422 in. (10.7 mm)
Clad (Zr-4) thickness			0.0243 in. (617 μm)
Total number of fuel rods			32 028
Core weight			226 200 lb (102 600 kg)
UO_2			175 600 lb (79 650 kg)
Zircaloy			36 300 lb (16 500 kg)
Misc.			14 300 lb (6 490 kg)
Fuel pellet diameter,	Region	1	0.3669 in. (9.319 mm)
		2 and 3	0.3659 in. (9.294 mm)
Fuel pellet length			0.6 in. (20 mm)
Diametral gap,	Region	1	0.0065 in. (165 μm)
		2 and 3	0.3659 in. (9.294 mm)
Fuel density, %	Region	1	94
		2	92
		3	91
Fuel enrichment, w/o	Region	1	1.85
		2	2.55
		3	3.10
No. of grid spacers			7
Neutron absorber			Ag-In-Cd
Clad			304 SS
Clad thickness			0.024 in. (610 μm)
No. of control assemblies			53
Full length			48
Part length			5
Rods per assembly			20
Burnable poison rods			816
No. per assembly			12
No. of assemblies			68
Material			Borosilicate glass
O.D.			0.4395 in. (11.16 mm)
I.D.			0.2365 in. (6.007 mm)
Clad			304 SS
Boron (natural) loading			0.0429 g/cm
Reactor vessel			
I.D. of shell			157 in. (4 m)
Belt line thickness (w/o clad)			7.875 in. (200 mm)
Head thickness			5.0 in. (127 mm)
Clad thickness			0.125 in. (3 mm)
Overall height			40 ft-5 in. (12.3 m)
Inlet nozzles			27.5 in. (0.7 m) tapered to 35.4 in. (0.9 m)
Outlet nozzles			29 in. (0.74 m)
Water volume with core and internals in place			3 718 ft^3 (105.3 m^3)
Core barrel I.D.			133.9 in. (3.40 m)
O.D			137.9 in. (3.50 m)

Table A-1 Surry plant data [adapted from BMI-2104, Vol V] (Concluded)

Thermal shield I.D.	142.6 in. (3.62 m)
O.D.	148.0 in. (3.76 m)
Safety Injection Charging Pumps	
Number	3
Design pressure, discharge (gage)	2 750 psi (19 MPa)
Design pressure, suction (gage)	250 psi (1.7 MPa)
Design temperature	250°F (121°C)
Design flow	150 gpm (9.46 L/s)
Maximum flow	600 gpm (37.9 L/s)
Design head	5 800 ft (1800 m)
Low Head Safety Injection Pumps	
Number	2
Design pressure, discharge (gage)	300 psi (2.1 MPa)
Design temperature	300°F (149°C)
Design flow	3 000 gpm (189 L/s)
Design head	225 ft (69 m)
Maximum flow	4 000 gpm (252 L/s)
Containment Spray Pumps	
Number	2
Design flow	3 200 gpm (202 L/s)
Design head	225 ft (69 m)
Design pressure (gage)	250 psi (1 724 MPa)
Recirculation Spray Pumps Inside Containment	
Number	2
Design flow	3 500 gpm (221 L/s)
Design head	230 gpm (14.5 L/s)
Recirculation Spray Pumps Outside Containment	
Number	2
Design flow	3 500 gpm (221 L/s)
Design head	249 ft (75.9 m)
Recirculation Spray Coolers	
Number	4
Design duty, each	55 5500 000 Btu/hr (16.3 MW)
Refueling Water Storage Tank	
Volume	350 000 gal (1325 m^3)
Boron concentration	2 500 ppm
Design pressure	Hydraulic head
Design temperature	150°F (66°C)
Water temperature	45°F (7°C)

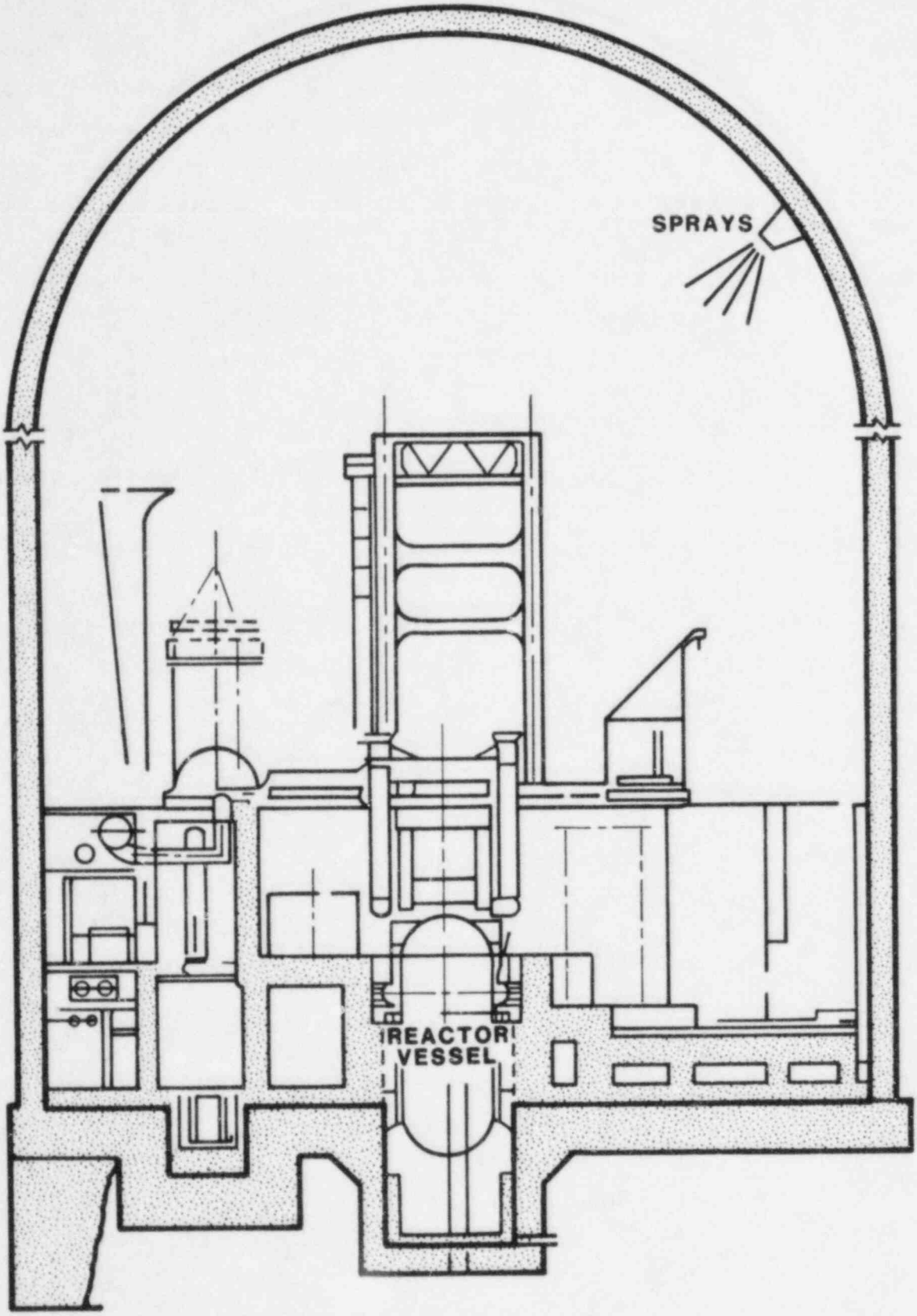

Figure A-1 Large, dry, high-pressure containment (typical of Surry). [BMI-2104, Vol V]

Because of the availability of containment cooling and the containment spray systems in sequence S_2D (a small loss-of-coolant accident, with an equivalent pipe diameter of less than 2 inches, and failure of the emergency core cooling injection system), the release of fission products to the environment could be quite small. As a result, the contribution to the predicted public health risk could also be small. This type of event is believed to be comparatively likely, however, relative to other core-melt sequences and is of interest for this reason. In this sequence, the effectiveness of the containment safety features is examined. The threat posed by hydrogen combustion in this case is of particular interest because the atmosphere cannot be made inert by the presence of steam as in other sequences. Core meltdown occurs with elevated reactor-coolant-system pressure as in the TMLB' case, but at somewhat lower pressures because of continuous leakage from the reactor coolant system. The rate of coolant loss and the timing of core uncovering and melting will be dependent on the size and location of the break in the primary system.

One possible flow path of fission products in the primary system is illustrated in Figure A-2. Other possible flow paths to the break through the intact loops are considered to be sealed by water in the low points of the primary system. If the flow path through the intact loops is also available, the residence time and retention of fission products in the primary system would be greater than for the case analyzed.

Two specific containment-failure modes are considered for the S_2D sequence, early failure due to a hydrogen burn and melt-through of the concrete basemat. For a hydrogen burn to present a significant threat to containment integrity, a large coherent burn is required. This would imply accumulation and distribution throughout the containment volume of a large quantity of hydrogen, followed by ignition. If the burning were spread out in time, or if a number of small burns were to take place, there would be no threat to the containment. Melt-through of the containment basemat would

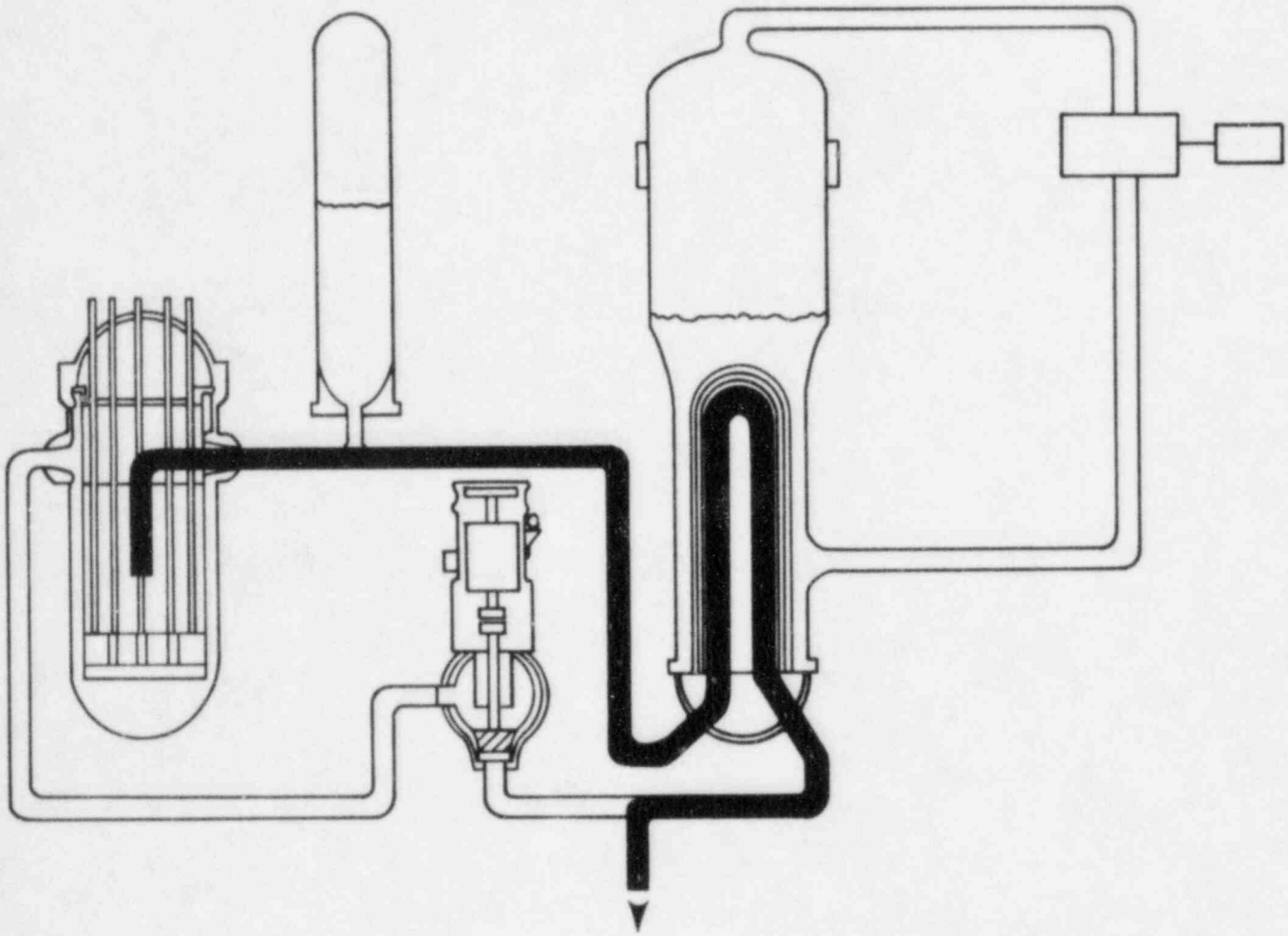

Figure A-2 Flow path for fission-product transport in sequence S_2D. [BMI-2104, Vol V]

be the most likely failure mode for this sequence. If a continuous supply of the containment spray water is available to the reactor cavity, a coolable debris configuration may be achieved, and the accident sequence may be terminated without a breach of containment.

Appendix B

Additional MARCH Sensitivity Studies for S_2D

J. M. Griesmeyer

B.1 Introduction

This appendix describes a short study of MARCH parameters that influence the results of S_2D simulations but which were not investigated in the sensitivity study for the TMLB' accident sequence.[1] The important parameters identified in that previous study are expected to be important for the S_2D sequence as well. Four additional MARCH input parameters were varied about their base case values for the S_2D sequence. The first three relate to the definition of the accident sequence.

- Break size - inches, diameter.
- Break elevation - feet from the bottom of the core.
- Spray recirculation flow - gallons per minute.

The last input parameter investigated in this study represents a model uncertainty:

- Effective spray droplet size - microns in diameter.

The sequence definition parameters were studied for two reasons. First, there are many variations that might influence the results of a particular accident sequence but which are not specified by its generic name. Second, MARCH uses rather simple models for some aspects of the calculations and relation between the MARCH treatment and the behavior that might actually occur is not known.

B.2 Results of the S_2D Sensitivity Study.

Each of the four parameters were varied about their base case values for the S_2D sequence. That base case is the Surry S_2D as described in Volume V of BMI-2104. A short summary of the results is given in Table B-1. The individual results are discussed below.

Table B-1 Short summary of the MARCH S_2D sensitivity study.

	Event Times (min)				Fraction Clad Reacted		
Case	Start Melt	Core Slump	Core Collapse	Head Failure	Core Slump	Core Collapse	Transfer to INTER
Base case	136.4	149.4	151.4	241.9	0.486	0.601	0.617
Break Size							
1.5"	78.9	92.5	93.9	108.9	0.456	0.563	0.563
2.5"	79.9	91.4	93.5	179.6	0.483	0.590	0.610
Break Elevation							
25 ft	124.1	137.1	139.0	227.7	0.481	0.612	0.627
16 ft	127.5	140.3	142.2	231.5	0.489	0.607	0.623
Recirculation Flow							
3500 gpm	136.4	149.4	151.4	241.9	0.486	0.601	0.617
Droplet Size							
200 microns	136.4	149.4	151.4	241.9	0.486	0.601	0.617
1000 microns	136.4	149.4	151.4	242.2	0.490	0.606	0.621

B.2.1 The Effect of Break Size.

The size of the break was varied from 1.5 to 2.5 inches in diameter and the base case was 2.0 inches. The results of the break size variations are shown in Figures B-1 through B-4. In the base case calculation, the core was uncovered at 35 minutes and started to heat up. The primary system fell below the accumulator pressure by 45 minutes into the accident and the discharge of the accumulator quenches the core. The resulting pressure rise shuts off the accumulator discharge until the water is boiled off and the core starts to reheat. When the pressure again falls below the 600 psi accumulator set point, the rest of the accumulator water is discharged and the core is requenched. After the last of the accumulator water is boiled off, the core heats up and finally melts at 136 minutes. The core collapses at 151 minutes and the vessel fails at 241 minutes. The combustible gases in the containment burn about 100 minutes later.

For the 1.5-inch case, the primary system pressure does not fall below the accumulator pressure until after the core melts and collapses into the bottom head of the vessel (93.9 minutes). The accumulator discharge quenches the debris increasing the pressure in the primary system so that the head fails at 109 minutes. Here also, a burn occurs about 100 minutes after vessel failure.

In the 2.5-inch case, the discharge of the accumulator water starts at 30 minutes. The pressure rise from the quench of the debris is not enough to shut off the accumulator discharge. The core heats up again and collapses into the bottom head at 93.5 minutes. As with the base case, the low primary system pressure delays vessel failure, which occurs 75 minutes after core collapse at 179 minutes.

The size of the break is not a model uncertainty and therefore not strictly part of the δ_p concerns in the QUEST study. The results presented here indicate that the break size used in the MARCH calculations can have a major influence on the temperature in the primary system and the progression of the in-vessel portion of the

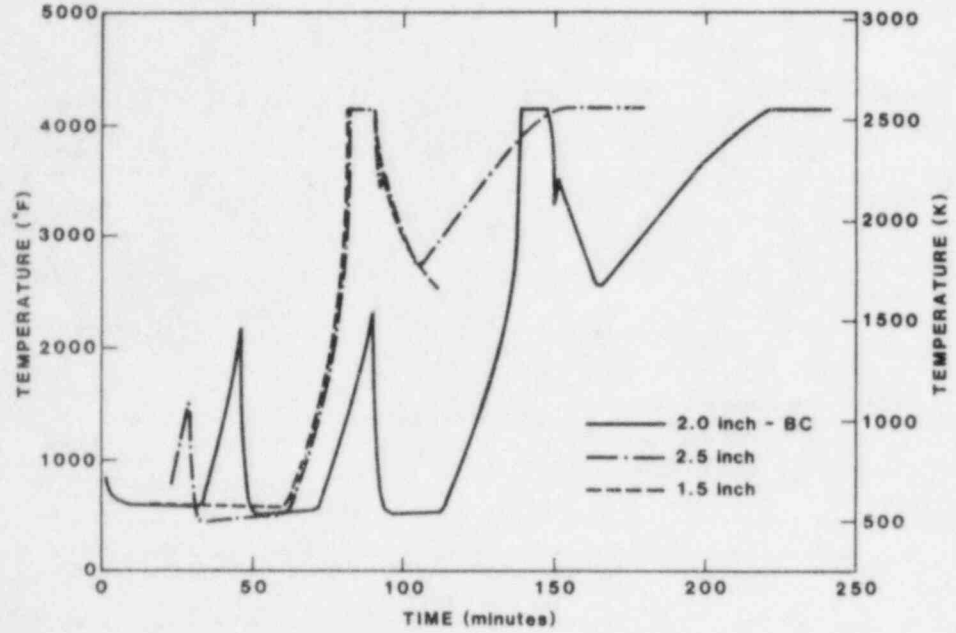

Figure B-1 MARCH variations on S_2D hole size - core temperature.

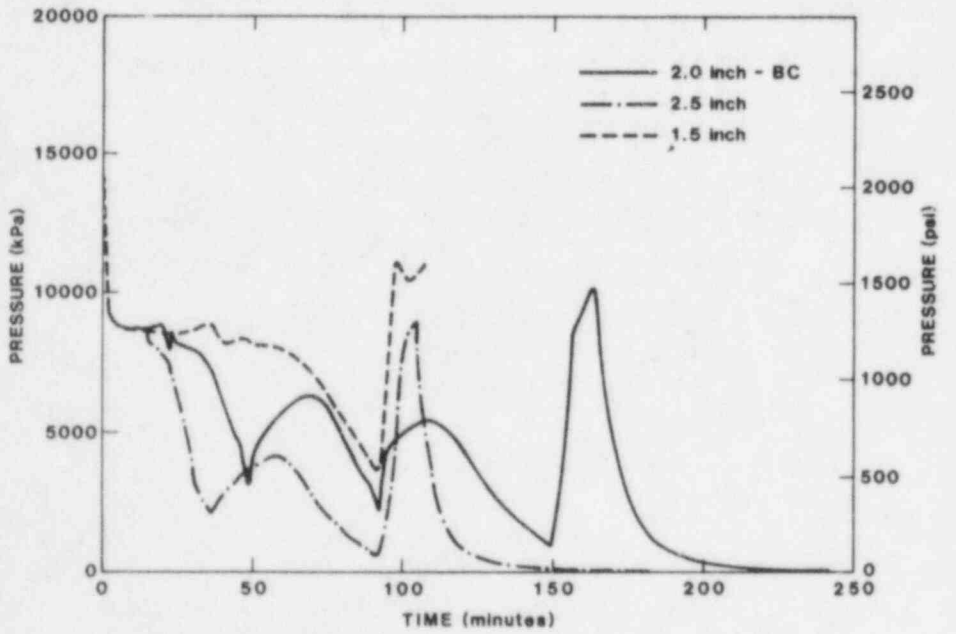

Figure B-2 MARCH variations on S_2D hole size - primary system pressure

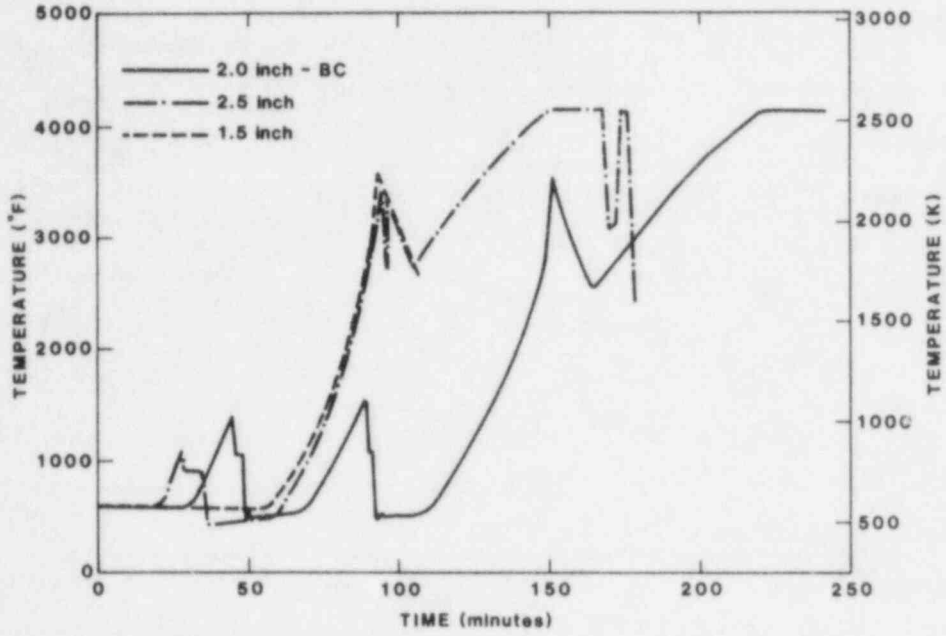

Figure B-3 MARCH variations on S_2D hole size - core exit gas temperature

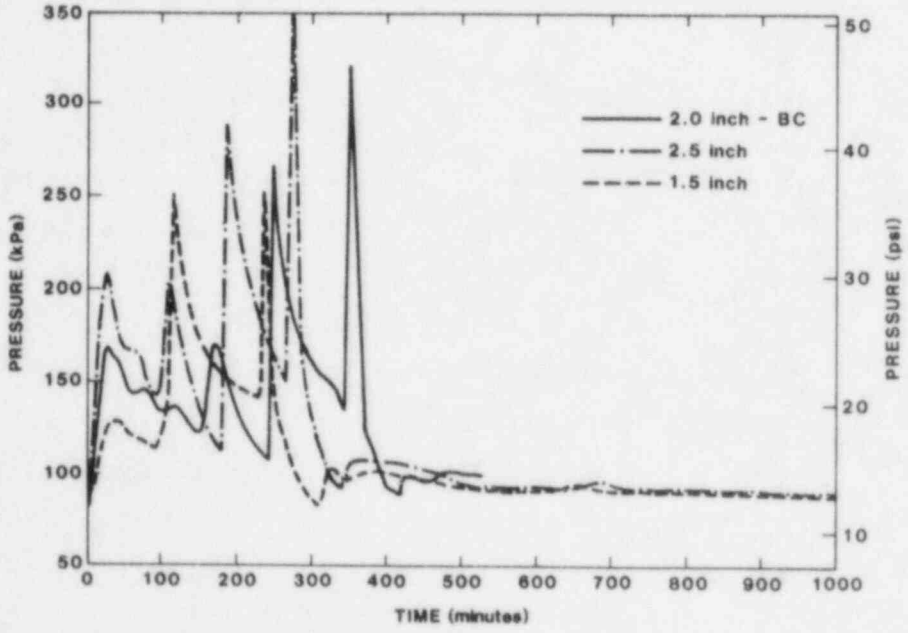

Figure B-4 MARCH variations on S_2D hole size - total containment pressure

calculation. However, the simple models in MARCH may not be able to accurately calculate the blowdown of the primary system for a particular break size. The effective size for a given break size used as an input parameter to MARCH is not known and it is not straightforward to determine an appropriate range of nominal break size for use in the δ_p calculations. Thus for the QUEST study this parameter has not been explored further.

B.2.2 The Effect of Break Elevation.

The elevation of the break is also a part of the specification of the accident sequence, and a break of two inches could occur at many elevations in the plant. The nominal elevation for the BMI-2104 study was 18 feet from the bottom of the core, which corresponds to the elevation of the coolant pump seals. The calculated water level and the elevation of the break determine whether water or steam is leaked from the primary system and thus the mass and energy loss rates. MARCH uses a simple level swell model, which may not lead to accurate determination of whether water or steam is leaking. The effective elevation of the break for a given input break elevation is not known and is not explored in the QUEST study.

However, the MARCH break elevation parameter can influence the depressurization of the primary system and thus change the timing of accumulator discharge and core melt. Figures B-5 through B-8 show the results of varying the break elevation from 16 to 25 feet. After the calculated water level falls below the break elevation, only steam can leak from the primary system, which then more slowly looses water inventory. For the 25-foot elevation case, depressurization is delayed and there is only one discharge of the accumulator. Note that here, as with the study of nominal break size discussed above, the base case provides the maximum estimate of the times to core melt and vessel failure.

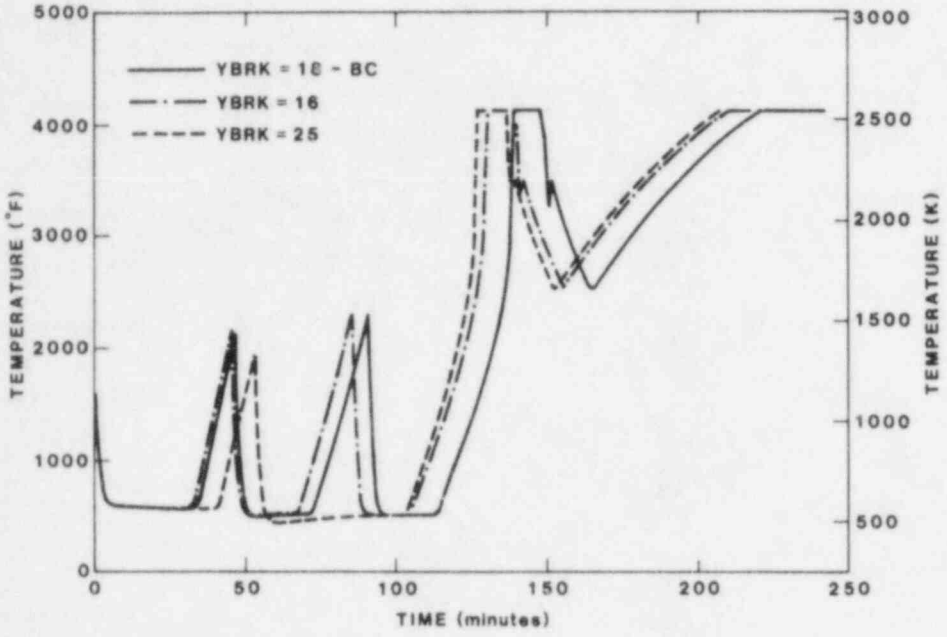

Figure B-5 MARCH variations on S_2D Break Elevation - core temperature

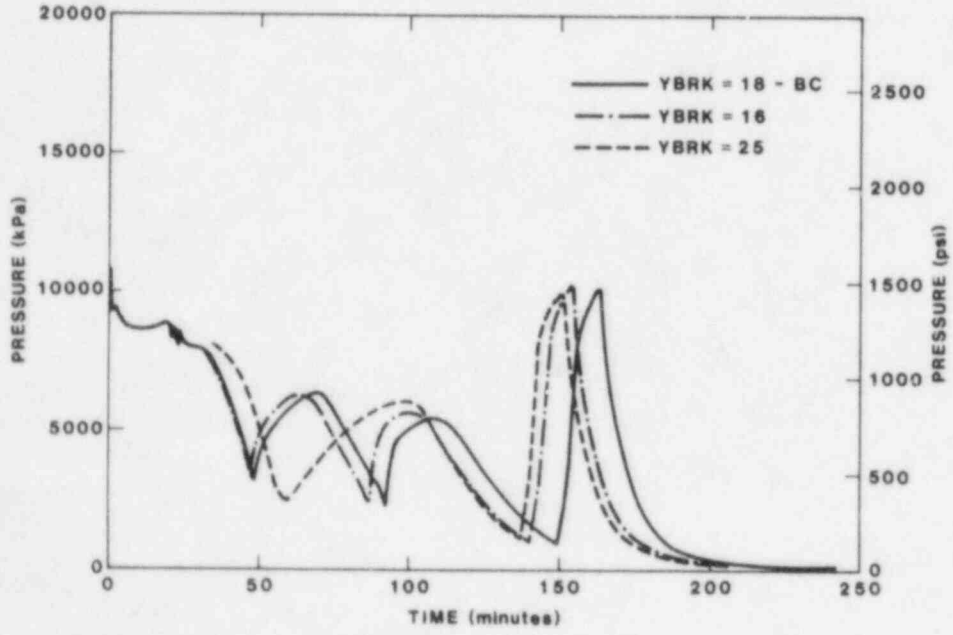

Figure B-6 MARCH variations on S_2D Break Elevation - primary system pressure

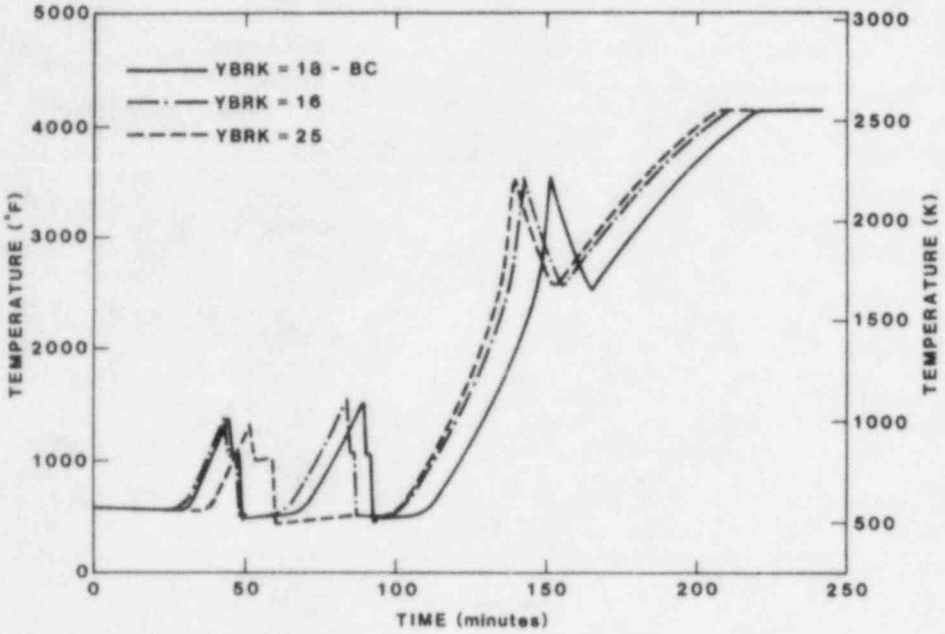

Figure B-7 MARCH variations on S_2D Break Elevation - core exit gas temperature

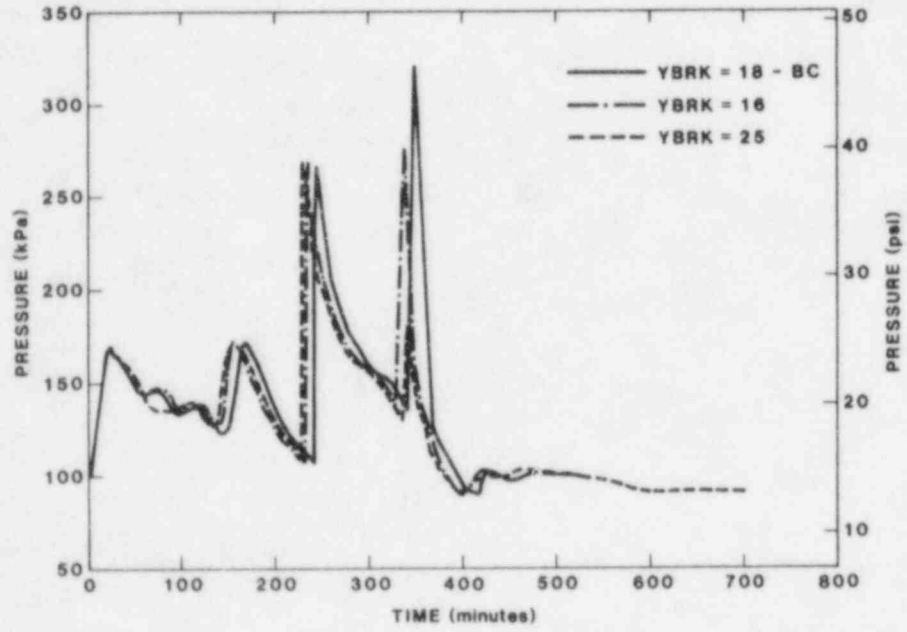

Figure B-8 MARCH variations on S_2D Break Elevation - total containment pressure

B.2.3 The Effect of Recirculation Flow

At Surry, one or two recirculation trains may be used. Figures B-9 and B-10 show the effect of using either one or two trains. For the single train case (3,500 gpm), the containment pressure rise at vessel failure is increased as expected and the burn of combustible gases is delayed because of the larger steam content in the containment atmosphere. While the maximum pressure at burn is not changed much from the two train case, the maximum temperature associated with the burn is reduced by 140 K.

Since the recirculation flow is part of the sequence definition, it is not explored further in the QUEST study.

B.2.4 The Effect of Spray Droplet Size.

Spray droplet size only effects the time constant for containment atmosphere heat removal in the variations studied here. This is illustrated in Figures B-11 and B-12, which show the calculated pressure and temperature in the containment for droplet sizes from 200 to 1000 microns. The maximum pressure at burn is increased by 10 psi, in the 1000 micron case and the maximum temperature at burn is increased by about 280 K. The time constants for the rest of the calculation are long so that the spray particle size has no effect.

The choice of droplet size for the δ_p calculations is discussed in Section 4.0 of this report.

B.3 Conclusions.

This short study has shown that two parameters, break size and elevation, can have a strong effect on the timing and progression of the in-vessel portion of the accident calculations. The uncertainty that they contribute to the source term calculations is not easily determined because it arises from the simple models used in MARCH and

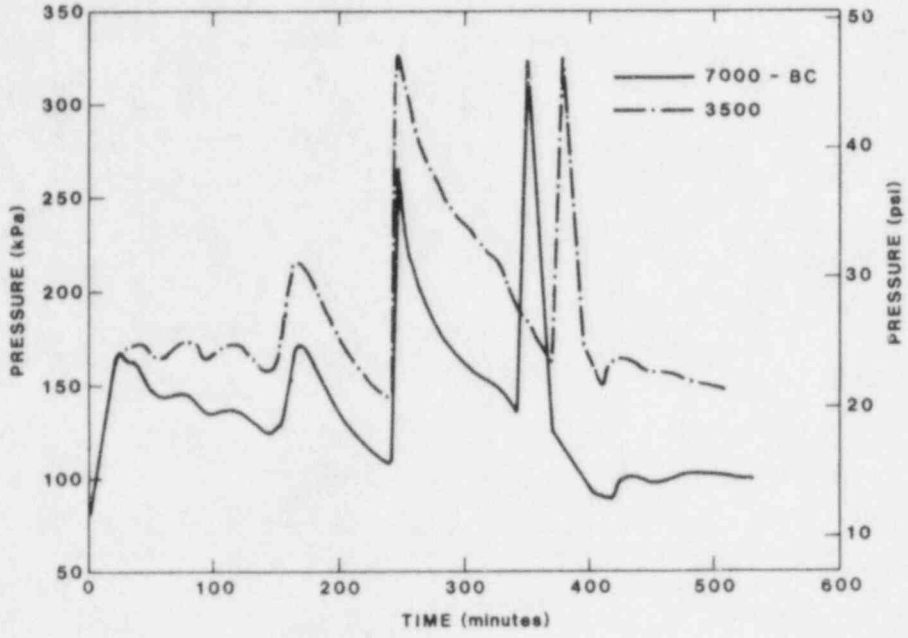

Figure B-9 MARCH variations on S_2D spray recirc flow - total containment pressure

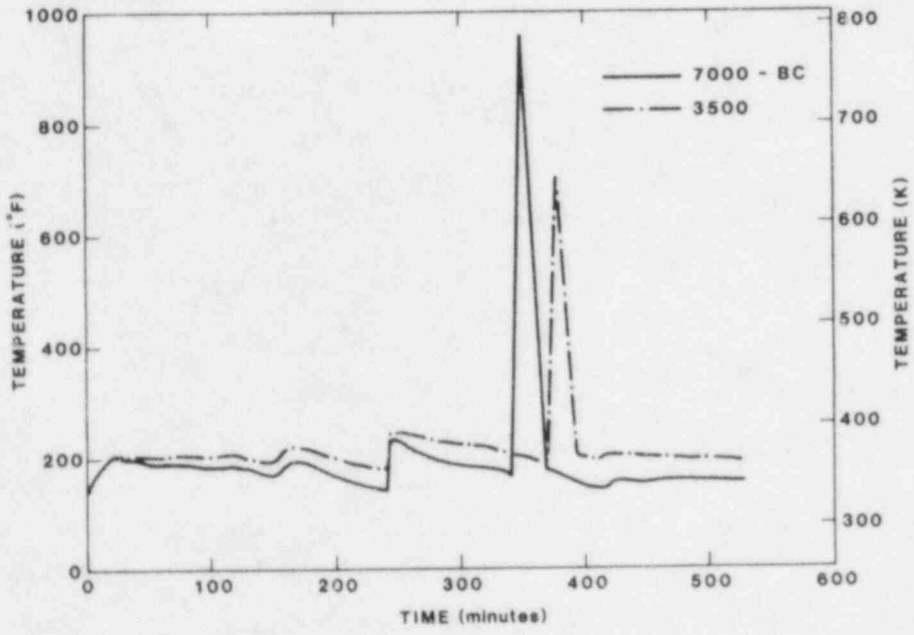

Figure B-10 MARCH variations on S_2D spray recirc flow - compartment temperature

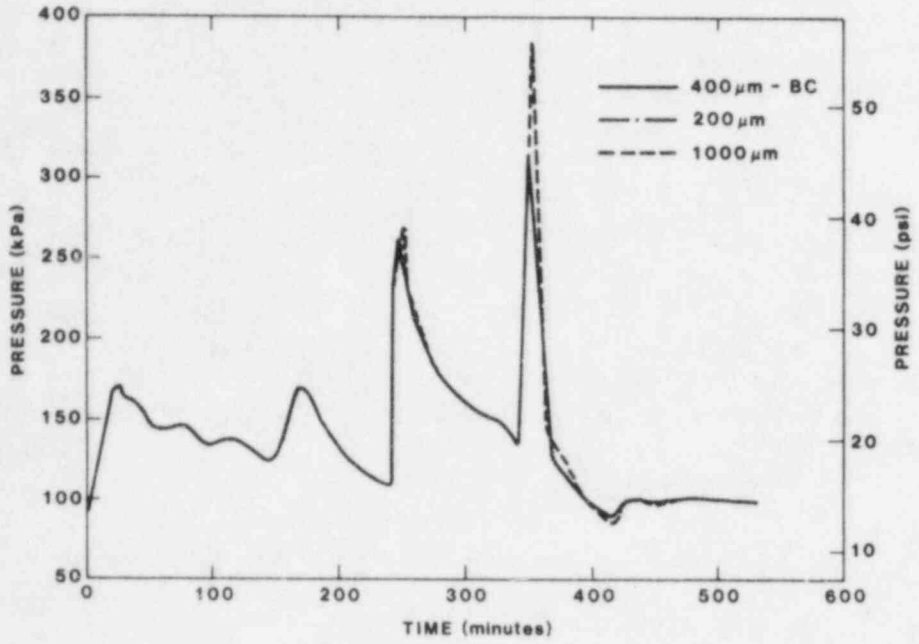

Figure B-11. MARCH variations on S_2D spray droplet diameter - total containment pressure

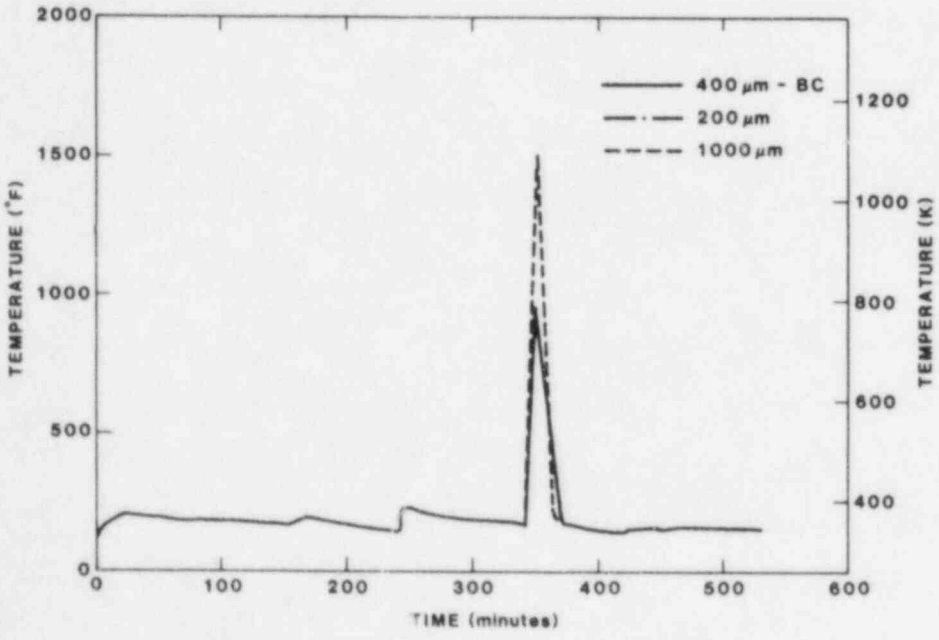

Figure B-12. MARCH variations on S_2D spray droplet diameter - compartment temperature

from the possible variations in the specification of S_2D accident sequence details.

B.4 References

1. R. J. Lipinski, et al, "Uncertainty in Radionuclide Release under Specific LWR Accident Conditions - Volume II: TMLB' Analyses," Sandia National Laboratories Report, SAND84-0410/2, February 1985.

Appendix C

Spray Efficiency Sensitivity Studies

D. C. Williams

C.1 Introduction

Many of the uncertainties in the S_2D source term analyses are qualitatively similar to uncertainties which arise in the TMLB' sequence and which were treated in some detail in the QUEST TMLB' analyses (Volume II of the QUEST report); hence, they have been studied in less detail in the QUEST S_2D analyses. Important exceptions are provided by a class of uncertainties related to the effectiveness of the sprays in removing aerosols and their associated radionuclides from the containment atmosphere. Since decontamination by sprays is a dominant phenomenon in the S_2D sequence, and since these uncertainties have no analogues in previous QUEST work, they will be addressed here. Uncertainties considered will include those related to the elementary collection efficiency of a falling drop for an aerosol particle, aerosol particle sizes, and spray parameters (effective drop size).

The QUEST base case assumed a 400-μm diameter for the spray drop size, in order to conform with the assumptions of the BMI-2104 study. In the present work, most uncertainties other than those associated with the drop size were studied by parameter variation about a base case defined to include a drop size of 1000 μm rather than 400 μm. This was done for two reasons. First, the larger size is much closer to the center of the range of sizes deemed credible for the "effective average" size (300 μm to 2000 μm; see Section 5.4). The second reason was computational: in CONTAIN, the coupling between the modeling of the spray thermal-hydraulic effects and other atmospheric thermal-hydraulic calculations is explicit, and this leads to unstable behavior in the calculations unless the timestep is kept below some maximum size. This maximum timestep

decreases rather rapidly with decreasing drop size, which increases computational costs, and sensitivity studies with a 400 μm drop size would have been unnecessarily expensive.

The modeling of sprays in CONTAIN has not been completely documented elsewhere, and a description of some of its main features will therefore be given in the next section. Emphasis will be on the modeling of the collection of aerosols by the spray drops. A brief comparison with the BMI-2104 modeling will also be given.

C.2 Spray Modeling in CONTAIN

The problem of collection of particles and small drops by larger drops falling through the atmosphere has been studied in many different contexts: nuclear safety, industrial pollution control, phenomena involving natural precipitation, etc. No attempt will be made to review in detail the experimental and theoretical literature here. However, in Section C.3.3, some examples of this work will be cited, and it will be noted that detailed modeling can be quite complex. Even with such modeling, obtaining good agreement between theory and experiment over wide ranges of conditions has proven to be an elusive goal.

In CONTAIN, the construction of detailed models for the collection efficiencies has not been attempted, in part because these efficiencies must be evaluated an extremely large number of times as the calculation proceeds and computational costs would quickly become excessive. Hence, simplified approximate expressions are required.

Five collection mechanisms are considered in the CONTAIN model for aerosol removal by spray droplets:

1. Inertial impaction, which occurs because the particle has a finite inertia, leading the trajectory of the particle center of mass to cross the flow streamlines around the drop and thus intersect the surface of the drop.

2. Interception, which arises because the finite size of the particle permits its surface to contact that of the drop, even when the particle center of mass is on a trajectory which does not intersect the drop.

3. Brownian diffusion, which results from molecular diffusion of the particles across the flow boundary layer around the drop.

4. Diffusiophoresis, which arises as a response of the particle to concentration gradients and vapor flow toward (or from) the drop surface when condensation on (or evaporation from) the drop is occurring.

5. Thermophoresis, which is the migration of a particle down a temperature gradient due to the effect of differential molecular impacts.

The above effects are assumed to be additive in CONTAIN. They will be discussed here in terms of the collection efficiencies of these processes. The collection efficiency may be defined as

$$\varepsilon = \frac{N_p(\text{collected})}{(\pi D^2/4)hn_p}. \qquad \text{(C-1)}$$

Here, N_p(collected) is the number of particles actually collected by a drop of diameter D as it falls a height h through an atmosphere containing n_p particles per unit volume. In CONTAIN, the efficiency is evaluated separately for each of the above five effects, and the

total collection efficiency is assumed to be the sum of the collection efficiencies for the individual effects.

The dominant effects for most containment conditions are interception and impaction, with Brownian diffusion becoming important for very small particle sizes. The treatment in CONTAIN utilizes expressions given by Fuchs[1] for interception and impaction. These efficiencies depend heavily upon whether one assumes viscous flow or potential flow around the drop. The former applies for small values of the drop Reynolds number, $Re_d < 1$, while the latter applies for very large values of Re_d. It must be acknowledged that these efficiencies are based upon a simplified theory, perhaps excessively simplified; however, better approaches suitable for general containment systems codes do not appear to be available at this time.

The expressions used in CONTAIN are:

Interception:

Viscous flow:

$$\varepsilon_{Dv} = 1.5(d/D)^2 \qquad \text{(C-2a)}$$

Potential flow:

$$\varepsilon_{Dp} = 3d/D \qquad \text{(C-2b)}$$

Impaction:

Viscous flow:

$$\varepsilon_{Iv} = 0, \qquad Stk \leq 1.214$$

$$\varepsilon_{Iv} = \left[1+\frac{0.75\ \ln(2Stk)}{(Stk-1.214)}\right]^{-2}, \quad Stk > 1.214 \qquad \text{(C-3a)}$$

Potential flow:

$$\varepsilon_{Ip} = 0.0, \qquad Stk \leq 1/12$$

$$\varepsilon_{Ip} = [Stk/(Stk+0.5)]^2, \quad Stk \geq 0.2 \qquad \text{(C-3b)}$$

(Interpolation is used on $1/12 > Stk > 0.2$)

In the above, d is the particle diameter and Stk is the Stokes number, given by

$$Stk = \frac{d^2 \rho_p U_d}{9\mu D}, \qquad \text{(C-3c)}$$

where ρ_p is the particle density, U_d is the drop fall velocity, and μ is the gas velocity. Eq. C-3c neglects the Cunningham slip correction, which can be important for $d << 1$ μm; however, the impaction effect is zero for such particles ($Stk << 1$) and this neglect is therefore not very important.

As given by Fuchs and as reproduced above, these relations make no allowance for nonspherical aerosol particles. In CONTAIN, an approximate allowance for the agglomeration and dynamic shape factors (Υ and χ, respectively) is made by multiplying the ratio d/D by Υ in Eqs. C-2a and C-2b, and by including a factor of χ in the denominator in Eq. C-3c. However, it should be noted that the sprays keep the degree of superheat

in the containment atmosphere very small during most of the S_2D sequence. Under these conditions, water uptake is expected to lead to approximately spherical aerosol particles, with shape factors close to unity. Hence, the shape factors were set equal to unity and variations in them were not studied in the QUEST S_2D analyses.

For spray drop sizes in the range of interest, Re_d ranges from about 15 to almost 1000. Hence, Re_d is expected to be always too large for the viscous flow relations to hold, but it is not clear that Re_d is large enough for the potential flow relations to provide a good approximation either, except perhaps for the larger drop sizes. In this intermediate regime, no simple expression is expected to be rigorously defensible. In early work, Langmuir[2] suggested a simple interpolation formula as an approximation to the impaction efficiency,

$$\varepsilon_I = \frac{\varepsilon_{Iv} + Re_d \varepsilon_{Ip}/60}{1 + Re_d/60}, \qquad (C\text{-}4)$$

and this formula has been adopted for CONTAIN. In addition, an equivalent interpolation formula has been adopted for the interception efficiency. Little justification can be given for the latter, except to note that the interception efficiency is governed by the same flow patterns about the drop that govern the impaction efficiency; hence, the transition from the viscous flow limit to the potential flow limit might reasonably be expected to show a qualitatively similar dependence upon drop Reynolds number in both cases.

The expressions for the Brownian and phoretic collection efficiencies assumed in CONTAIN are as follows:

Brownian diffusion:

$$\varepsilon_B = 4\mathcal{D}_p(2+0.6Re_d^{1/2}Sc_p^{1/3})/DU_d \qquad (C\text{-}5)$$

In Eq. C-5, $\mathcal{D}_p$ is the diffusivity of the particles in the atmosphere and Sc_p is the particle Schmidt number, equal to $\nu/\mathcal{D}_p$, where ν is the kinematic viscosity.

Thermophoresis:

$$\varepsilon_{th} = 4C_{th}(2+0.6Re_d^{1/2}Pr^{1/3})(T_{gas}-T_{drop})/DU_d \qquad (C\text{-}6)$$

$$C_{th} = \frac{3\mu C(c_t Kn + k_g/k_p)}{2\chi\rho_g T(1+3c_m Kn)(1+2c_t Kn+2k_g/k_p)}$$

Here, Pr is the Prandtl number, T the temperature, C the Cunningham slip correction, Kn the Knudsen number ($2\lambda/d$, where λ is the molecular mean free path), and k_g/k_p is the ratio of gas thermal conductivity to particle conductivity. The constants c_t and c_m are related to thermal accommodation and slip, respectively; the values assumed are 1.0 and 1.37, respectively.

Diffusiophoresis:

$$\varepsilon_{df} = 4\mathcal{D}(2+0.6Re_d^{1/2}Sc^{1/3})\frac{m_1^{1/2}\ln\left(\frac{P_g-P_{vd}}{P_g-P_2}\right)}{\left(X_1 m_1^{1/2}+X_2 m_2^{1/2}\right)DU_d} \qquad (C\text{-}7)$$

In Eq. C-7, $\mathcal{D}$ is the vapor diffusivity in the atmosphere; Sc is the Schmidt number, $\nu/\mathcal{D}$; the subscripts 1, 2, and g refer, respectively, to the vapor, the noncondensible gas (treated as

being dry air), and the total atmosphere; m and X are the molecular weight and the mole fraction, respectively; P is the pressure; and P_{vd} is the vapor pressure of the drop.

The expressions given above for the phoretic collection efficiencies are basically equivalent to those used to calculate phoretic deposition of aerosols upon surfaces in CONTAIN. The phoretic effects can be negative under certain conditions; for example, the diffusiophoretic effect is negative when the drop is evaporating. In such cases, the phoretic effects are still evaluated from Eqs. C-6 and C-7 and added algebraically to the other collection efficiencies. The total collection efficiency is constrained to be nonnegative, however.

At the start of the drop fall, the drop temperature initially changes rapidly, with large and rapid changes in the phoretic efficiencies resulting. Under certain conditions, the drop diameter also changes significantly as it falls, which affects all the collection efficiencies. In CONTAIN, the equations of heat and mass transfer between the atmosphere and the drop are integrated numerically over the drop fall history, and the aerosol collected is evaluated at each timestep in the drop fall integration. Hence, the time variation of the collection efficiencies is taken into account.

Comparison with BMI-2104. It is of interest to compare the CONTAIN spray calculation with that performed for the BMI-2104 S_2D analyses. The latter were performed by incorporating expressions for the spray collection efficiency into the NAUA code. Phoretic effects were not included. The expressions utilized for the interception, impaction, and Brownian collection efficiencies were:

Interception:

$$\varepsilon_D = \frac{1.5(d/D)^2}{(1+d/D)^{1/3}} \qquad \text{(C-8a)}$$

Impaction:

$$\varepsilon_I = [Stk/(Stk+0.35)]^2 \qquad \text{(C-8b)}$$

Brownian diffusion:

$$\varepsilon_B = 3.5Pe^{-2/3} \qquad \text{(C-8c)}$$

$$Pe = \text{Peclet No.} = U_d D/\mathscr{D}_p$$

The BMI-2104 expression for interception differs negligibly from that given previously for the viscous flow limit, Eq. C-2a. On the other hand, the BMI-2104 expression for the impaction efficiency is much closer to that given previously for the potential flow limit; in fact, it gives efficiencies that are even somewhat larger than does Eq. C-3b. As will be seen in Section C.3.1, the difference between results obtained assuming viscous flow versus potential flow efficiencies is large. Hence, the difference between the CONTAIN treatment and the BMI-2104 treatment of interception and impaction effects is potentially quite significant.

In order to compare the treatments of collection by Brownian diffusion, it is useful to note that Eq. C-5 can be rewritten in the form

$$\varepsilon_B = 8/Pe + 2.4Re_d^{1/6}Pe^{-2/3} \qquad (C\text{-}9)$$

For all particle and drop sizes of interest, $Pe \geq 10^6$, and the second term of Eq. C-9 therefore dominates. For values of Re_d in the range of interest, the CONTAIN value of ε_B is 1.1 to 2 times the BMI-2104 value. This difference is not large, and, except for the smallest particle sizes, Brownian diffusion is only a minor contributor to the total aerosol collection in the CONTAIN calculations. Hence, the effects of the different treatments of Brownian diffusion are not expected to be important.

C.3 Sensitivity to Elementary Collection Efficiencies

C.3.1 Impaction and Interception Efficiencies

As noted above, the prescription employed in CONTAIN for estimating collection efficiencies in the transition regime between viscous and potential flow is at best a crude approximation. In order to illustrate the possible importance of this issue, calculations were carried out for the S_2D base case (1000 μm drop) assuming the limiting viscous flow relations and repeated assuming the limiting potential flow relations. Results for total curies airborne are compared with the results of the normal CONTAIN calculation in Fig. C-1. Also shown in the figure are the results obtained assuming no spray at all. It is apparent that assuming the viscous relations largely eliminates the benefits of the sprays; that is, the resulting curve for total curies airborne lies considerably closer to the curve obtained with the sprays off than it does to the normal CONTAIN calculation. This result follows from the fact that Eq. C-2a gives exceedingly small collection efficiencies for interception, and Eq. C-3a gives zero collection by impaction for particles smaller than about 4 μm in these calculations.* (In contrast, the

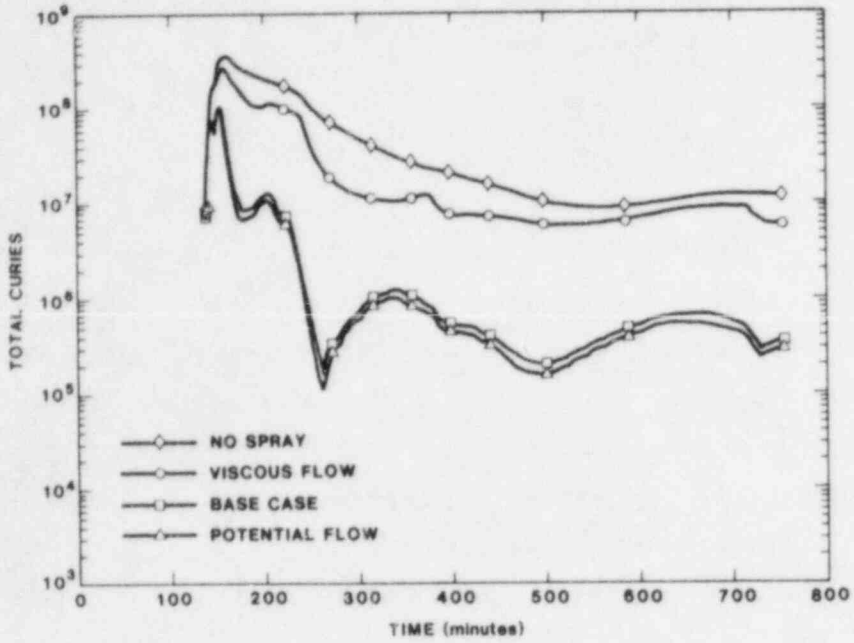

Figure C-1 Influence of spray flow modeling on collection efficiency

potential flow impaction formula, Eq. C-3b, gives substantial collection efficiencies for all particle sizes larger than about 1.3 μm.*)

On the other hand, assuming the limiting potential flow relations results in airborne radionuclide concentrations that are only slightly lower than the standard CONTAIN results. This result follows from the fact that a 1000 μm drop has a relatively large Reynolds number, of the order of 200, and the interpolation formula, Eq. C-4, yields a net efficiency close to the potential flow limit. For smaller drops, e.g. 300 or 400 μm, this would not be true and assuming the potential flow limit could result in aerosol concentrations considerably lower than those given by the standard calculation. Even for these drop sizes, the standard calculation gives radionuclide concentrations much lower than

*These threshold sizes correspond to the particle densities of 3000 kg/m^3 assumed in the QUEST S_2D calculations.

what would be calculated assuming the limiting relations for viscous flow.

It should be emphasized that the range between the viscous and potential flow limiting results is not intended to represent a realisitic estimate of the actual uncertainty range associated with these effects. In particular, the collection efficiencies obtained assuming the viscous limit are believed to be unrealistically small, possibly by large factors. The simple theoretical arguments underlying the results cited in Eq. C-2 indicate that there is little justification for assuming the viscous limit, since $Re_d >> 1$, but this theory may be too simple to provide an adequate guide. A brief additional discussion of the CONTAIN collection efficiencies, including some comparison with other work in this area, will be given in Section C.3.3.

C.3.2 Uncertainties in Phoretic Effects

The CONTAIN calculation of spray collection efficiencies associated with phoretic effects is rather simplified, and the BMI-2104 calculations did not include phoretic effects at all. The expressions given in Eqs. C-6 and C-7 would appear to imply that the phoretic collection efficiency increases strongly as the drop size decreases, but this is rather misleading. When the variation of collection efficiency as the drop falls is taken into account, it can be shown that, in most cases, the total amount of aerosol collected by a given mass of spray water due to phoretic effects is not sensitive to drop size. Since the net effect of other collection mechanisms tends to decrease with increasing drop size, it is expected that phoretic effects are most likely to be relatively significant for the larger drop sizes.

In order to examine the potential significance of uncertainties in phoretic effects, CONTAIN calculations were run for the S_2D base case with a 2000 μm (not 1000 μm) drop size,

both with and without phoretic effects. Results for total curies airborne are shown in Fig. C-2. It is clear that phoretic effects have relatively little influence on the results in this sequence, and uncertainties in their exact magnitude are not expected to be important. Likewise, any uncertainties in the BMI-2104 results due to omission of phoretic effects in their spray model appear to be unimportant.

This result should not be overgeneralized. In general, phoretic effects (principally diffusiophoresis) may be be large whenever the moles of steam condensed by the sprays constitute a large fraction of the total moles of (steam+gas) present in the atmosphere. This condition is not satisfied in the present sequence, but it might be satisfied in other situations. The phoretic effects could also prove important (and possible negative) whenever the containment atmosphere is superheated to a significant extent.

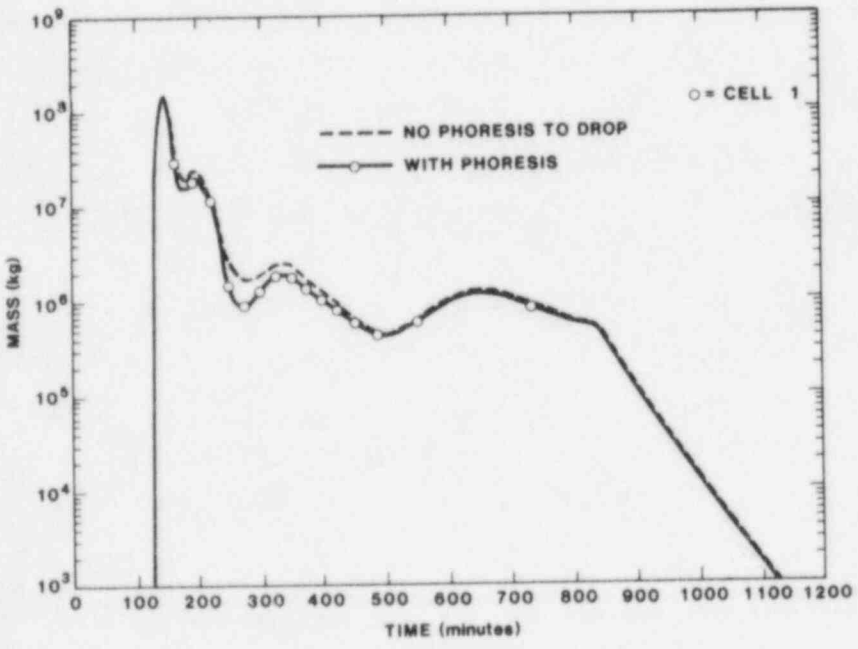

Figure C-2 Influence of phoresis to drop

C.3.3 Comparison of CONTAIN Efficiencies with Other Work

As noted at the the start of Section C.2.1, the problem of particle collection by falling drops has been studied in a variety of contexts. A partial sampling of the theoretical and experimental literature in this area showed the subject to be complex, with some of the results difficult to reconcile with one another. For cases with $D >> d$, as is generally the case here, typical detailed theoretical treatments involve solution of the Navier-Stokes equations for the flow around the drop, followed by numerical integration of the particle trajectory as it moves through the drop flow field under the influence of the various forces acting upon it. When the size ratio D/d is not large, other methods have been used.

The detailed theoretical treatments typically yield rapid increases in collection efficiency with increasing particle size above ~ 1-4 microns, a behavior that is characteristic of the impaction mechanism. The threshold size generally lies close to the potential flow value or somewhat above it[3-6]; even for smaller drop sizes (100-200 μm), the threshold particle size generally lies significantly below the viscous flow value[4-6]. Experimental data in this regime are in reasonable accord with the theoretical results. Hence, it appears likely that the CONTAIN calculations do give an adequate representation of the inertial impaction effect, although there may be some tendency to overestimate the effect by underestimating the threshold particle size for onset of inertial impaction, especially for drops in the smaller part of the size range of interest ($D < 1000$ μm).

For micron-sized particles and smaller, the situation is less clear. Theoretical treatments often disagree with one another and with experimental data, which themselves often disagree with one another[3]. Some of the detailed theoretical results, and some laboratory experiments, give values of the

collection efficiencies which are in reasonable agreement with the CONTAIN values,[3,5] while others fall below the CONTAIN values by as much as an order of magnitude.[3,5] Some (not all) of the experimental and theoretical results indicate that, for micron-sized particles, the collection efficiency tends to decrease with decreasing drop size in the size regime 300-1000 μm.[3,5] The CONTAIN collection efficiencies show a qualitatively similar behavior because the interpolation formula introduces a shift from the predictions of Eq. C-2b toward the much smaller values predicted by Eq. C-2a as the drop size is reduced. Quantitatively, this behavior in CONTAIN is limited to drop sizes smaller than 400-500 μm, while Refs. 3 and 5 suggest that it arises for drops smaller than about 1000 μm. Hence, for micron-sized particles, there may be some tendency for CONTAIN to overestimate collection efficiencies for drops in the hundreds of microns size range, while doing a better job for larger drops.

Some of the results (e.g., Ref. 3) show increasing collection efficiencies with decreasing <u>particle</u> size for micron-sized particles and smaller. The behavior differs from the CONTAIN (and BMI-2104) modeling, in which efficiencies decrease with decreasing particle size until Brownian diffusion becomes the dominant mechanism, at particle sizes of about 0.1 μm and less. Particle capture by wake eddies at the rear of the drop has been invoked to explain such behavior.[3] The same effect has been invoked[3,5] to explain the increase in collection efficiency with increasing drop size in the 300-1000 μm regime that was noted above. This same approach has been interpreted[3] to imply that wake shedding of eddies, beginning at $Re_d \sim$ 300-400, could yield a decrease in collection efficiency with increasing drop size for D > 1000 μm, with this decrease possibly being more rapid than that given by CONTAIN. It also indicates that CONTAIN may underpredict the collection of submicron particles ($d \leq 0.5$ μm) for drops on the order of 1000 μm.[3,5]

The experimental results alluded to above involve laboratory measurements on drops falling under more or less carefully controlled conditions. Field measurements in the natural precipitation environment typically imply washout efficiencies higher (by an order of magnitude or more) than either the theoretical or experimental results cited above, and higher than would be given by CONTAIN[3,7]. Likewise, the CONTAIN collection efficiencies would lie near the lower limit of the rather wide range of collection efficiencies inferred from the Containment Systems Experiments (CSE)[8]. Uptake of water by aerosol particles in saturated or near-saturated environments has been invoked as an explanation for these results[3,8].

It is acknowledged that the above discussion is based upon only a sampling of the available literature, and has not considered some potentially-important effects (e.g., electrostatic interactions). In order to better define the collection efficiencies and their associated uncertainties, a comprehensive literature review should be carried out, including a critical evaluation of the various results and evaluation of the various factors each study has taken into account, or not taken into account, and how these factors might affect the results. It has not been possible to perform this rather time-consuming task in the present work, and any conclusions offered here must be regarded as very tentative. Subject to this qualification, it is suggested that most (but not all) of the available results are consistent with the use of a CONTAIN calculation with D = 2000 μm as providing a reasonable lower limit to the spray effectiveness. The theoretical treatments and laboratory measurements also suggest that CONTAIN calculations with D = 300 or 400 μm provide a reasonable upper limit to spray effectiveness, although some field measurements and CSE results suggest greater effectiveness is possible under some conditions. Pending more careful study, the collection efficiency uncertainties remain rather large and difficult to quantify.

C.4 Uncertainties Associated with Particle Sizes

In the QUEST CONTAIN calculations, it was assumed that all aerosol sources had a lognormal size distibution, with a mass median diameter (mmd) of 1 μm and a σ_g of 2. The mmd calculated by VANESA generally ranged from 0.4 μm to 1.0 μm, with brief periods when it was slightly larger in some runs. The mmd of the aerosols released from the RCS generally is within a factor of two of 1 μm, as estimated from TRAP-MELT calculations. It should be emphasized that both the VANESA and TRAP-MELT estimates of the mmd have considerable uncertainty associated with them.

In many aerosol calculations, the dominant aerosol depletion mechanism is agglomeration to larger sizes followed by gravitational settling. In such cases, results are relatively insensitive to initial particle size because, if the initial particle size is assumed reduced, the number density of particles is correspondingly increased, the initial agglomeration rates are rapid, and the system relatively quickly looses its "memory" of the small initial particle size. In the present case, however, the sprays provide the dominant mechanism for aerosol removal, and most of the collection mechanisms depend more or less strongly upon the particle size. Hence, it appeared to be desirable to consider the order of magnitude of the uncertainties that might be introduced by uncertainties in particle size.

Based upon the range of particle sizes observed in the VANESA calculations, it was judged that a reasonable estimate of the uncertainty range associated with the particle size uncertainty could be obtained by varying the aerosol source mmd from 0.4 to 1.0 μm. Results for total airborne radioactivity obtained for these two values of the mmd are compared in Fig. C-3. The effect of varying the particle size is seen to be nontrivial, but it is less than a factor of two. Hence, this

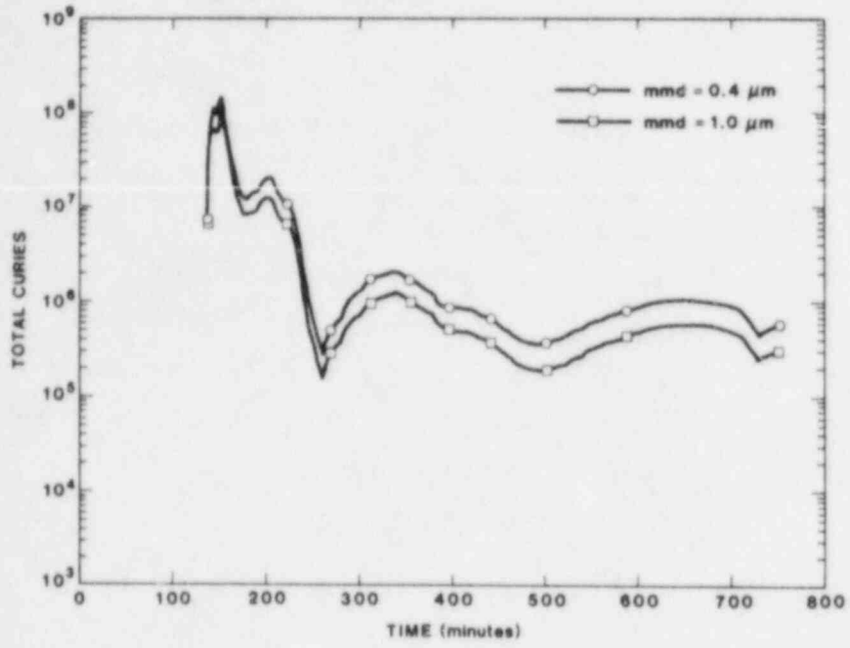

Figure C-3 Comparison of 0.4 and 1.0 micron particle sizes

uncertainty is potentially of some significance, but it is not one of the dominant uncertainties.

C.5. Effect of Drop Size

Before presenting the computational results on the effect of drop size, it is of some interest to consider the expected size dependence of the individual collection mechanisms as given in Section C.2. As noted in Section C.3.2, the effectiveness of the phoretic effects, for a given mass of spray water, is not expected to be very size-dependent. The Brownian diffusion collection efficiency depends upon size through the factor $Re_d^{1/2}/DU_d$, which varies as $(DU_d)^{-1/2}$. For drops in the size range of interest, the dependence of U_d upon D does not depart greatly from linearity, and thus the Brownian efficiency is roughly inversely proportional to D.

The situation is somewhat more complex for the impaction and interception collection efficiencies. The size dependence of the impaction efficiency is through the Stokes parameter, Stk, which varies as U_d/D. Since U_d increases as D increases, this ratio turns out to be fairly insensitive to D in the size regime of interest. The impaction efficiency exhibits threshold behavior, being zero below the threshold and increasing rapidly above it. For particle sizes just above the threshold, the collection efficiency can be sensitive to small changes in Stk. However, since efficiencies become large so rapidly above the threshold, all particles significantly larger than the threshold will be very rapidly removed by the sprays, and the effect of drop size will be significant only insofar as it alters the threshold. From Eqs. C-3 and C-4, it is apparent that the threshold varies as $Stk^{1/2}$ and, hence, as $(U/D)^{1/2}$. Hence, the threshold particle size is not very sensitive to drop size, and a large effect of drop size upon impaction is not expected, for drops in the size range of interest. (For several reasons, these arguments would break down if extended to larger or smaller drops than the 300 - 2000 μm range considered in QUEST).

In the case of interception, the potential flow and viscous flow formulae give, respectively, D^{-1} and D^{-2} as the dependence of the collection efficiency upon the drop size. For $D \geq 1000$ μm, the interpolation formula, analogous to Eq. C-4, gives efficiencies close to the potential flow limit and the interception efficiency assumed by CONTAIN does show the expected decrease with increasing drop size. For sizes less than 1000 μm, the increase in the efficiency given by Eq. C-2b with decreasing drop size is compensated for by the shift away from the potential flow limit given by the interpolation formula. The net effect is that there is relatively little variation in the interception efficiency over the 300 - 1000 μm range; for drops smaller than about 500 μm, the efficiency actually declines as the drop size is reduced further.

It must be reiterated that the above discussion of the impaction and interception efficiencies and their dependence upon drop size is subject to the uncertainties involved in the use of the interpolation formula, Eq. C-4. These are no doubt quite significant, as was discussed in Section C.3.3.

In estimating the effectiveness of a given mass of spray water in removing aerosol, the efficiencies discussed above must be multiplied by the surface/volume ratio of the drops, which varies as 1/D. This factor strengthens the inverse dependence of the Brownian diffusion effectiveness upon drop size. It leads to a monotonic decrease in interception effectiveness with increasing drop size, although the dependence is quite flat in the lowest part of the size range ($D < 400$ μm). It does not greatly alter the threshold behavior of the impaction effect as a function of particle size, and the importance of impaction is still not expected to be a very strong function of drop size.

In Fig. C-4, the total curies airborne is plotted as a function of time for drop sizes of 400, 1000, and 2000 μm (a 300 μm drop gave results differing negligibly from the 400-μm drop results). Also shown are results for the run with no spray operating. Over most of the time span studied, the range of drop sizes considered leads to factors of five to ten variation in the airborne radioactivity. Even the 2000 μm drop size gives an order of magnitude decontamination relative to the no-spray case, except that decontamination factors are less during periods of rapid release early in the sequence.

In Figure C-5, the particle size distribution is shown for the three drop sizes, and for the no-spray case, at times of about 315 minutes into the accident. For all drop sizes, the

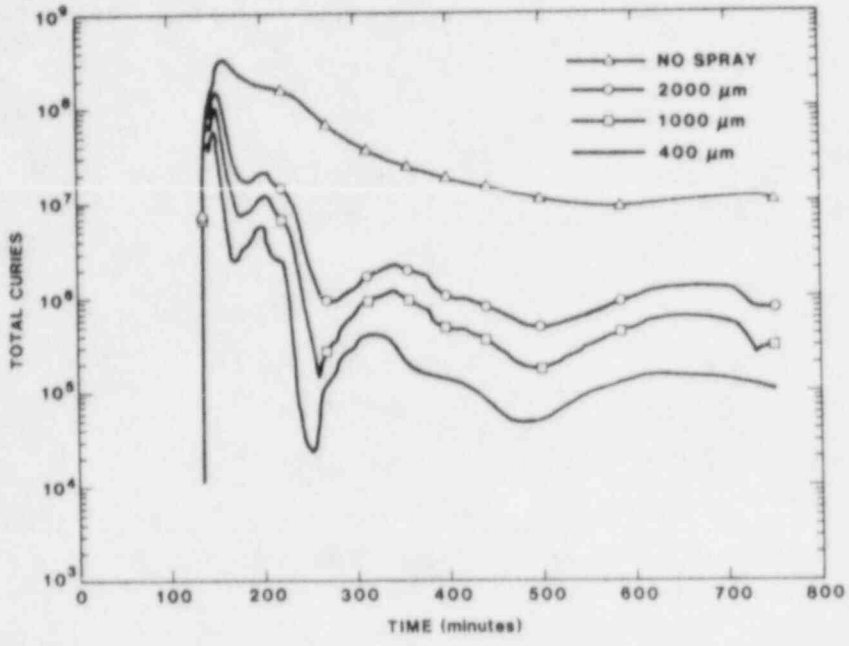

Figure C-4 Dependence upon drop size

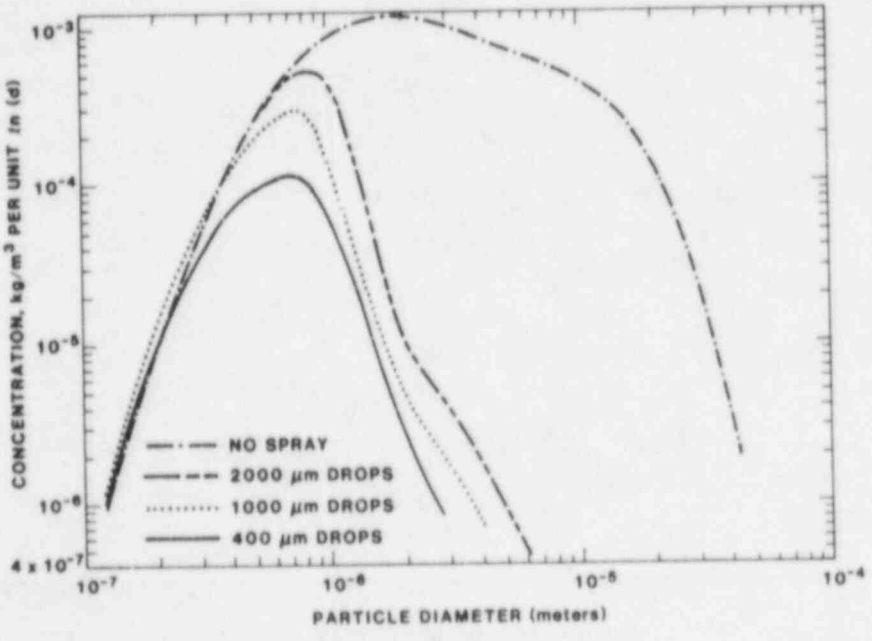

Figure C-5 Particle size distribution at 315 minutes

size distribution shows a rapid fall-off for sizes much larger than about 1 μm, due to the onset of the impaction effect. As expected, the particle size at which this rapid decline begins does not depend strongly upon drop size. For all cases with sprays on, the concentrations of particles with diameters a few microns or greater are seen to be quite small, but they appear to be substantially lower for the 400 μm drop size than for the larger drops. This is largely (not entirely) a numerical effect, related to certain approximations used in CONTAIN and the fact that the calculations with the larger drop size were run with larger timesteps. If calculations were run for the larger drop sizes with timesteps as small as those used for the 400 μm drop, the concentrations of the larger particle sizes would not be much greater than those calculated for the 400 μm drop.

C.6 Summary and Conclusions

It is concluded that uncertainties associated with the collection of aerosols by containment sprays are not large enough to compromise the basic conclusion that containment sprays offer substantial decontamination factors in the Surry S_2D sequence analyzed. The airborne radionuclide concentrations are calculated to be at least an order of magnitude lower than what they would be without sprays, except during times when rapid release of radionuclides to the containment atmosphere gives the sprays inadequate time to take effect.

The exact magnitude of the decontamination factors to be expected is subject to considerable uncertainty, approaching an order of magnitude. The principal sources of uncertainty involve uncertainty in the drop collection efficiencies by impaction and interception and uncertainty in the choice of a representative drop size for the sprays. A smaller, but still significant uncertainty may be that resulting from uncertainty in the aerosol particle sizes associated with the sources to containment.

Uncertainty in the collection efficiencies associated with Brownian diffusion and phoretic effects do not appear to be important, primarily because these effects are themselves only minor contributors to the total aerosol collection efficiency, at least in this particular sequence. Significant uncertainties due to other collection mechanisms not considered can not be ruled out, although it is likely that these would tend to be in the downward direction.

Considering the dependence of the various collection efficiencies upon drop size, the effective spray drop size appropriate for these calculations should be smaller than the mass median diameter but larger than the number median diameter; either a linear median or surface median diameter might be appropriate. In view of this conclusion, the data on spray drop size discussed in Section 5.4 and summarized in Table 2 of the main report indicate that the size range used in QUEST, 300 - 2000 μm, could be considered excessively wide. However, this judgment does not take into account the other uncertainties involved.

The particle size uncertainty appears to be capable of contributing something approaching, but probably not exceeding, a factor of two in the upward direction. If combined with the largest drop diameter justified by the present arguments and the data of Table 2 (surface median diameter for Spray Systems Nozzle A80, 1360 μm), the particle size effect might reasonably be expected to give results approaching those obtained with a 2000-μm drop for the base case. There is still the difficult-to-quantify uncertainty in the impaction and interception efficiencies to consider; these were discussed in Section C.3.3, where it was tentatively concluded that they probably do not invalidate use of the 2000 μm CONTAIN calculations as representing a minimum spray effectiveness calculation.

It is concluded, therefore, that the 2000 μm drop size provides a reasonable estimate of the minimum spray effectiveness to be expected, and is therefore suitable for use in those QUEST "high" calculations in which the sprays are operating. In a similar vein, a 300 μm drop size appears reasonable for the "low" case, although it is more difficult to offer a quantitative justification. Hence, the range in drop size adopted for QUEST is 300 - 2000 μm. It should be understood that this range is used partly as a surrogate representation of other uncertainties, in addition to the actual uncertainty in effective drop size. The latter is believed to be somewhat less than this range would indicate.

References

1. Fuchs, N. A., The Mechanics of Aerosols, pp. 162-165, Pergamon, New York, 1964.

2. Langmuir, Irving, "The Production of Rain by a Chain Reaction in Cumulus Clouds at Temperatures Above Freezing", J. Meteor., 5, 175 (1948).

3. Beard, K. V., "Experimental and Numerical Collision Efficiencies for Submicron Particles Scavenged by Small Raindrops", J. Atmos. Sci., 31, 1595 (1974).

4. Leong, K. H., Beard, K. V., and Ochs, H. T., "Laboratory Measurements of Particle Capture by Evaporating Cloud Drops", J. Atm. Sci., 39, 1130 (1982).

5. Wang, P. K., "A Theoretical and Experimental Determination of the Efficiency ...", 4th Joint Conference on Sensing of Environmental Pollutants

6. Pilat, M. J., and Prim, A., "Calculated Particle Collection Efficiencies ....",

7. Glasstone, S., and Dolan, D. J., The Effects of Nuclear Weapons, pp.418-419., U. S. DOD and U. S. DOE (1977).

8. Hilliard, R. K., Postma, A. K., McCormack, J. D., and Coleman, L. F., "Removal of Iodine and Particles in the Containment Systems Experiment", Nucl. Tech., 10, 499 (1971).

DISTRIBUTION:

Division of Technical Information
and Document Control
NRC Distribution Contractor
U.S. Nuclear Regulatory Commission
15700 Crabbs Branch Way
Rockville, MD 20850
350 copies for R5

U.S. Nuclear Regulatory Commission (16)
Office of Nuclear Regulatory Research
Washington, DC 20555
Attn: O. E. Bassett
B. S. Burson
R. T. Curtis
C. N. Kelber
J. T. Larkins
G. Marino
L. Chan (5)
M. Silberberg
M. Jankowski
R. W. Wright
T. J. Walker
W. Pasedag

U.S. Nuclear Regulatory Commission (4)
Office of Nuclear Reactor Regulation
Washington, DC 20555
Attn: L. G. Hulman
P. Easky
J. Rosenthal
J. Mitchell

U.S. Department of Energy (2)
Albuquerque Operations Office
P. O. Box 5400
Albuquerque, NM 87185
Attn: J. R. Roeder, Director
Operational Safety Division
D. K. Nowlin, Director
Special Programs Division
For: C. B. Quinn
D. Plymale

U.S. Department of Energy
Office of Nuclear Safety Coordination
Washington, DC 20545
Attn: R. W. Barber

Electric Power Research Institute
3412 Hillview Avenue
Palo Alto, CA 94303
Attn: R. Vogel

Brookhaven National Laboratory
Upton, NY 11973
Attn: R. A. Bari
T. Pratt
G. A. Greene

Professor R. Seale
Department of Nuclear Engineering
University of Arizona
Tucson, AZ 85721

Oak Ridge National Laboratory (5)
P. O. Box Y
Oak Ridge, TN 37830
Attn: T. Kress
R. P. Wichner
R. Lorenz
G. Parker
R. Spencer

K. Holtzclaw
General Electric - San Jose
Mail Code 682
175 Kurtner Ave
San Jose, CA 95125

Argonne National Laboratory
9700 S. Cass Ave
Argonne, IL 60439
Attn: J. Rest

Cathy Anderson
Nuclear Safety Oversight Commission
1133 15th St., NW
Room 307
Washington, DC 20005

Battelle's Columbus Laboratory (3)
505 King Ave
Columbus, OH 43201
Attn: P. Cybulskis
R. Denning
J. Gieseke

J. E. Antill
Berkeley Nuclear Laboratory
Berkeley GL 139 PB
Gloucestershire
United Kingdom

DISTRIBUTION (Continued)

W. G. Cunliffe
Bldg. 396
British Nuclear Fuels, Ltd.
Springfields Works
Salwick, Preston
Lancashire
United Kingdom

Reactor Development Division (4)
UKAEA - Atomic Energy Establishment
Winfrith, Dorchester
Dorset
United Kingdom
Attn: R. G. Tyror, Head
T. Briggs
R. Potter
A. Nichols

Projekt Nucleare Sicherheit (3)
Kenforschungszentrum Karlsruhe
Postfach 3640
D-7500 Karlsruhe 1
Federal Republic of Germany
Attn: J. P. Hosemann
H. Albrecht
H. H. Rininsland
A. Feige

G. Petrangeli
Direzione Centrale della Sicurezza
Nucleare e della Protezione Sanitaria
(DISP)
Entre Nazionale Energie Alternative
(ENEA)
Viale Regina Margherita, 125
Casella Postale N. 2358
I-00100 Roma A.D., Italy

K. J. Brinkman
Reactor Centrum Nederland
P.O. Box 1
1755 ZG Petten
The Netherlands

H. Bairiot, Chief
Department LWR Fuel
Belgonucleaire
Rue de Champde Mars. 25
B-1050 Brussels, Belgium

S. Saito
Japan Atomic Energy Research Institute
Takai Research Establishment
Tokai-Mura, Naku-Gun
Ibaraki-ken
Japan

Wang Lu
TVA
400 Commerce, W9C157-CK
Knoxville, TN 37902

M. Fontana
Director, IDCOR Program
Technology for Energy, Inc.
P. O. Box 22996
10770 Dutchtown Rd.
Knoxville, TN 37922

UKAEA
Safety and Reliability Directorate
Wigshaw Lane
Culcheth
Warrington, WA3 4NE
United Kingdom
Attn: H. J. Teague (3)
M. Hayns

Frau Reusenbach-Berger
Gesellschaft fuer Reaktorsicherheit
(GRS mbH)
Postfach 101650
Glockengasse 2
D-5000 Koeln 1
Federal Republic of Germany

S. J. Niemczyk
Union of Concerned Scientists
1346 Connecticut Avenue, N.W.
S.1101
Washington, DC 20036

M. Jankowski
IAEA
Division of Nuclear Reactor Safety
Wagranerstrasse 5
P.O. Box 100
A/1400 Vienna, Austria

DISTRIBUTION (Continued)

3141	C. M. Ostrander (5)	6422	J. E. Brockmann (5)
3151	W. L. Garner (1)	6422	R. M. Elrick
6000	E. H. Beckner	6423	P. S. Pickard
6400	A. W. Snyder	6425	W. J. Camp
6410	J. W. Hickman	6425	D. R. Bradley (5)
6411	A. S. Benjamin	6425	P. K. Mast (5)
6411	D. M. Kunsman	6425	M. Pilch
6415	J. M. Griesmeyer	6427	M. Berman
6415	C. D. Leigh	6440	D. A. Dahlgren
6415	F. E. Haskin	6449	K. D. Bergeron
6420	J. V. Walker (5)	64[illegible]	K. K. Murata
6420	J. B. Rivard	6449	D. C. Williams
6422	D. A. Powers (5)	8024	M. A. Pound

NRC FORM 335 (2-84) NRCM 1102, 3201, 3202

U.S. NUCLEAR REGULATORY COMMISSION

BIBLIOGRAPHIC DATA SHEET

SEE INSTRUCTIONS ON THE REVERSE

1. REPORT NUMBER (Assigned by TIDC, add Vol. No., if any)

SAND84-0410
Vol. 3

2. TITLE AND SUBTITLE

Uncertainty in Radionuclide Release Under Specific LWR Accident Conditions
Volume III: S_2D Analyses

3. LEAVE BLANK

4. DATE REPORT COMPLETED

MONTH	YEAR
March	1985

5. AUTHOR(S)

R.J. Lipinski, D.R. Bradley, J.E. Brockmann, J.M. Griesmeyer, D.A. Powers, A.R. Taig*, J. Tills**, D.C. Williams

6. DATE REPORT ISSUED

MONTH	YEAR
April	1985

7. PERFORMING ORGANIZATION NAME AND MAILING ADDRESS (Include Zip Code)

Sandia National Laboratories
Albuquerque, NM 87185

8. PROJECT/TASK/WORK UNIT NUMBER

9. FIN OR GRANT NUMBER

A1227

10. SPONSORING ORGANIZATION NAME AND MAILING ADDRESS (Include Zip Code)

Office of Nuclear Regulatory Research
U.S. Nuclear Regulatory Commission
Washington, DC 20555

11a. TYPE OF REPORT

Technical

b. PERIOD COVERED (Inclusive dates)

12. SUPPLEMENTARY NOTES

* On attachment from Safety and Reliability Directorate, United Kingdom Atomic Energy Authority
** J. Tills and Associates, Inc.

13. ABSTRACT (200 words or less)

An estimation of the uncertainty in the calculated radiological source term for an assumed S_2D accident in the Surry plant has been made. The major conclusions of the study are: (1) The method of calculating a specific source term for a particular LWR accident, as demonstrated in the BMI-2104 reports, allows the determination of the effect on the source term of various phenomena uncertainties. (2) For the S_2D accident, a very important uncertainty is whether or not the core materials in the reactor cavity are coolable by the continuous flow of water from the sprays. This uncertainty leads to a late-time source term uncertainty that ranges from about a megacurie of suspended radioactivity, down to many orders of magnitude lower. The uncertainty in debris coolability also induces a larger uncertainty in the early source term than was found in the TMLB' analyses (reported in Volume II). The uncertainty in debris coolability is primarily due to uncertainty in debris configuration after contacting water in the reactor cavity. (3) At late times another important uncertainty is the effectiveness of the containment sprays. This single uncertainty leads to a factor of ten uncertainty in late-time source term, all of it upward with respect to the BMI-2104 evaluation. (4) In all cases considered, the total suspended aerosol radioactivity declined by a factor of one hundred in one hundred minutes or less. This is due to the cleansing action of the sprays.

14. DOCUMENT ANALYSIS – a. KEYWORDS/DESCRIPTORS

QUEST
Uncertainty
S_2D
Radionuclide release

b. IDENTIFIERS/OPEN-ENDED TERMS

15. AVAILABILITY STATEMENT

Unlimited

16. SECURITY CLASSIFICATION

(This page) Unclassified
(This report) Unclassified

17. NUMBER OF PAGES

18. PRICE

*U.S. GOVERNMENT PRINTING OFFICE: 1985-461-721:20089

UNITED STATES
NUCLEAR REGULATORY COMMISSION
WASHINGTON, D.C. 20555